A cytoskeletal network maintains filament shape in the multicellular cyanobacterium *Anabaena* sp. PCC 7120

Benjamin L. Springstein[1]*, Dennis J. Nürnberg[2,†], Ann-Katrin Kieninger[3], Christian Woehle[1¥], Julia Weissenbach[1,‡], Marius L. Theune[1], Andreas O. Helbig[4], Andreas Tholey[4], Iris Maldener[3], Tal Dagan[1], Karina Stucken[5*+]

[1] Institute of General Microbiology, Christian-Albrechts-Universität zu Kiel, Kiel, Germany

[2] Department of Life Sciences, Imperial College, London SW7 2AZ, United Kingdom

[3] Department of Microbiology/Organismic Interactions, University of Tübingen, Tübingen, Germany

[4] AG Proteomics & Bioanalytics, Institute for Experimental Medicine, Christian-Albrechts-Universität zu Kiel, Kiel, Germany

[5] Department of Food Engineering, University of La Serena, La Serena, Chile.

[†] Present address: Institute of Experimental Physics, Free University of Berlin, Berlin, Germany

[¥] Present address: Max Planck Institute for Plant Breeding Research, Max Planck-Genome-center Cologne, Cologne, Germany

[‡] Present address: Faculty of Biology, Technion-Israel Institute of Technology, Haifa, 32000, Israel

* Corresponding authors: KS kstucken@userena.cl; BLS bspringstein@ifam.uni-kiel.de

Abstract

The determinants of bacterial cell shape are extensively studied in unicellular forms. Nonetheless, the mechanisms that shape bacterial multicellular forms remain understudied. Here we study coiled-coil rich proteins (CCRPs) in the multicellular cyanobacterium *Anabaena* sp. PCC 7120 (hereafter *Anabaena*). Our results reveal two CCPRs, termed LfiA and LfiB (for linear filament), which assemble into a heteropolymer that traverses the longitudinal cell axis. Two additional CCRPs, CypS (for cyanobacterial polar scaffold) and CeaR (for cyanobacterial elongasome activity regulator), form a polar proteinaceous scaffold and regulate MreB activity, respectively. Deletion mutants of these CCRPs are characterized by impaired filament shape and decreased viability. Our results indicate that the four CCRPs form a proteinaceous network that stabilizes the *Anabaena* multicellular filament. We propose that this cytoskeletal network is essential for the manifestation of the linear filament phenotype in *Anabaena*.

Introduction

Bacterial multicellularity ranges from transient associations, such as colonies and biofilms to permanent multicellular forms[1]. The basic characteristics of prokaryotic organisms that are considered as multicellular are mechanisms of cell-cell adhesion and intercellular communication[2]. Biofilms are considered as transient forms of prokaryotic multicellularity since they lack a reproducible multicellular shape[3]. The shape of the individual cell has been shown to have a strong impact on the spatial biofilm formation. Example is the different composition of cell morphologies within an *Escherichia coli* biofilm[4]. Studies of biofilm formation in *Rhodobacter sphaeroides* showed that wild type (WT) rod-shaped cells readily form biofilms on costal water surfaces, while coccoid-like cells that were treated with an inhibitor of MreB – a well-known cell shape determinant – lacked the ability to form biofilms and failed to attach to surfaces[5]. Hence, cytoskeletal structures that determine cell shape through the remodeling of the peptidoglycan (PG) sheet are key regulators of biofilm formation, specifically in environments that are subjected to constant changes[5–8]. MreB, together with the elongasome

49 (a multi-enzyme complex), is a regulator of longitudinal PG biogenesis, and thus it plays a
50 crucial role in the adaption to different environments and prokaryotic multicellularity.

51 The key hallmarks of permanent bacterial multicellularity are morphological
52 differentiation and a well-defined and reproducible shape, termed patterned multicellularity[3].
53 Unlike biofilms, patterned multicellular structures are the result of either coordinated swarming
54 or developmental aggregation behavior as in myxobacteria[9]. Additional factors include cell
55 division, proliferation and cell differentiation as in sporulating actinomycetes[10] and
56 cyanobacterial filaments[11,12]. In myxobacteria as well as in actinomycetes, it has been shown
57 that patterned multicellular traits are dependent on the coordinated function of different coiled-
58 coil-rich proteins (CCRPs). Reminiscent of eukaryotic intermediate filaments (IFs)[13,14], many
59 bacterial CCRPs were shown to perform analogous cytoskeletal functions through their ability
60 to self-assemble into distinct filaments *in vitro* and *in vivo*[15–19]. Unlike FtsZ or MreB[20,21],
61 bacterial IF-like CCRPs do not require any additional co-factors for polymerization *in vitro*[22].
62 For example, in *Myxococcus xanthus*, the coordinated swarming and aggregation into fruiting
63 bodies is mediated by its gliding motility[23], which strictly depends on the filament-forming
64 CCRP AglZ[24]. AglZ is organized in a large multi-protein complex that governs gliding motility
65 in synergy with MreB, which still retained its PG synthesis function but was also co-opted for
66 gliding motility in *M. xanthus*[25–28]. Actinobacteria, such as *Streptomyces* species, grow by
67 building new cell wall (i.e. PG) only at the cell poles, independent of MreB[29,30], which is
68 strikingly different from how most other bacteria grow[31]. This characteristic polar growth mode
69 is organized by a cytoskeletal network of at least three CCRPs - DivIVA, Scy and FilP – that
70 form the polarisome[16,17,32,33]. Similar to eukaryotic intermediate filaments (IFs), FilP and Scy
71 self-assemble into filaments *in vitro*[17,32], thereby fulfilling a major criterium of cytoskeletal
72 proteins[34]. Although of essential importance for growth and cell shape, the polarisome is not
73 directly involved in the hallmark patterned multicellular trait of Actinobacteria. In contrast,
74 patterned multicellularity in Actinobacteria is governed by a highly reproducible and
75 coordinated cell division event during sporulation where up to 100 FtsZ-driven Z-rings are

76 formed. This then leads to the formation of evenly spaced septa, resulting in long chains of
77 spores[3,35].

78 Cyanobacteria are characterized by a large phenotypic diversity, ranging from
79 unicellular species to complex filamentous cyanobacteria of which some can undergo
80 morphological differentiation[36]. Filamentous cyanobacteria that differentiate multiple cell types
81 are considered the peak of prokaryotic complexity. The cell biology of multicellular
82 cyanobacteria has been studied in the context of cytoplasmic continuity, intercellular
83 communication, and cell differentiation[37]. Species of the Nostocaceae are characterized by the
84 formation of linear filaments, where equally interspaced heterocysts (specialized cells for
85 nitrogen fixation) are differentiated upon nitrogen starvation in a highly reproducible pattern[37].
86 Studies of multicellular growth in the model multicellular cyanobacterium *Anabaena* showed
87 that FtsZ - the prokaryotic tubulin homolog - is an essential protein that localizes to future
88 septum sites in a typical Z-ring structure, while MreB - the prokaryotic actin homolog -
89 determines the cell shape of a single cell within an *Anabaena* filament but is dispensable for
90 filament viability[38,39]. Deletion of MreB[39] or of a class B penicillin-binding-protein (PBP)[40]
91 resulted in swollen and rounded cell morphotypes, a phenotype commonly associated with
92 defects in PG biogenesis[41,42]. As a true-multicellular organism, *Anabaena* contains functional
93 analogs to the eukaryotic gap-junctions, termed septal junctions, which facilitate intercellular
94 communication[43] by direct cell connections[44]. These structures involve the septum localized
95 proteins SepJ, FraC and FraD[37,45,46] and a nanopore array in the septal PG[47]. The importance
96 of SepJ, FraC and FraD for multicellularity in *Anabaena* is highlighted by a defect in filament
97 integrity and a resulting loss of multicellularity under diazotrophic growth conditions in strains
98 lacking any of the three genes[46,48–50]. Besides the canonical cytoskeletal proteins FtsZ and
99 MreB, no other cytoskeletal proteins have been described in *Anabaena.* Here we study the
100 contribution of coiled-coil-rich filament-forming proteins to the *Anabaena* phenotype. For this
101 purpose, we predicted *Anabaena* CCRPs with presumed IF-like functions and evaluated their
102 cytoskeletal properties using *in vivo* and *in vitro* approaches.

103 **Results**

104 **Prediction of CCRP candidates in *Anabaena***

105 Potential filament-forming proteins were predicted computationally by surveying the *Anabaena*
106 genome for CCRPs, which putatively have IF-like function[15,24,32,51,52]. *Anabaena* CCRPs were
107 filtered according to the presence of a central rod-domain, which is characteristic to eukaryotic
108 IF and prokaryotic IF-like proteins[14,53,54]. Similar to Bagchi *et al*. (2008), who identified the
109 filament-forming CCRP FilP in *Streptomyces coelicolor*[32], we defined the presence of a rod-
110 domain as 80 amino acids in coiled-coil conformation. This analysis resulted in the
111 identification of 186 rod-domain-containing CCRPs (Supplementary File 1). The 186 CCRPs
112 were further filtered to include only hypothetical proteins of unknown function, yielding a set of
113 13 candidates for further analysis (Supplementary Fig. 1 and Supplementary Table 1). The
114 distribution of homologs to these 13 candidates in cyanobacteria showed that eight *Anabaena*
115 CCRPs have homologs in multicellular cyanobacteria as well as in unicellular cyanobacteria
116 while five have homologs present only in multicellular cyanobacteria (Fig. 1a; Supplementary
117 Table 1).

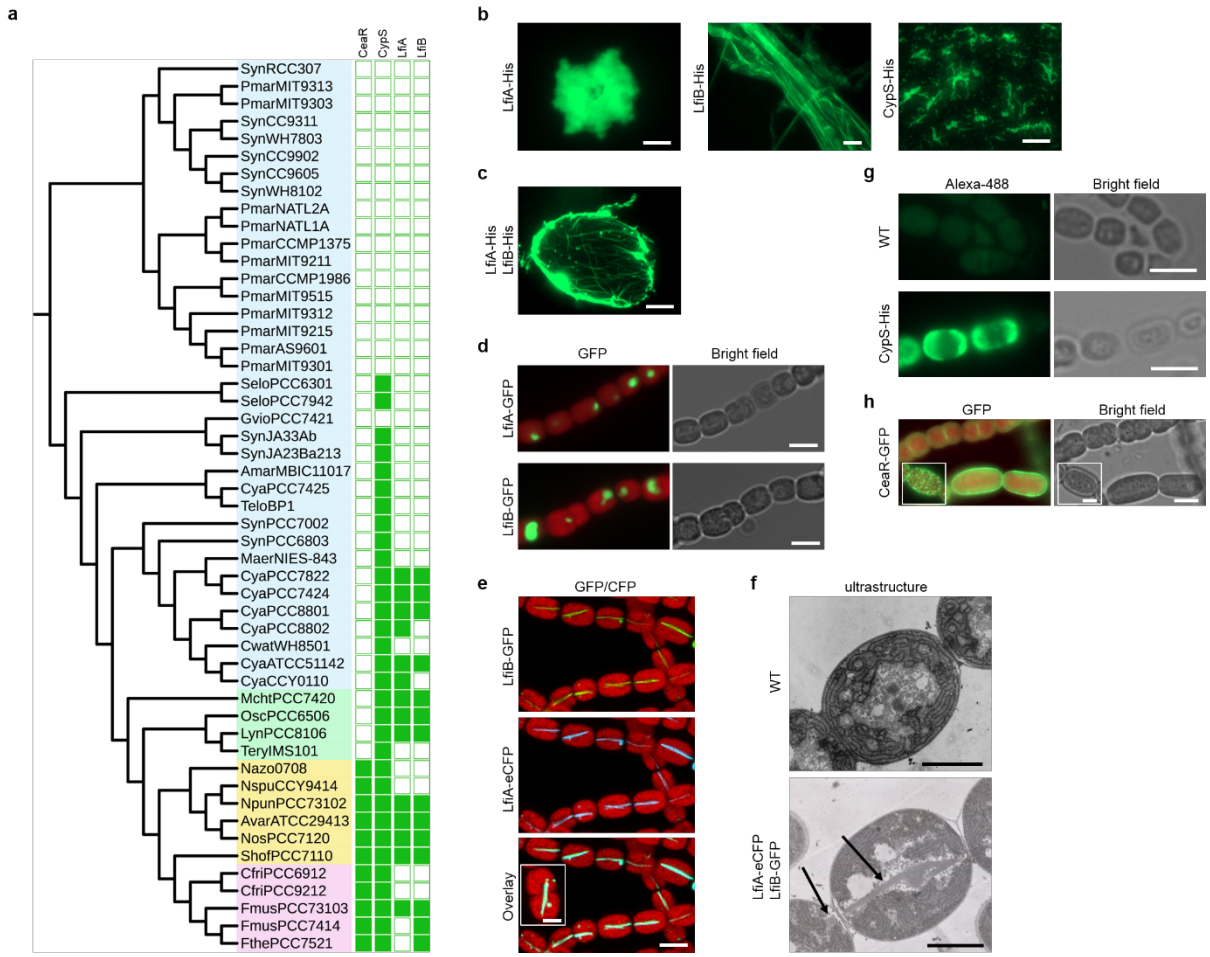

Fig. 1: Cyanobacterial CCRPs polymerize *in vitro* and *in vivo*

(**a**) Distribution of protein candidate homologs in cyanobacteria. Organism names include the genus first letter and species first three letters. The presence of homologous genes is marked by a green rectangle. Organism names are shaded according to cell or colony morphology; blue: unicellular, green: filamentous, yellow: filamentous and heterocyst forming, pink: heterocyst forming and true branching or multiseriate filaments. Homologs accession numbers are supplied in Supplementary File 2. (**b**-**c**) Epifluorescence micrographs of NHS-Fluorescein-stained *in vitro* filaments formed by purified and renatured (**b**) LfiA-His (1 mg ml^{-1}), LfiB-His (0.5 mg ml^{-1}) and CypS-His (0.5 mg ml^{-1}) or (**c**) co-renatured LfiA-His and LfiB-His (0.25 mg ml^{-1} each) in 25 mM HEPES, pH 7.4 (LfiB), HLB (LfiA and co-renatured LfiA/B) or PLB (CypS) renaturation buffer. (**d**) Merged GFP-fluorescence and chlorophyll autofluorescence (red) and bright field micrographs of *Anabaena* WT cells expressing LfiA-GFP or LfiB-GFP from P_{petE}. LfiA-GFP-expressing cells were grown in BG11 without copper and induced for 2 d with 1 µM $CuSO_4$. LfiB-GFP-expressing cells were grown in $BG11_0$. (**e**) Merged GFP and/or eCFP fluorescence and chlorophyll autofluorescence (red) micrographs of *Anabaena* WT cells co-expressing LfiA-eCFP and LfiB-GFP from P_{petE} and grown in $BG11_0$. Localization of LfiA/B grown in BG11 is depicted in Supplementary Fig. 7. (**f**) Electron micrographs of ultrathin sections of *Anabaena* WT and *Anabaena* cells co-expressing LfiA-eCFP and LfiB-GFP. Black arrows indicate electron-dense structures coinciding with the LfiA/B heteropolymer observed in Fig. 1e. Filaments appear to anchor or attach to the cell poles. (**g**) Alexa Fluor 488 and bright field micrographs of anti-His immunofluorescence staining of *Anabaena* WT and *Anabaena* cells expressing CypS-His from P_{petE} grown in liquid $BG11_0$ supplemented with 0.25 µM $CuSO_4$ for 2 d. Polar sites loaded with CypS-His plugs coincide with sites of retracted chlorophyll autofluorescence observed prior to immunofluorescence (Supplementary Fig. 6b). (**h**) Merged GFP fluorescence and chlorophyll autofluorescence and bright field micrographs of *Anabaena* WT cells expressing CeaR-GFP from P_{petE} grown on BG11. Notably, no enlarged cells were identified in the Δ*ceaR* mutant strain expressing CeaR-GFP from P_{ceaR} (Supplementary Fig. 8a), indicating that CeaR level in WT cells is tightly regulated. Inlay shows patchy and cell periphery-localized CeaR-GFP. N-terminal YFP translational fusion of CCRPs did not reveal coherent structures, suggesting that the N-terminus is essential for protein localization. Scale bars: 5 µm, (e) 1.25 µm, (f) 1.6 µm or (h inlay) 2.5 µm.

145 ***In vivo and in vitro* filamentation of CCRP candidates**

146 Out of the 13 candidates, four CCRPs showed self-association and filamentation properties,
147 including LfiA together with LfiB, CypS and All4981 (that will be investigated in a separate
148 report). The remaining nine candidates failed to form filamentous structures *in vivo* and *in vitro*
149 and consequently were excluded from further analysis. An exception is CeaR whose
150 computational structural prediction suggested similarity to the well-characterized prokaryotic
151 IF-like protein crescentin from *Caulobacter crescentus*[15] (Supplementary Table 1). To evaluate
152 the ability of candidate CCRPs to self-associate, we ectopically expressed C and N-terminally
153 tagged (His_6, YFP, eCFP or GFP) recombinant proteins and investigated *in vitro* polymerization
154 properties and *in vivo* localization pattern. The assembly of CCRPs into filaments *in vitro* was
155 tested by fluorescence microscopy using the NHS-Fluorescein dye, which was previously
156 successfully used to visualize FtsZ filaments[55]. For this, we purified His_6-tagged candidates by
157 Ni-NTA affinity chromatography under denaturing conditions and renatured them by dialysis
158 followed by NHS-fluorescein staining. As a positive control for our approach we used
159 crescentin[15,56]. The NHS-fluorescein staining of crescentin revealed an extensive filamentous
160 network in our *in vitro* assay (Supplementary Fig. 2). As negative controls, we included empty
161 vector-carrying BL21 (DE3) cells, GroEL1.2 from *Chlorogloeopsis fritschii* PCC 6912 (known
162 to self-interact[57]) and the maltose binding protein (MBP), all of which were tested negatively
163 for filament formation *in vitro* using our approach (Supplementary Fig. 2).

164 **LfiA and LfiB are interdependent for polymerization *in vitro* and *in vivo***

165 Since the candidate proteins were annotated as hypothetical proteins, we initially investigated
166 and confirmed the transcription of all four genes under standard (BG11) and diazotrophic
167 ($BG11_0$) growth conditions (Supplementary Fig. 3a,b). An additional inspection of the genomic
168 loci suggested that *lfiA* and *lfiB* are encoded in an operon structure, however, RT-PCR data
169 indicated that they are not co-transcribed (Supplementary Fig. 3a,c). Applying our *in vitro*
170 polymerization assay to LfiA revealed amorphous non-filamentous aggregates while LfiB
171 assembled into sheet-like filamentous structures (Fig. 1b). Nonetheless, most LfiB precipitated

172 upon renaturation, suggesting that LfiB has only a partial capacity to form filaments. Next,
173 inspired by the close genomic localization of *lfiA* and *lfiB*, we tested for co-polymerization of
174 both proteins. Upon co-renaturation, LfiA and LfiB assembled into a meshworks of
175 heteropolymers (Fig. 1c). This demonstrates that LfiA and LfiB are interdependent for
176 filamentous assembly *in vitro*. To examine the *in vivo* localization pattern of LfiA and LfiB, we
177 expressed translational GFP fusions of both proteins from the replicative pRL25C plasmid, a
178 derivate of the pDU1 plasmid[58], which is commonly used in experimental work in
179 *Anabaena*[39,59,60]. The expression of LfiA-GFP and LfiB-GFP from their respective native
180 promoters (as predicted using BPROM[61]) revealed no discernible expression of LfiB-GFP
181 (Supplementary Fig. 4a). Consequently, we investigated the *in vivo* localization of both proteins
182 from the frequently used copper-regulated *petE* promoter (P_{petE})[59,60,62,63], which has been
183 previously used to study the localization of FtsZ and MreB in *Anabaena*[39,59,60]. We generally
184 observed that the P_{petE}-driven gene expression does not always lead to expression of the
185 translational fusion protein in every cell under standard growth conditions (BG11 medium).
186 Notably, this was not observed under diazotrophic growth conditions (i.e. $BG11_0$) or upon
187 supplementation with additional $CuSO_4$, where we saw more pronounced expression. The
188 expression of LfiA-GFP and LfiB-GFP from P_{petE} in *Anabaena* independently did not reveal
189 filamentous structures (Fig. 1d). However, upon co-expression of LfiA-eCFP and LfiB-GFP
190 from P_{petE}, a distinct filamentous structure along the longitudinal cell axis could be observed
191 (Fig. 1e). To confirm that the localization of LfiA-GFP and LfiB-GFP is not affected by the
192 wildtype (WT) *lfiA* or *lfiB* alleles, we localized both proteins in a Δ*lfiA*Δ*lfiB* double mutant strain.
193 This experiment revealed the same localization pattern as in the WT (Supplementary Fig. 4b),
194 suggesting that co-polymerization is a dosage-dependent process. In support of this idea, we
195 only observed pronounced *in vitro* co-polymerization with equal amounts of LfiA-His and LfiB-
196 His (Supplementary Fig. 5). We further validated the co-polymerization of LfiA and LfiB by
197 heterologous expression in the Δ*lfiA*Δ*lfiB* double mutant background and in *E. coli*; both
198 experiments revealed the same interdependent polymerization pattern (Supplementary Fig. 4c
199 and 7). The intracellular localization of the LfiA/LfiB heteropolymer in *Anabaena* suggests that

200 the polymer is either anchored at the cell poles or specifically broken up during cell division,
201 as LfiA/LfiB filaments were never observed to cross cell-cell borders and only traversed
202 through not yet fully divided cells (Figs. 1e inlay and 1f). Our results so far suggest that LfiA
203 and LfiB form a heteropolymer *in vitro* and *in vivo* and that heteropolymer assembly may
204 depend on LfiA and LfiB relative dosage.

205 **CypS localizes to the cell poles in *Anabaena***

206 The *in vitro* polymerization assay of CypS revealed that CypS assembled into star-like
207 structures of short filamentous strings (Fig. 1b). The expression of CypS-GFP in *Anabaena*
208 WT cells from the predicted native promoter (P_{cypS}; using BPROM) did not reveal coherent
209 fluorescence signals (Supplementary Fig. 6a). However, when expressed from P_{petE}, CypS-
210 GFP was localized to the cytosol and the cell envelope (Supplementary Fig. 5a). The same
211 localization to the cell envelope and the cytoplasm was also observed upon expression of
212 CypS-GFP from P_{cypS} in a *ΔcypS* mutant background (Supplementary Fig. 5a). Notably, CypS-
213 GFP only partially complemented the Δ*cypS* mutant swollen cell phenotype (Supplementary
214 Fig. 6a). Consequently, we examined whether the addition of a C-terminal His-tag may
215 reconstitute the CypS WT phenotype and found that CypS-His forms a functional protein fusion
216 (Supplementary Fig 9a,c). Immunolocalization of CypS-His in *Anabaena* WT revealed that the
217 protein forms large plugs at the cell poles (Fig. 1g) that appeared to displace the thylakoid
218 membranes (Supplementary Fig. 6b). This suggests that the comparably large C-terminal GFP
219 tag negatively affects CypS localization *in vivo*. However, upon additional induction of CypS-
220 GFP expression, polar assemblies can also be seen (Supplementary Fig. 6a), suggesting that
221 the GFP-tag only partially interferes with CypS localization. Further induction of CypS-His
222 expression also resulted in the formation of swollen cells (Supplementary Fig. 6b), indicating
223 that CypS has morphogenic properties. To test for a possible interplay between LfiA/LfiB and
224 CypS we tested for the localization of LfiA/LfiB in the Δ*cypS* mutant strain. This revealed that
225 in the absence of CypS, LfiA and LfiB co-localization in the form of a filamentous structure is

226 lost (Supplementary Fig. 7). Our results thus indicate that CypS forms polar plugs that are
227 putative anchor sites for the LfiA/LfiB filament.

228 **CeaR is morphogenic and is localized to the cell envelope and the Z-ring**

229 Attempts to overexpress CeaR-His in *E. coli* for the *in vitro* polymerization assay were not
230 successful, possibly due to the N-terminal transmembrane domains (TMDs; Supplementary
231 Fig. 1). Removal of the CeaR N-terminal TMDs enabled overexpression in *E. coli,* but
232 nonetheless no filamentous CeaR *in vitro* structures were observed. We note that genomes of
233 unicellular cyanobacteria do not have a homologous gene to *ceaR* (Fig. 1a), and furthermore,
234 unlike CypS, LfiA and LfiB, recombinant expression of CeaR-GFP in *Synechocystis* was
235 unsuccessful. This suggests that CeaR function is specific to the multicellular cyanobacterial
236 phenotype. Expression of a functional CeaR-GFP fusion protein (Supplementary Fig. 11b,d,e)
237 from P_{ceaR} and from P_{petE} in *Anabaena* WT showed that the protein localized to the cell
238 periphery in a patchy pattern (Fig. 1h, Supplementary Fig. 8a), yet it also accumulated at the
239 septa or had localization at the Z-ring. Z-ring or septal localization was found in 25% of cells
240 (589 out of 2301 counted cells) carrying P_{petE}::*ceaR-gfp* and in 17% of cells (206 out of 1237
241 counted cells) carrying P_{ceaR}::*ceaR-gfp*. In addition, we observed that the expression of CeaR-
242 GFP from P_{petE} led to a swollen cell phenotype in a large proportion of cells (1754 (76%) of
243 2301 counted cells) and a similar proportion of swollen cells when CeaR-GFP was expressed
244 from P_{ceaR} (789 (64%) of 1237 counted cells; Fig. 1h, Supplementary Fig. 8a). A similar swelling
245 of cells was also identified in *Anabaena* WT cells expressing untagged CeaR from P_{ceaR} (435
246 (32%) of 1346 counted cells; Supplementary Fig. 8a). Strikingly, expression of both, CeaR-
247 GFP or untagged CeaR in the Δ*ceaR* mutant strain did not induce cell swelling (Supplementary
248 Figs. 8a and 9a). The localization pattern of CeaR indicates that CeaR is associated with the
249 FtsZ-driven divisome. In agreement with our suggestion, CeaR-GFP localization to the Z-ring
250 was lost upon deletion of the N-terminal TMDs from CeaR (Supplementary Fig. 8a). This
251 indicates that membrane anchorage is key for proper CeaR function and localization.

252 ***Anabaena* CCRP deletion strains show defects in filament shape and viability**

253 To further study the function of the four CCRPs, we generated Δ*cypS,* Δ*ceaR* and a double
254 Δ*lfiA*Δ*lfiB* mutant strain and examined their phenotype. Notably, single Δ*lfiA* or Δ*lfiB* mutant
255 strains could not be generated, suggesting that the presence of only one of those proteins is
256 lethal for *Anabaena*. Our results show that the Δ*cypS* and Δ*lfiA*Δ*lfiB* mutant strains were
257 characterized by altered filament and cell shape phenotypes and reduced filament viability (Fig
258 2a, Supplementary Fig. 10a,b). Unlike the linear filament growth pattern of the *Anabaena* WT,
259 both Δ*cypS* and Δ*lfiA*Δ*lfiB* mutant strains showed filaments with a zigzagged pattern (Fig. 2a,
260 Supplementary Fig. 9d). Additionally, Δ*cypS* and Δ*lfiA*Δ*lfiB* cells were significantly larger and
261 more rounded in comparison to the WT, reminiscent of Δ*mreB* mutant[39] (Fig. 2c). The defect
262 phenotype of the Δ*cypS* and Δ*lfiA*Δ*lfiB* mutant strains could be complemented with pRL25C
263 carrying P_{cypS}::*cypS* or $P_{lfiA/lfiB}$::*lfiA-lfiB*, respectively (Supplementary Fig. 9a,b). We also
264 observed a slight decrease in cell volume in older Δ*ceaR* mutant cultures that also exhibited a
265 shortened filament length phenotype (Fig. 2c, Supplementary Figs. 9d and 11c). This is in
266 accordance with our observation of cell volume increase upon CeaR-GFP overexpression in
267 *Anabaena* WT (Figs. 1h, Supplementary Fig. 8a). Our results thus show that CeaR expression
268 level influences *Anabaena* cell shape and suggest a role of CeaR in PG biogenesis and cell-
269 shape determination.

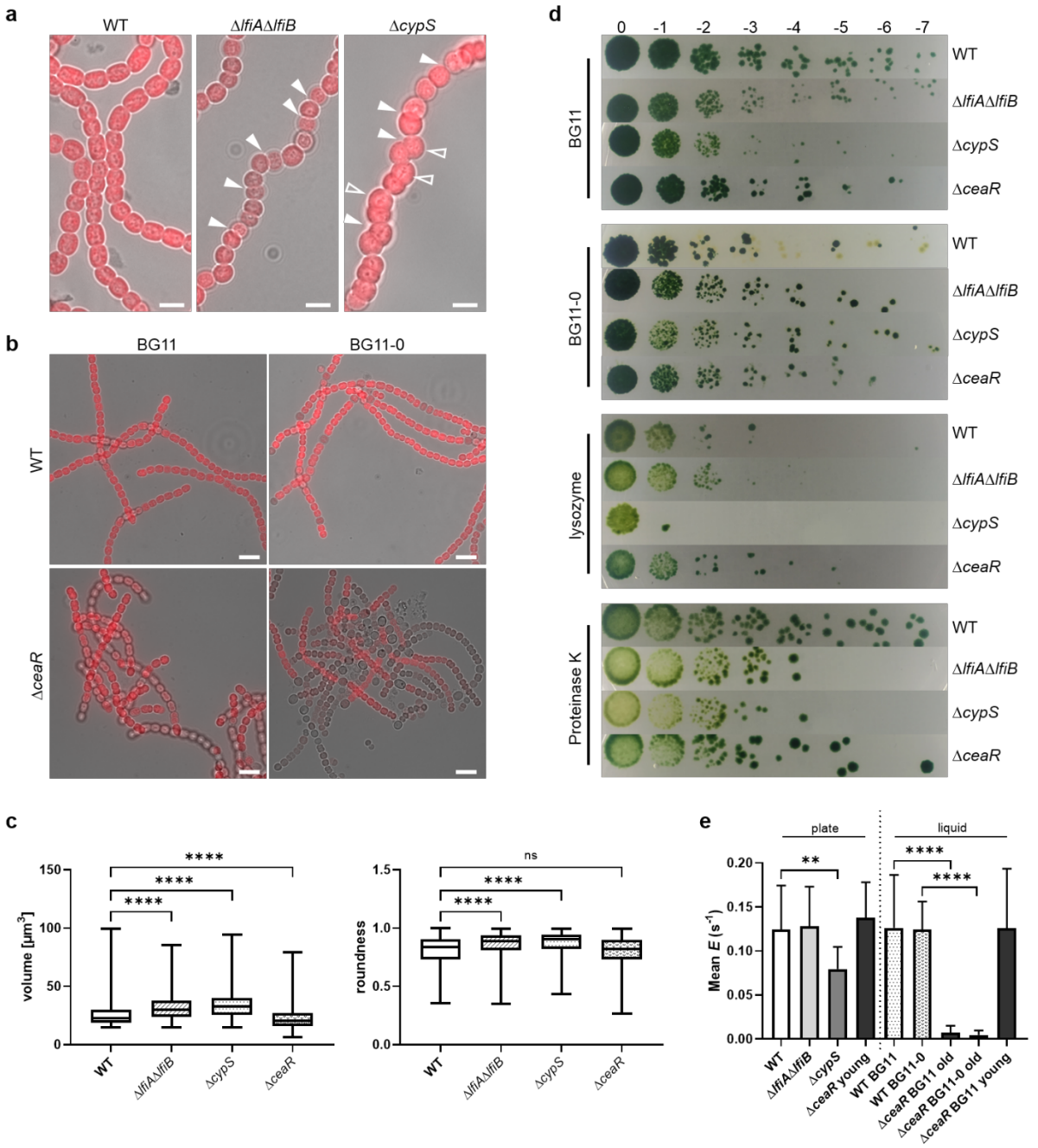

Fig. 2: *Anabaena* CCRP mutant strains reveal altered filament and cell shape phenotypes

(**a**-**b**) Merged chlorophyll autofluorescence and bright field micrographs of (**a**) *Anabaena* WT, Δ*lfiA*Δ*lfiB* and Δ*cypS* mutant strains grown on BG11 plates and (**b**) *Anabaena* WT and Δ*ceaR* mutant strain grown in BG11 and 5 d after transfer into $BG11_0$. Similar to what was observed upon transfer into $BG11_0$, reduced Δ*ceaR* filament length was also observed during prolonged cultivation on BG11 plates (Supplementary Figs. 9d and 11c). Unlike in the WT, we commonly observed bright red fluorescent filaments in the Δ*ceaR* mutant (Fig. 3d, Supplementary Fig. 9e). Ultrastructures revealed that those structures do not consist of thylakoid membranes (Supplementary Fig. 15), leaving the nature of those filaments unknown. White triangles indicate zigzagged growth and translucent triangles show swollen cells. Scale bars: (a) 5 µm and (b) 10 µm. (**c**) Cell roundness and volume of *Anabaena* WT, Δ*lfiA*Δ*lfiB*, Δ*cypS* and Δ*ceaR* mutant strains grown on BG11 plates measured with Fiji imaging software. *Anabaena* WT: n = 537; Δ*ceaR*: n = 796; Δ*lfiA*Δ*lfiB*: n = 404; Δ*ceaR*: n = 369. (**d**) *Anabaena* WT, Δ*lfiA*Δ*lfiB*, Δ*cypS* and Δ*ceaR* mutant strains were spotted onto BG11, $BG11_0$ or BG11 plates supplemented with lysozyme or Proteinase K in triplicates of serial dilutions of factor 10 and grown until no further colonies arose in the highest dilution (n = 2). (**e**) Mean exchange coefficients (*E*) of fluorescence recovery after photobleaching (FRAP) experiments from calcein-labelled *Anabaena* WT and CCRP mutant strains. Liquid *Anabaena* WT and Δ*ceaR* cultures were grown in BG11 and

286 partially transferred to $BG11_0$ 1 d prior labelling. Plate grown *Anabaena* WT, Δ*lfiA*Δ*lfiB* and Δ*cypS* mutant strains
287 were grown on BG11 plates. Data present the number of recordings of bleached cells (n). *Anabaena* WT BG11
288 plate: n = 21; *Anabaena* WT liquid BG11: n = 10; *Anabaena* WT liquid $BG11_0$: n = 11; Δ*cypS*: n= 23; Δ*lfiA*Δ*lfiB*: n =
289 17; Δ*ceaR* liquid BG11: n = 16; Δ*ceaR* liquid $BG11_0$: n = 6. Representative FRAP micrographs are shown in
290 Supplementary Fig. 12. Representative fluorescence recovery curves are shown in Supplementary Fig. 13. Values
291 indicated with * are significantly different from the WT. *: $P < 0.05$, **: $P < 0.01$, ***: $P < 0.001$, ****: $P < 0.0001$. ns
292 indicates no significant difference to the WT (using one-way ANOVA with Dunnett's multiple comparison test).

293 The round and swollen cell phenotypes of the Δ*cypS* and Δ*lfiA*Δ*lfiB* mutant strains are
294 indicative of an impairment in cell wall integrity and/or defects in PG biogenesis as well as an
295 elevated sensitivity to turgor pressure[41,42,64,65]. Similarly, the resemblance of the phenotypes of
296 CeaR with MreB raised the hypothesis that the four investigated CCRPs could be involved in
297 cell wall integrity or the PG biogenesis machinery. Consequently, we tested the sensitivity of
298 the deletion strains to cell wall degrading enzymes and osmotic stressors. Our results show
299 that the Δ*cypS* mutant had elevated sensitivity to lysozyme, and both, the Δ*cypS* and Δ*lfiA*Δ*lfiB*
300 mutant strains, were slightly more sensitive to Proteinase K compared to the WT (Fig 2d).
301 These results suggest that both mutants have a defect in cell wall integrity. An increased
302 sensitivity to lysozyme has been previously been associated with a defect in elongasome
303 function[39], suggesting that CypS could be associated with the *Anabaena* elongasome.
304 Furthermore, Δ*cypS* and Δ*lfiA*Δ*lfiB* mutants were unable to grow in liquid culture
305 (Supplementary Fig. 10a) with Δ*cypS* mutant cells readily bursting upon transfer to liquid
306 culture (Supplementary Fig. 10b), hinting for an elevated sensitivity to fluid shear stress or
307 turgor pressure. In contrast, the Δ*ceaR* mutant was unaffected by the presence of cell wall
308 stressors (Fig. 2d) and grew well in BG11 growth medium (Fig. 2b). However, upon nitrogen
309 stepdown (i.e., transfer into $BG11_0$), the Δ*ceaR* mutant strain readily fragmented into shorter
310 filaments that aggregated into large-scale cell clumps (Fig. 2b, Supplementary Figs. 10a and
311 11d,e). Cells in those clumps also gradually lost their chlorophyll auto-fluorescence signal (an
312 indicator for a decreased viability) and ultimately died within a few days (Fig 2b, Supplementary
313 Fig. 11a,b,d). This shows that filament viability in the Δ*ceaR* mutant is impaired under
314 diazotrophic conditions. The defect in filament viability could be complemented with pRL25C
315 carrying P_{ceaR}::*ceaR* or P_{ceaR}::*ceaR-gfp* (Supplementary Fig. 11b,d,e).

316 Previous studies showed that mutants of genes involved in intercellular communication
317 in *Anabaena* show a similar, albeit more pronounced fragmentation phenotype (producing
318 unicellular forms) when transferred from BG11 to $BG11_0$ due to the loss of diazotrophy[46,48–50].
319 Proper nutrient exchange through septal junctions is essential for *Anabaena* viability,
320 especially under diazotrophic growth[37]. Consequently, we investigated the level of intercellular
321 communication using FRAP experiments of calcein stained *Anabaena* CCRP mutant strains.
322 Our results show that the Δ*lfiA*Δ*lfiB* mutant is not impaired in intercellular solute diffusion while
323 diffusion is reduced in the Δ*cypS* mutant and virtually absent in the Δ*ceaR* mutant grown in
324 liquid medium (Fig. 2e, Supplementary Figs. 12 and 13). Notably, solute diffusion was not
325 decreased in young Δ*ceaR* mutant cells (i.e. cultures up to 10 days; Fig. 2e), indicating the
326 effect of *ceaR* knockout on cell-cell communication depends on the culture age. This culture
327 age effect on cell-cell communication is also reflected by the different Δ*ceaR* mutant filament
328 length in younger and older (i.e. 3-4 weeks old) cultures. While young Δ*ceaR* mutant filaments
329 showed normal filament lengths, filaments from older Δ*ceaR* mutant cultures were shortened
330 (Supplementary Figs. 9d,e and 11c). To further investigate the underlying cause for the
331 impaired cell-cell communication, we isolated sacculi and observed that the Δ*ceaR* and the
332 Δ*cypS* mutant partially contained significantly larger septa with decreased nanopore counts
333 compared to the WT. We suggest that the larger septa may be responsible for the decrease in
334 solute diffusion (Supplementary Fig. 14). In addition, we observed that some nanopores in the
335 Δ*ceaR* mutant strain were large and irregular (Supplementary Fig. 14), which as well could
336 contribute to the decreased efficiency in solute diffusion.

337 ***Anabaena* CCRPs are involved in MreB function and localization**

338 The swollen cell phenotype of *Anabaena* Δ*mreB* mutant strain has been previously reported
339 to have no effect on intracellular structures[39]. To assess whether the altered cell and filament
340 shape of *Anabaena* CCRP mutant strains has any effect on intracellular arrangements, we
341 compared ultrathin sections of *Anabaena* WT and CCRP mutant strains. Except for Δ*ceaR*
342 mutant cells that contain a red fluorescent filament (Fig. 3d; Supplementary Figs. 9e and 15),

343 intercellular ultrastructures of the mutant strains were largely unaffected regardless of their
344 impact on filament viability and shape (Supplementary Fig. 15). The red fluorescent filaments
345 are not assemblies of thylakoid membranes but appear to be void entities, whose nature is yet
346 to be identified. However, the observed cell wall defects and altered cell shape phenotypes
347 indicates that CypS, LfiA/LfiB and CeaR function is related to PG biogenesis, possibly through
348 association with FtsZ or MreB. To test for a link with the FtsZ-driven divisome, we visualized
349 Z-ring placement in *Anabaena* WT and in each of the mutant strains by immunofluorescence.
350 No alterations in Z-ring placement were observed, indicating that Z-ring formation is unaffected
351 in the mutant strains (Supplementary Fig. 16). To test for an association with the elongasome,
352 we compared the MreB localization in cells ectopically expressing a functional GFP-MreB
353 fusion[39] from P_{petE}. Notably, unlike in the previously reported P_{petE}::GFP-MreBCD
354 overexpression strain[39], we never saw polar aggregate-like structures in our GFP-MreB-
355 expressing strain (Fig. 3a). This suggests that the previously observed aggregations in the
356 GFP-MreBCD strain[39] are specific to the *mre* operon overexpression rather than the
357 overexpression of MreB only. In contrast, we observed short GFP-MreB filaments and
358 occasionally GFP-MreB patches within the cells (Fig. 3a). When grown on $BG11_0$ plates, which
359 we found to increase P_{petE}-driven expression levels, more pronounced GFP-MreB filaments
360 were visible, readily spanning the whole cells (Supplementary Fig. 17). Expression of GFP-
361 MreB in the mutant strains revealed considerable alterations of GFP-MreB localization (Fig
362 3a). Even though GFP-MreB filaments were present in the Δ*lfiA*Δ*lfiB* mutant strain, we only
363 detected those in non-rounded cells that seemingly had a WT-like phenotype (Fig 3b inlay; 245
364 (24%) of 1040 cells counted), whereas in rounded cells of zigzagged filaments, the GFP-MreB
365 signals were restricted to the cell poles (Fig. 3b; 795 (76%) of 1040 counted cells). These
366 observations suggest that LfiA/LfiB are important for proper localization of MreB. Unlike
367 LfiA/LfiB, CypS seems to have no direct influence on GFP-MreB localization, as indicated by
368 the WT-like localization of GFP-MreB in the Δ*cypS* mutant strain (Fig. 3c). In contrast, in the
369 Δ*ceaR* mutant, GFP-MreB only localized as aggregate-like patches and never formed
370 filamentous strings as seen in the WT (Fig. 3d). This suggests that CeaR is important for proper

371 MreB polymerization. The negative effect of the absence of CeaR on GFP-MreB function and
372 localization became even more evident during growth in liquid culture. There, P_{petE}-driven
373 expression of GFP-MreB led to a prominent rounding of Δ*ceaR* mutant cells and a zigzagged
374 filament shape (Fig. 3d). Despite being expressed from the P_{petE}, GFP-MreB signal intensity
375 was strongly elevated in these cells, which suggests a role of CeaR in MreB turnover
376 regulation. The induced cell rounding of the Δ*ceaR* mutant upon GFP-MreB expression argues
377 for a defect in proper MreB function as the rounded phenotype resembles the previously
378 described Δ*mreB* mutant phenotype[39]. Similarly, the swollen cell phenotype of *Anabaena* cells
379 expressing CeaR-GFP (Fig. 1h, Supplementary Fig. 8a) is reminiscent of the enlarged cells
380 observed upon GFP-MreBCD overexpression[39]. An association of CeaR with MreB is further
381 reinforced by a banded and helical-like assembly of CeaR-GFP in *E. coli* (Supplementary Fig.
382 8b), resembling the localization of YFP-MreB in *E. coli*[66]. Thus, our observations suggest that
383 CeaR is involved in longitudinal PG synthesis by affecting MreB localization and function.

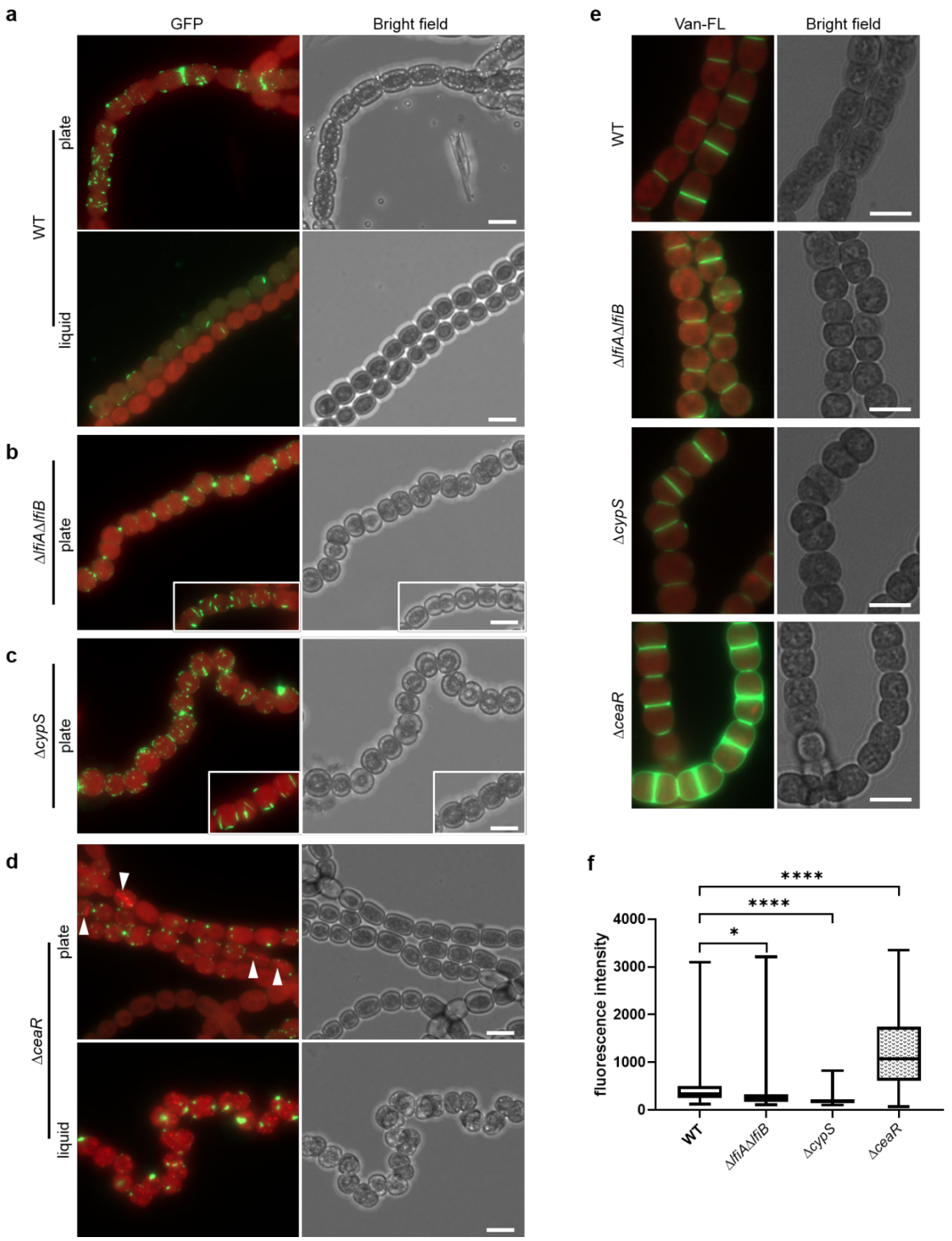

Fig. 3: CCRPs affect MreB localization and PG biogenesis

(**a**-**d**) Merged GFP fluorescence and chlorophyll autofluorescence and bright field micrographs of *Anabaena* WT, Δ*lfiA*Δ*lfiB*, Δ*cypS* and Δ*ceaR* mutant strains expressing GFP-MreB from P_{petE}. Cells were either grown on BG11 plates or in BG11 liquid medium prior visualization. White triangles indicate red fluorescent filaments within Δ*ceaR* mutant cells. Exposure time for GFP fluorescence excitation was 70 ms except for 14 ms in the Δ*ceaR* mutant grown in liquid BG11. Consequently, despite being expressed from the non-native P_{petE}, absence of CeaR detrimentally affects GFP-MreB localization and turnover. (**e**) Merged BODIPY™ FL Vancomycin (Van-FL) fluorescence and chlorophyll autofluorescence and bright field micrographs of *Anabaena* WT, Δ*lfiA*Δ*lfiB*, Δ*cypS* and

393 Δ*ceaR* mutant strains stained with 5 µg ml^{-1} Van-FL. As a result of the low Van-FL staining and for better visibility,
394 Van-FL fluorescence intensity in Δ*lfiA*Δ*lfiB* and Δ*cypS* mutants was artificially increased about twofold after image
395 acquisition. Unlike in the WT and the other two mutants, Δ*ceaR* mutant cells show longitudinal Van-FL staining,
396 indicating an altered PG biogenesis activity or localization of enzymes involved in PG biogenesis. (**f**) Analysis of the
397 arithmetic mean fluorescence intensities of cells from Fig. 3e. For all measurements, Van-FL fluorescence intensity
398 from cell septa was recorded using 130 ms exposure time from an area of 3.52 $µm^2$. Sample size (n) was 200
399 stainings for each strain. Values indicated with * are significantly different from the WT. *: $P < 0.05$, **: $P < 0.01$, ***:
400 $P < 0.001$, ****: $P < 0.0001$. ns indicates no significant different to the WT (using one-way ANOVA with Dunnett's
401 multiple comparison test). Scale bars: 5 µm.

402 **PG biogenesis is altered in *Anabaena* CCRP mutants**

403 To further assess the function of *Anabaena* CCRPs in MreB and elongasome-driven PG
404 turnover, we stained active sites of PG synthesis by fluorescently labeled vancomycin
405 (Van-FL). This revealed alterations in the PG remodeling between WT and CCRP mutant
406 strains (Fig. 3e,f). While Δ*lfiA*Δ*lfiB* and Δ*cypS* mutants showed a similar Van-FL staining pattern
407 compared to the WT, both mutants revealed a significantly reduced staining intensity (Fig 3e,f).
408 Hence, it is likely that CypS and LfiA/LfiB are linked to PG biogenesis. Unlike the other two
409 mutants, the Δ*ceaR* mutant is characterized by an increased mean intensity of Van-FL staining
410 that is observed not only in the septal wall, as in the WT, but also in the lateral cell wall (Fig.
411 3e). Consequently, we suggest that CeaR acts as a regulator PG biogenesis and/or localization
412 of the PG biogenesis machinery. This is in agreement with the altered expression and
413 localization pattern of GFP-MreB in the Δ*ceaR* mutant (Fig. 3d). The suggested role of the four
414 CCRPs in PG turnover is furthermore in agreement with the observed swollen cell phenotype
415 in the Δ*cypS* and Δ*lfiA*Δ*lfiB* mutant and with the altered MreB localization in the mutant strains.
416 Since we observed that CCRP mutants affect cell wall integrity, we next examined the
417 heterocyst-development in the CCRP mutants. Heterocysts contain an extra cell envelope with
418 specific heterocyst glycolipids and envelope polysaccharides[37]. Therefore, we cultivated the
419 CCRP mutant strains on $BG11_0$ plates and inspected heterocyst-formation and staining pattern
420 with alcian blue, a dye that specifically binds to the heterocysts polysaccharide sheet. Our
421 results so far did not reveal an observable defect in heterocyst-development in any of the
422 mutants (Supplementary Fig. 18).

423 ***Anabaena* CCRPs have the capacity to form an interconnected network and interact with**
424 **SepJ and MreB**

425 As our *Anabaena* CCRP mutant strains displayed similar phenotypes and the four *Anabaena*
426 CCRPs were all linked to MreB function and localization as well PG biogenesis, we next
427 investigated whether the four proteins interact with each other and with other known
428 morphological determinants in *Anabaena*. Using bacterial two hybrid assays, we found that all
429 of our four CCRPs were able to self-interact (Fig 4a). Additionally, all four CCRPs could cross-
430 interact with each other (Fig. 4a) and we found that LfiA, LfiB and CeaR but not CypS,
431 interacted with MreB. Additionally, CeaR weakly interacts with FtsZ (Fig. 4a, Supplementary
432 Fig. 18), which is in agreement with the Z-ring-like *in vivo* localization of CeaR-GFP (Fig. 1h,
433 Supplementary Fig. 8a). Furthermore, all proteins were identified as interaction partners of the
434 septal protein SepJ, but not with FraC and FraD (Fig. 4a, Supplementary Fig. 19), two other
435 septal junction proteins[45]. Since coiled-coil motifs are well-known protein-protein interaction
436 domains[67–69], they are putatively prone for false-positive results in the interaction assays.
437 Indeed, interactions of coiled-coil containing proteins are usually considered to be specific[67,70–
438 76]; nonetheless, we further tested the interaction specificity of our four CCRPs – Cyps, LfiA,
439 LfiB and CeaR – in the bacterial two-hybrid assay by including Alr3364, another *Anabaena*
440 CCRP (Supplementary Fig. 1), as a negative control in our screening. Our results show that
441 Alr3364 only weakly interacted (< 500 Miller Units/mg LacZ) with LfiA and LfiB and failed to
442 interact with CypS and CeaR (Supplementary Fig. 20). This confirms that the strong
443 interactions (all > 500 Miller Units/mg LacZ) observed between CypS, LfiA, LfiB and CeaR are
444 indeed specific interactions. We attempted to further confirm our interaction results with affinity
445 co-elution experiments. However, we found that Ni-NTA-bound *Anabaena* CCRPs readily
446 precipitated upon transfer from denaturing to native buffer conditions, precluding further co-
447 elution studies. Additionally, we observed that non-denaturing conditions failed to purify
448 overexpressed CCRPs from *E. coli*, confirming their inherent insoluble nature, a property
449 known to eukaryotic IFs[54,77]. Instead, we surveyed for further interaction partners in *Anabaena*
450 WT cells expressing CeaR-GFP or LfiA-GFP by co-immunoprecipitation experiments

451 (Supplementary Fig. 21) and analyzed co-precipitated proteins by LC-MS/MS analytics
452 (Supplementary File 3). This analysis confirmed that LfiA and LfiB interact with each other *in*
453 *vivo* and validated the association of CeaR and LfiA with MreB in *Anabaena* (Supplementary
454 Fig. 21c). Corroborating a role of CeaR in PG biogenesis and MreB function, CeaR was also
455 found to be associated with three penicillin binding proteins (Supplementary Fig. 21c), which
456 are known regulators of PG synthesis and are part of the elongasome[78,79]. Furthermore, both,
457 CeaR and LfiA, co-precipitated ParA, and CeaR was additionally found to be associated with
458 MinD (Supplementary Fig. 21c). Both ParA and MinD belong to a protein family of Walker-A-
459 type ATPases and mediate plasmid and chromosome segregation[77,80,81]. To test for a similar
460 function in our CCRPs, we compared the DNA distribution among the CCRP mutant cells as
461 measured by distribution of 4′,6-Diamidin-2-phenylindol (DAPI) staining intensity. For that, we
462 calculated the width of the DAPI focal area as the range of DAPI staining around the maximum
463 intensity focus (±10 grey intensity in arbitrary units). This revealed that the staining focal area
464 size was significantly different among the four tested strains ($P=3.14x10^{-41}$, using Kruskal-
465 wallis). Post-hoc comparison showed that the focal area size in the *ΔceaR* mutant was larger
466 than the others, and the area size in *Anabaena* WT was not significantly different than Δ*cypS*.
467 The DAPI signal observed in the Δ*lfiA*Δ*lfiB* mutant appears as the most condensed, and
468 indeed, the Δ*lfiA*Δ*lfiB* mutant focal DAPI area was smallest in comparison to the other strains
469 (alpha=0.05, using Tukey test; Supplementary Fig. 22ab). Unlike the *ΔceaR* mutant and the
470 WT, DAPI signals in the Δ*lfiA*Δ*lfiB* and Δ*cypS* mutant strains were also observed between two
471 neighboring cells (Supplementary Fig 21a), indicating that DNA distribution is not properly
472 executed during cell division in those strains.

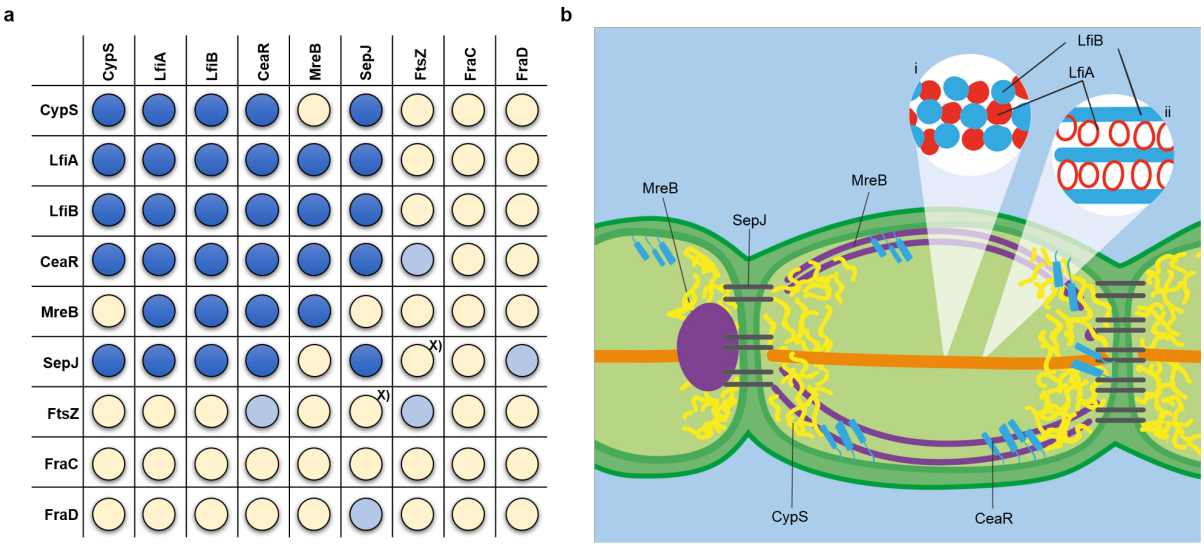

Fig. 4: *Anabaena* CCRPs form a putative cytoskeletal network that links the septal junction protein SepJ and the MreB cytoskeleton

(**a**) Graphical visualization of beta-galactosidase assay results of *E. coli* BTH101 cells co-expressing indicated translational fusion constructs of *Anabaena* proteins with the T18 and T25 subunit, investigating all possible pair-wise combinations. Corresponding data are shown in Supplementary Fig. 19. Blue spots indicate strong verified interactions (>500 Miller units mg^{-1}) while light blue dots mark moderate interactions (< 500 Miller units mg^{-1}) and no interactions are depicted with yellow-colored dots. Dots marked with "X" were previously reported by Ramos-León *et al.* (2015)[82]. (**b**) A model for an interconnected cytoskeletal network in *Anabaena*. Septal junctions, comprised of, among others, SepJ (grey), are directly connected to the CypS polar scaffold (yellow) that provides anchoring sites for the LfiA/B filament (orange). (i) Similar to α-tubulin and β-tubulin, the LfiA/B heteropolymer could be composed of alternating LfiA (red) and LfiB (blue) monomers. (ii) However, based on *in vivo* localizations, *in vitro* polymerization, domain predictions and structural similarities to eukaryotic plectin, it is more likely that LfiA acts as a cytolinker protein for LfiB, enabling proper polymerization. The LfiA/B filament spans through the cells, anchoring to CypS but never passes through the septal junctions. The identified *Anabaena* filament stabilizing effect of LfiA/B could then be relayed to the neighboring cells via interactions with CypS, CeaR (light blue), SepJ and MreB (purple). MreB localization is adapted from Hu *et al.* (2007)[39] in which MreB plugs accumulate at the septa (indicated in the dividing cell on the left) but also forms cell-traversing filaments (right cell). MreB activity and localization is dependent on CeaR. Furthermore, according to FRAP results, it is conceivable that CeaR regulates *Anabaena* filament viability through interaction with SepJ.

Discussion

Here we provide evidence for the capacity of three *Anabaena* CCRPs - CypS, LfiA together with LfiB - to form IF-like polymers *in vitro* and *in vivo*. The characterization of multiple CCRPs in our study was possible thanks to the easy to use and comparably high-throughput approach for the screening of novel filament-forming CCRPs using the NHS-Fluorescein dye. Our approach supplies an alternative for the examination of protein-filament formation by electron microscopy; instead it allows for a simplified protocol for the detection of protein filaments using fluorescence microscopy. In accordance with previous studies of eukaryotic IF proteins[83,84], *Anabaena* CCRPs N-terminally tagged with a YFP-tag failed to produce a discernible

502 structures/fluorescence signal. This suggests that the N-terminus is essential for localization
503 or function of the *Anabaena* CCRPs and supports our observations of CypS and LfiA/LfiB as
504 *bona fide* prokaryotic CCRPs with IF-like function. While the previously described prokaryotic
505 IF-like proteins form homopolymers[15,24,32,52,85], LfiA and LfiB assemble into a heteropolymer
506 comprising the two proteins. Furthermore, LfiA and LfiB have the capacity to co-polymerize in
507 a heterologous *E. coli* system, similarly to other known CCRPs such as Scc from *Leptospira*
508 *biflexa*[85] or crescentin[86,87]. We note, however, that the results from our *in vivo* experiments of
509 LfiA/LfiB co-polymerization are based on artificial expression of the two CCRPs. We
510 hypothesize that the absence of a LfiA/LfiB heteropolymer in strains expressing LfiA-GFP or
511 LfiB-GFP alone (with the WT alleles still present) may be due to a dosage-dependent effect,
512 where the presence of unequal concentration of LfiA and LfiB in the cell leads to protein
513 aggregates. Our observation of LfiA-GFP or LfiB-GFP aggregates when they were expressed
514 alone in the Δ*lfiA*Δ*lfiB* mutant strain supports the dosage effect hypothesis. Also, in our *in vitro*
515 polymerization assay, LfiA and LfiB only formed clear filamentous structures when both
516 proteins are present in equal concentrations. Furthermore, the genomic neighbourhood of LfiA
517 and LfiB suggests that the LfiA/LfiB heteropolymer formation is relying on co-translational
518 assembly (e.g., as observed for LuxA/LuxB[88]). Co-translational assembly of the WT LfiA/LfiB
519 would lead to an efficient binding of the two subunits such that the expression of one unit only
520 in excess (i.e., LfiA-GFP or LfiB-GFP) would lead to the formation of aggregates.

521 Our results demonstrate that the four CCRPs described here form an interconnected
522 cytoskeletal network in *Anabaena*. The network is likely anchored to the cell poles through the
523 interaction with the septal junction protein SepJ. Together with the cell shape-determining
524 protein MreB[89], *Anabaena* CCRPs possibly contribute to the cell shape and relay filament
525 shape-stabilizing properties to neighboring cells, thereby maintaining the linear *Anabaena*
526 filament phenotype (Fig. 4b). The interaction of *Anabaena* CCRPs with SepJ suggests that not
527 only filament integrity[46,48] but also filament shape is strongly dependent on proper septal
528 junction function and stability. Hence the four CCRPs are likely involved in filament integrity,
529 similarly to the integral membrane proteins SepJ and FraC/FraD. The *Anabaena* CCRPs might

530 constitute stabilizing platforms or scaffolds for other proteinaceous structures, similarly to the
531 stabilizing function of the eukaryotic cytoskeleton for cell-cell contacts (i.e. desmosomes)[90].
532 Notably, LfiA shares structural similarities with the spectrin repeats of plectin (Supplementary
533 Table 1), a well-described eukaryotic cytolinker protein. Plectins link the three eukaryotic
534 cytoskeletal systems (actin filaments, microtubules and IFs), thereby contributing to the
535 resistance to deformation of vertebrate cells[90,91]. They furthermore stabilize desmosomes and
536 are hence directly involved in cell-cell connection integrity[92]. An analogous cytolinker function
537 of LfiA could explain why LfiB alone did not form filaments and suggests that LfiB requires LfiA
538 as the linking protein for polymerization. Based on the structural similarity to spectrin, it is also
539 conceivable that LfiA and LfiB possess similar functions as α and β-spectrin. Together, spectrin
540 α/β-heteropolymers produce a cell shape-maintaining interconnected cytoskeletal network (the
541 so called spectre) below the plasma membrane of erythrocytes[93]. Furthermore, similar to
542 LfiA/LfiB, spectrins are directly linked to the actin cytoskeleton[90]. This link of LfiA/LfiB to the
543 actin-like MreB cytoskeleton is evident in the altered localization of GFP-MreB in the Δ*lfiA*Δ*lfiB*
544 mutant strain. The observed-PG staining pattern where PG staining was strongly elevated in
545 the Δ*ceaR* mutant strain suggests that in *Anabaena* WT, CeaR acts to (down)regulate MreB
546 or elongasome function (hence its name: cyanobacterial elongasome regulator). Although less
547 pronounced, PG staining was decreased in both *ΔcypS* and Δ*lfiA*Δ*lfiB* mutants, suggesting
548 that CypS and LfiA/LfiB could act as positive regulators of elongasome function. These
549 observations further imply an association of CypS with the elongasome, despite the failure of
550 CypS to directly interact with MreB (Fig. 4a). MreB and the elongasome are the main
551 determinants of the PG exoskeleton, which provides the cell with structural integrity and
552 resistance to turgor pressure[79,94]. Notably, both Δ*cypS* and Δ*lfiA*Δ*lfiB* mutant strains were
553 unable to grow in liquid culture, hinting for a defect in the resistance to turgor pressure. The
554 growth defect in liquid culture of the Δ*cypS* and Δ*lfiA*Δ*lfiB* mutant strains may result from
555 altered elongasome functionality due to the absence of CypS and LfiA/LfiB. The association of
556 *Anabaena* CCRPs with proper elongasome function is further supported by the elevated
557 sensitivity of the Δ*cypS* mutant strain to lysozyme, similar to the Δ*mreB* mutant strain[39]. An

558 interaction of prokaryotic IF-like proteins with MreB and PG synthesis has been previously
559 described in other bacteria. Examples are the gliding motility in *M. xanthus,* where a multi-
560 protein complex, including the IF-like CCRP AglZ and MreB was found to coordinate type A-
561 motility[25]. Similarly, the curved morphotype of *C. crescentus* is induced by crescentin, which
562 modulates PG biogenesis by exuding local mechanical forces to the cell membrane[22,56]. Thus,
563 our results are in agreement with a functional link between IF-like CCRPs and the MreB
564 cytoskeleton in bacteria.

565 The conserved combination of all four CCRPs in heterocystous cyanobacteria that form
566 linear filaments (or false branching; Fig. 1a) suggests that the linear filament formation has a
567 selective advantage. Both Δ*cypS* and Δ*lfiA*Δ*lfiB* mutants had a zigzagged phenotype and were
568 unable to grow in liquid culture. The zigzagged mutants provide more accessible surface for
569 the acting mechanical forces in liquid[95], including fluid shear stress[96], ultimately resulting in
570 forces that cannot be endured by the abnormal mutant filaments. Notably, while the selective
571 advantage of cell shape is considered to be mostly a manifestation of biotic and abiotic
572 selective factors in the cell environment[97], the selective advantage of multicellular shapes is
573 likely related to the efficiency of intercellular communication and transport[95]. Indeed, the results
574 of our FRAP experiments show that the efficiency of flow in the zigzagged Δ*cypS* mutant
575 filament is reduced. Furthermore, the Δ*ceaR* mutant failed to grow in diazotrophic conditions
576 where transport of metabolites in the filament is considered essential for *Anabaena* viability. A
577 similar observation has been made for knockout mutant strains of SepJ, FraC and FraD that
578 are essential for *Anabaena* multicellularity[46,49,50]. Additionally, the decrease in solute diffusion
579 in the Δ*ceaR* mutant strain suggests that CeaR is involved in the buildup or stabilization of the
580 septal junctions. This notion is further supported by the abnormal nanopore formation observed
581 in some Δ*ceaR* mutant septa. Our results thus suggest that CeaR is important for *Anabaena*
582 multicellularity while CypS, LfiA and LfiB serve as regulators of *Anabaena* patterned
583 multicellularity. The evolution of patterned multicellularity is considered an important step
584 towards a sustainable division of labor and the development of cell differentiation[3]. Our study

585 reveals the role of cytoskeletal proteins in the evolution and maintenance of bacterial
586 multicellular form.

587 **Acknowledgments**

588 We thank Katrin Schumann, Myriam Barz, Lisa Stuckenschneider, Lisa-Marie Philipp and
589 Claudia Menzel for their assistance in the experimental work. We thank Tanita Wein for critical
590 comments on the manuscript. FRAP experiments were done at the Facility for Imaging by Light
591 Microscopy (FILM) at Imperial College London. We thank Tine Pape for assistance with
592 graphic illustrations (funded by the cluster of excellence ''The Future Ocean'' at Kiel
593 University). The study was supported by the German science foundation (DFG) (Grant No.
594 STU513/2-1 awarded to KS). DJN was supported by the BBSRC as part of the joint NSF Ideas
595 Lab grant on 'Nitrogen: improving on nature' (grant BB/L011506/1). IM and AK were supported
596 by German science foundation (DFG) (Grant SFB766).

597 **Author contribution**

598 BLS and KS designed the study. BLS established and performed the experimental work with
599 contributions from MT and JW. CW and TD performed comparative genomics analysis. DJN
600 and AKK performed FRAP assays and AKK and IM carried out ultrathin structures and
601 nanopore analyses. AOH and AT analyzed protein samples by mass spectrometry. BLS, TD
602 and KS drafted the manuscript with contributions from all coauthors.

603 **Competing interests**

604 The authors declare no competing interests.

605 **Supplementary information**

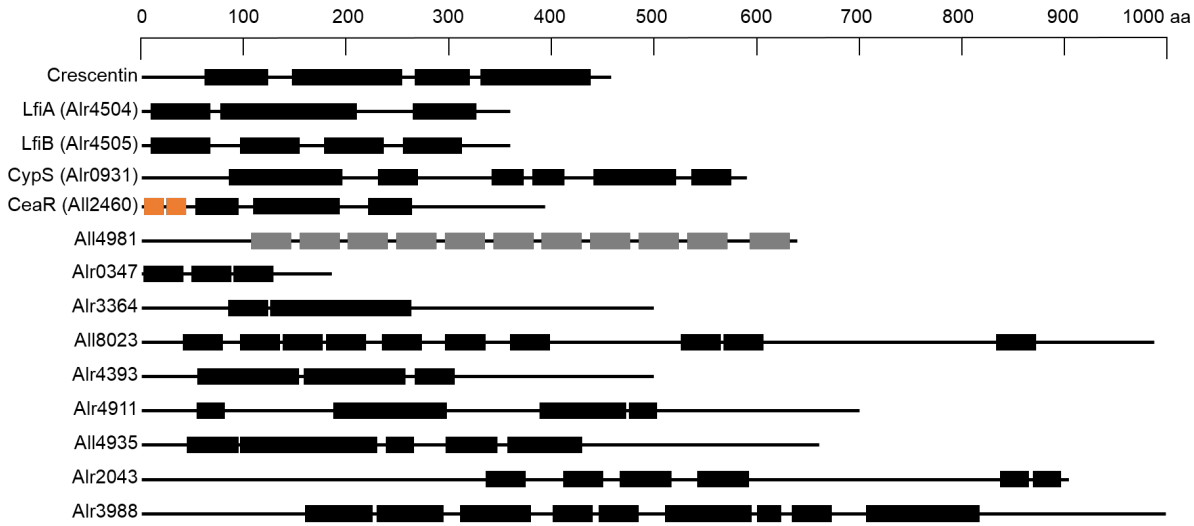

606

607 **Supplementary Fig. 1:Domain architecture of IF-like protein candidates**

608 Depiction of coiled-coil domains of protein candidates and Crescentin from *Caulobacter crescentus* based on the
609 COILS algorithm[98] with a window width of 21. The scale on top is given in amino acid residues (aa) and amino acid
610 sequences in coiled-coil conformation are depicted by black bars, transmembrane domains are shown in orange
611 bars, while non-coiled-coil sequences are represented by black lines. Tetratricopeptide repeats (TRPs) are shown
612 as grey bars. Cyanobacterial proteins are given as cyanobase locus tags.

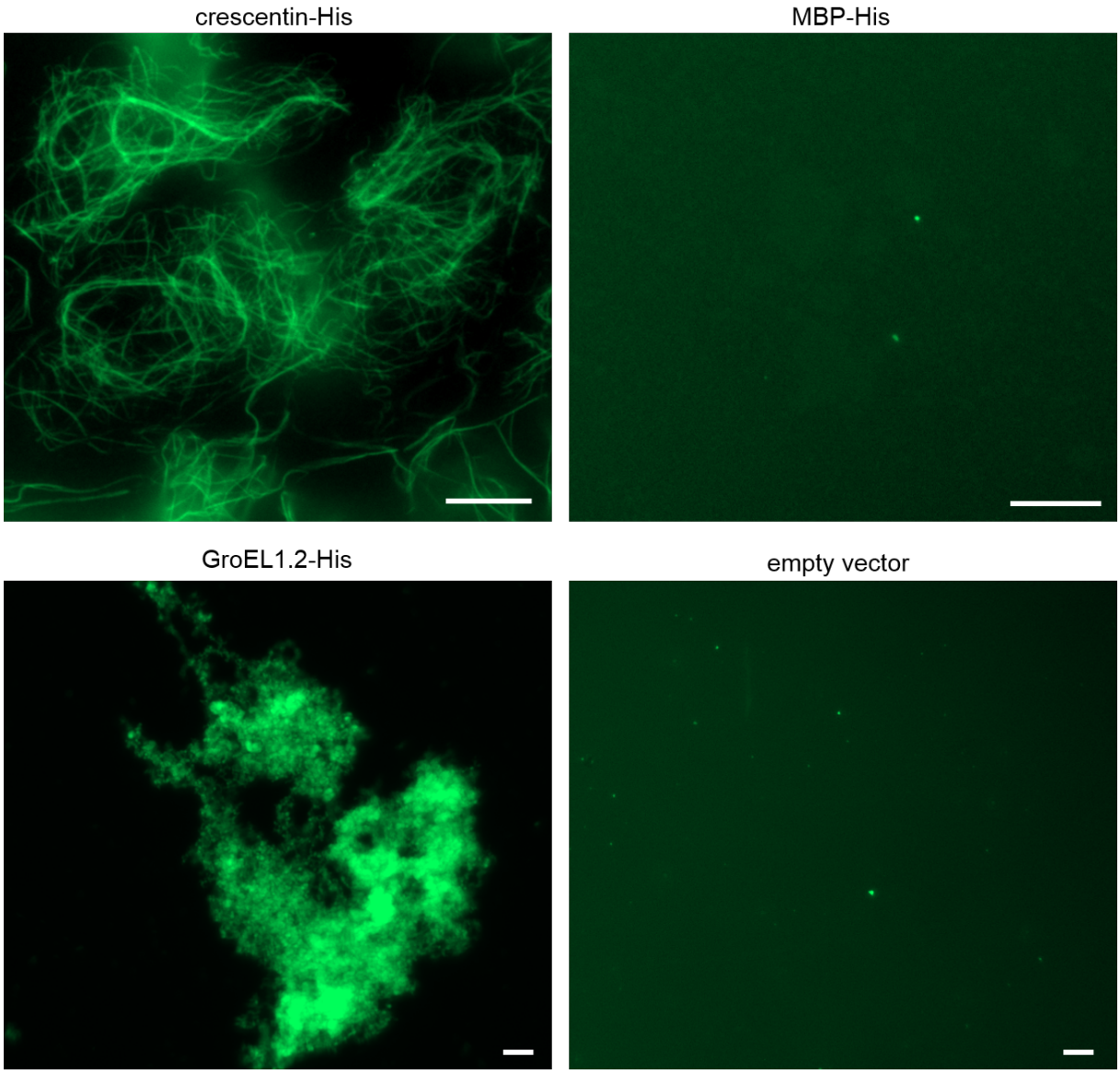

613

614 **Supplementary Fig. 2: *In vitro* polymerization assay controls**

615 NHS-fluorescein fluorescence micrographs of purified and renatured Crescentin-His, MBP-His and GroEL1.2 from
616 *Chlorogloeopsis fritschii* PCC 6912 (0.5 mg ml^{-1} each) as well as purified cell-free extracts of *E. coli* BL21 (DE3)
617 carrying empty vector (pET21a(+)) in HLB. Notably, GroEL1.2, able to self-interact[57], collapses into indistinct
618 aggregates, showing that oligomerizing proteins do not form filaments in our assay. Proteins and cell-free extracts
619 (empty vector) were dialyzed in a step-wise urea-decreasing manner and stained with an excess of NHS-
620 Fluorescein. Scale bars: 10 µm.

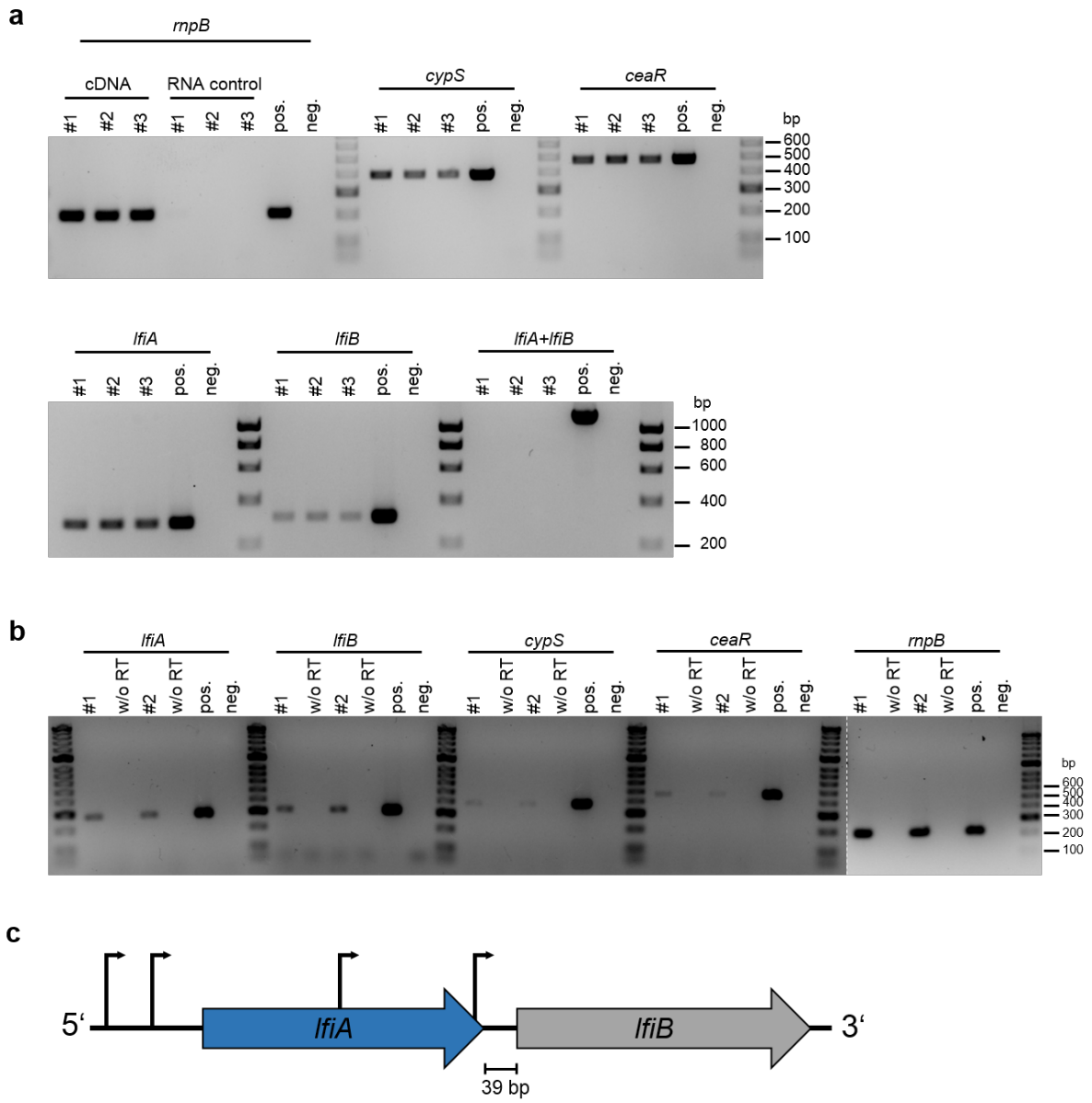

Supplementary Fig. 3: *Anabaena* CCRPs are expressed at standard growth conditions

(a,b) RT-PCR of whole RNA from *Anabaena* WT cultures grown in (a) BG11 or (b) $BG11_0$ liquid medium from (a) three or (b) two independent biological replicates. Gene transcripts were verified using internal gene primers (*rnpB*: #1/#2; *cypS*: #3/#4; *ceaR*: #5/#6; *lfiA*: #7/#8; *lfiB*: #9/#10; *lfiA* and *lfiB*: #7/#10). As negative control (neg), PCR reactions were performed with water instead of cDNA or RNA and as a positive control (pos) *Anabaena* gDNA was included. PCR fragments were resolved on a 2% agarose gel in TAE buffer. For each RT-PCR reaction, 100 ng cDNA was used. Absence of residual genomic DNA in DNase I-treated samples was verified with (a) 100 ng DNase I-treated RNA (RNA control) or (b) 100 ng DNase I-treated RNA that was subjected to cDNA synthesis reaction lacking reverse transcriptase (w/o RT). No common transcript for *lfiA* with *lfiB* was detected, suggesting that both proteins are not encoded in an operon.

(c) Depiction of the genomic environment of *lfiA* (blue) and *lfiB* (grey) within the *Anabaena* genome and their respective *in silico* predicted promoters depicted by black arrows (as predicted by BPROM[61]). Promoters of *lfiA* are predicted to reside 204 bp and 543 bp upstream of the open reading frame (ORF) and promoters of *lfiB* are located 22 bp and 450 bp upstream of the ORF, thereby residing within the *lfiA* ORF.

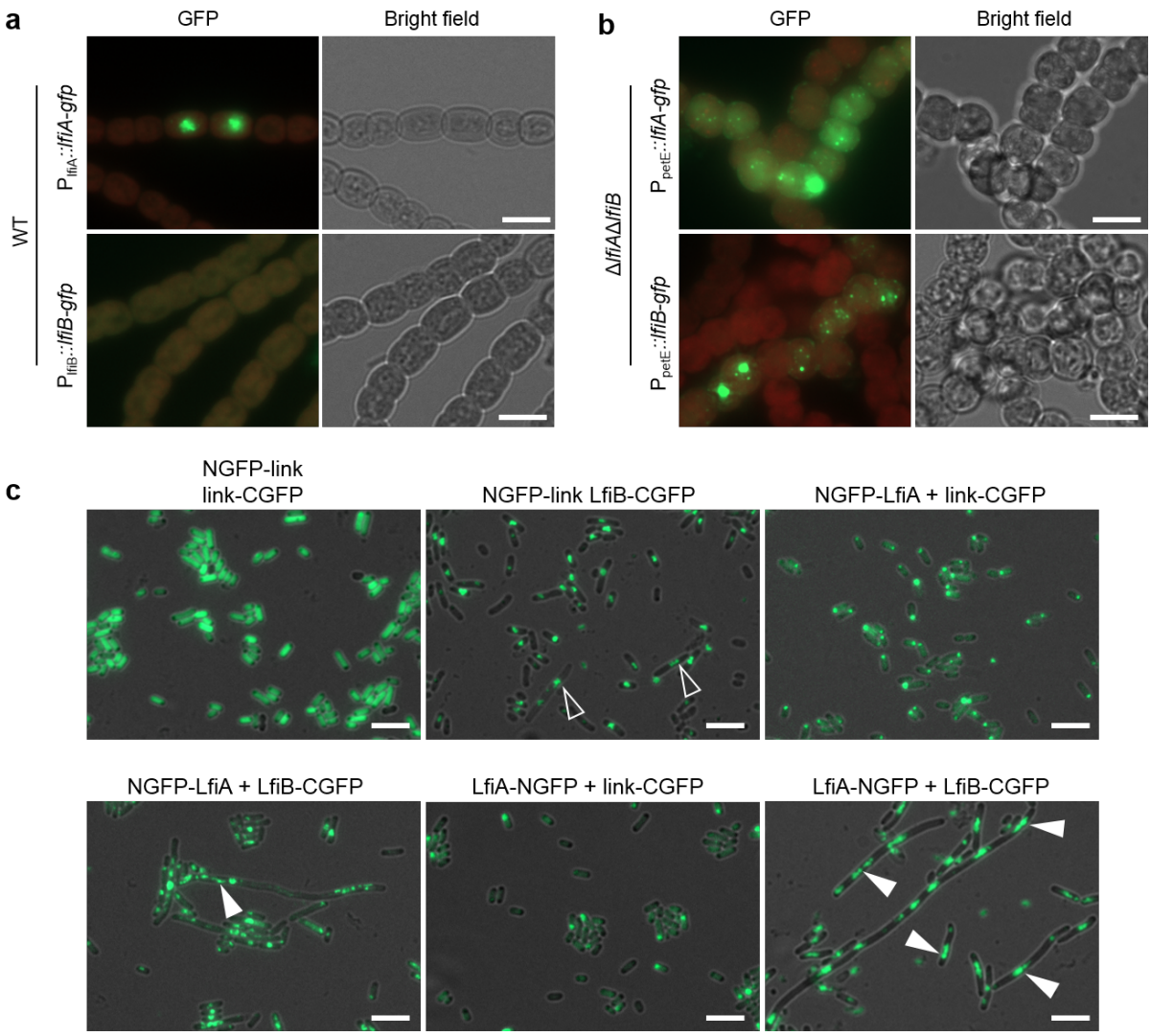

Supplementary Fig. 4: Heterologous expression of LfiA and LfiB

(a) Merged GFP fluorescence and chlorophyll autofluorescence (red) and bright field micrographs of *Anabaena* WT cells expressing LfiA-GFP or LfiB-GFP from P_{lfiA} and P_{lfiB}. No expression of LfiB-GFP is detectable from P_{lfiB} while expression of LfiA-GFP from P_{lfiA} leads to similar patchy clumps within the cells as observed from P_{petE} in Fig. 1d. Scale bars: 5 µm.

(b) Merged GFP fluorescence and chlorophyll autofluorescence and bright field micrographs of Δ*lfiA*Δ*lfiB* mutant strain expressing LfiA-GFP or LfiB-GFP from P_{petE}. Cells were grown on BG11 growth plates. For expression of LfiA-GFP, BG11 plates were supplemented with 1 µM $CuSO_4$. This experiment shows that LfiA-GFP and LfiB-GFP from P_{petE} (Fig. 1d) expression and localization in *Anabaena* WT is not affected by native LfiA or LfiB present in the WT background. Scale bars: 5 µm.

(c) Detection of protein-protein interactions with the GFP-fragment reassembly assay[99]. Merged GFP fluorescence and bright field micrographs of *E. coli* BL21(DE3) cells co-expressing NGFP-link (empty pET11a-link-NGFP) and -link-CGFP (empty pMRBAD-link-CGFP), NGFP-link and LfiB-CGFP, NGFP-LfiA and link-CGFP, NGFP-LfiA and LfiB-CGFP, LfiA-NGFP and link-CGFP or LfiA-NGFP and LfiB-CGFP. Cells were grown to an OD_{600} of 0.5, induced with 0.2% L-arabinose and 0.05 mM IPTG and incubated for 48 h at 20 °C. Transparent triangles point to structures resembling LfiB-His *in vitro* polymers. White triangles indicate FilP-GFP-like[32] filamentous structures that resemble structures indicated with translucent triangles but span longer distances. Co-expression of both, LfiA and LfiB leads to an elongated cell phenotype. FilP-like structures and elongated cells can already be seen upon co-expression of NGFP-LfiA with LfiB-CGFP but only upon co-expression of LfiA and LfiB with C-terminal GFP-fragments leads to a clear filamentous cell phenotype and abundant intracellular filamentous structures. This suggests that the N-terminus is important for heteropolymerization. Scale bars: 5 µm.

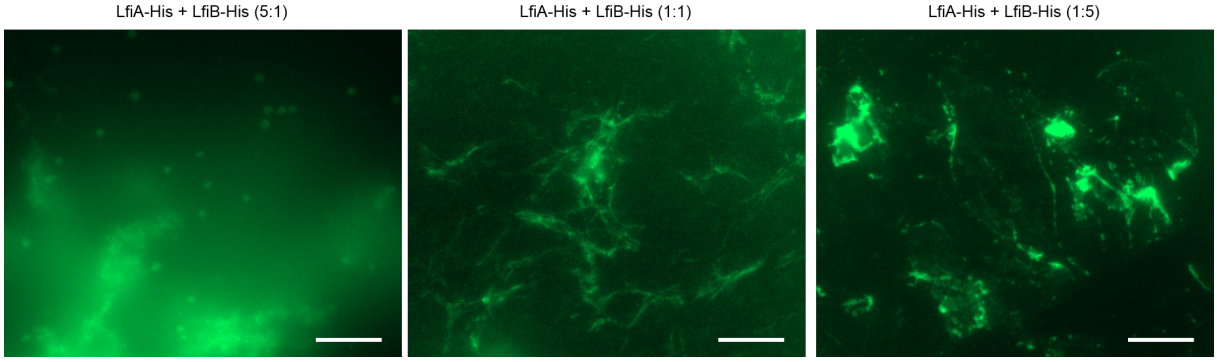

Supplementary Fig. 5: Co-polymerization of LfiA and LfiB is dosage-dependent

NHS-fluorescein micrographs of purified and co-renatured LfiA-His and LfiB-His in HLB. LfiA-His and LfiB-His were combined in different ratios, either with a fivefold excess of LfiA-His (left image; corresponding to 0.25 mg ml^{-1} LfiA-His and 0.05 mg ml^{-1} LfiB-His), a fivefold excess of LfiB-His (right image; corresponding to 0.25 mg ml^{-1} LfiB-His and 0.05 mg ml^{-1} LfiA-His) or an equal concentration of LfiA-His and LfiB-His (central image; 0.25 mg ml^{-1} each). Proteins were dialyzed in a stepwise urea-decreasing manner and stained with an excess of NHS-Fluorescein. Fine heteropolymers only form when equal concentrations of LfiA-His and LfiB-His are present. In concert with the partial self-polymerization capacity of LfiB-His (Fig. 1b), certain filamentous structures are also detected in the LfiB-His excess samples. However, most protein still precipitated under those conditions. Scale bars: 10 µm.

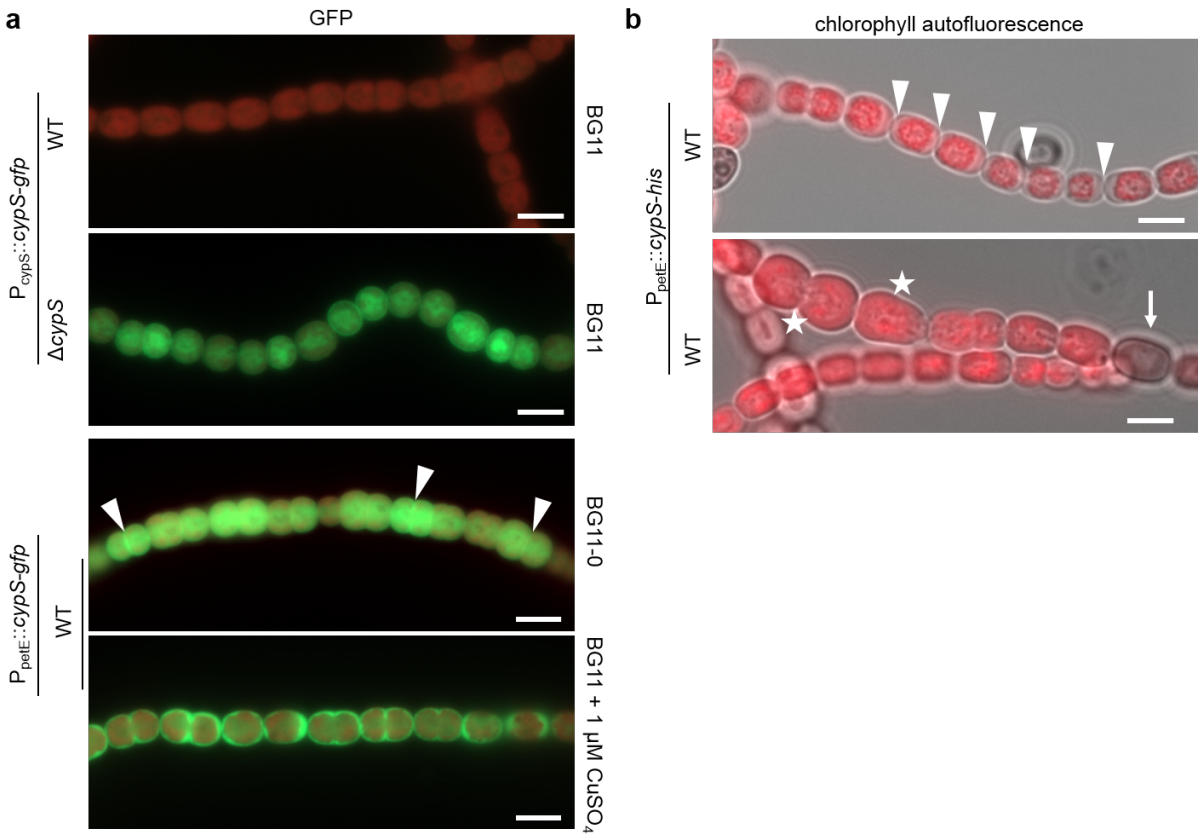

669

670 **Supplementary Fig. 6: CypS *in vivo* localization is tag orientation-dependent**

671 (a) Merged GFP fluorescence and chlorophyll autofluorescence micrographs of *Anabaena* WT and Δ*cypS* mutant
672 strain expressing CypS-GFP from P_{petE} or P_{cypS}. Strains carrying P_{cypS}::*cypS-gfp* were grown in BG11, while the
673 strains carrying P_{petE}::*cyps-gfp* are grown in indicated media with or without $CuSO_4$ supplementation. White triangles
674 indicate membrane localization, which is most pronounced in dividing cells. Further induction of protein expression
675 shows polar localization of CypS-GFP, similar to CypS-His. In the presence of native *cypS* (i.e. *Anabaena* WT), no
676 CypS-GFP expression was detected from P_{cyps}, indicating that CypS dosage is tightly controlled in the WT. Control
677 is likely exerted at the transcriptional level as overexpression from P_{petE} still produces detectable protein in the WT
678 background. Scale bars: 5 µm.

679 (b) Merged bright field and chlorophyll autofluorescence micrographs of *Anabaena* WT cells expressing CypS-His
680 from P_{petE} grown in $BG11_0$ supplemented with 0.25 µM $CuSO_4$ (upper image) or with 2.5 µM $CuSO_4$ for 2 d (lower
681 image). White triangles mark cell septa with the most prominent retraction of chlorophyll signal away from the poles.
682 White stars indicate swollen cells. White arrow points to a heterocyst. Note that the areas devoid of chlorophyll
683 signal are occupied by CypS-His plugs (Fig. 1g), suggesting that CypS forms a dense proteinaceous meshwork at
684 the cell poles. Scale bars: 5 µm.

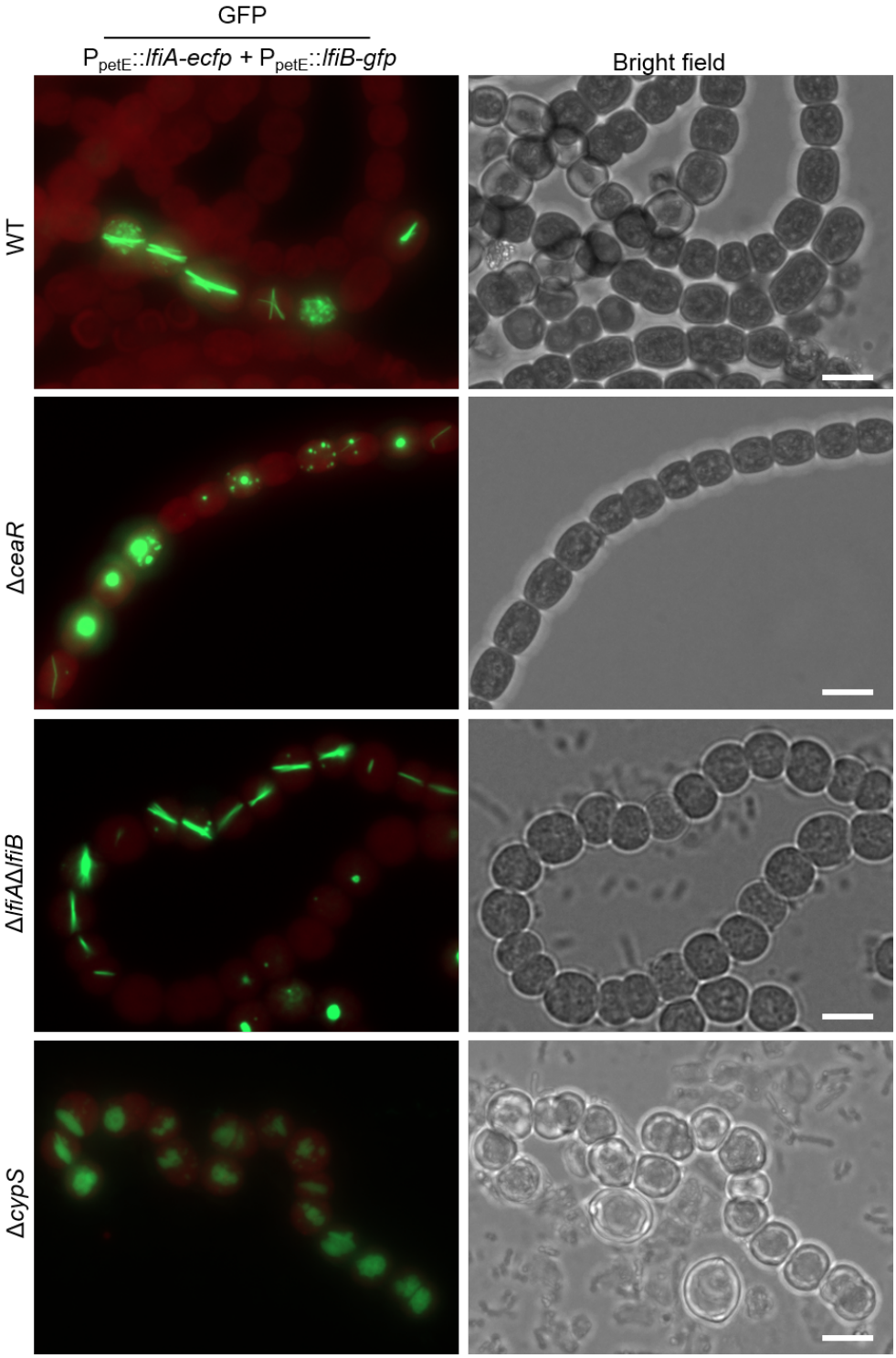

Supplementary Fig. 7: *Anabaena* CCRPs affect LfiA/B *in vivo* localization

Mergend GFP-fluorescence and chlorophyll autofluorescence and bright field micrographs of *Anabaena* WT and *Anabaena* mutant strains co-expressing LfiA-eCFP and LfiB-GFP from P_{petE}. First, second and fourth images are maximum intensity projections of a Z-stack. Localization of the LfiA/B filament is slightly altered in the Δ*ceaR* mutant strain and fully deranged in the Δ*cypS* mutant strain. This suggests that CypS is involved in LfiA/B polar attachment, possibly by providing a proteinaceous scaffold for LfiA/B anchorage. Also, Δ*cypS* mutant strain expressing LfiA/B showed a decrease in filament viability. Colonies arose upon transformation with the LfiA/B-expressing construct but did not grow upon re-streaking on fresh plates. Lack of fluorescence signal in some of the depicted cells is likely due to the phenotypic variation of copy numbers of the pRL25C plasmid in different cells within an *Anabaena* filament[100]. Scale bars: 5 µm.

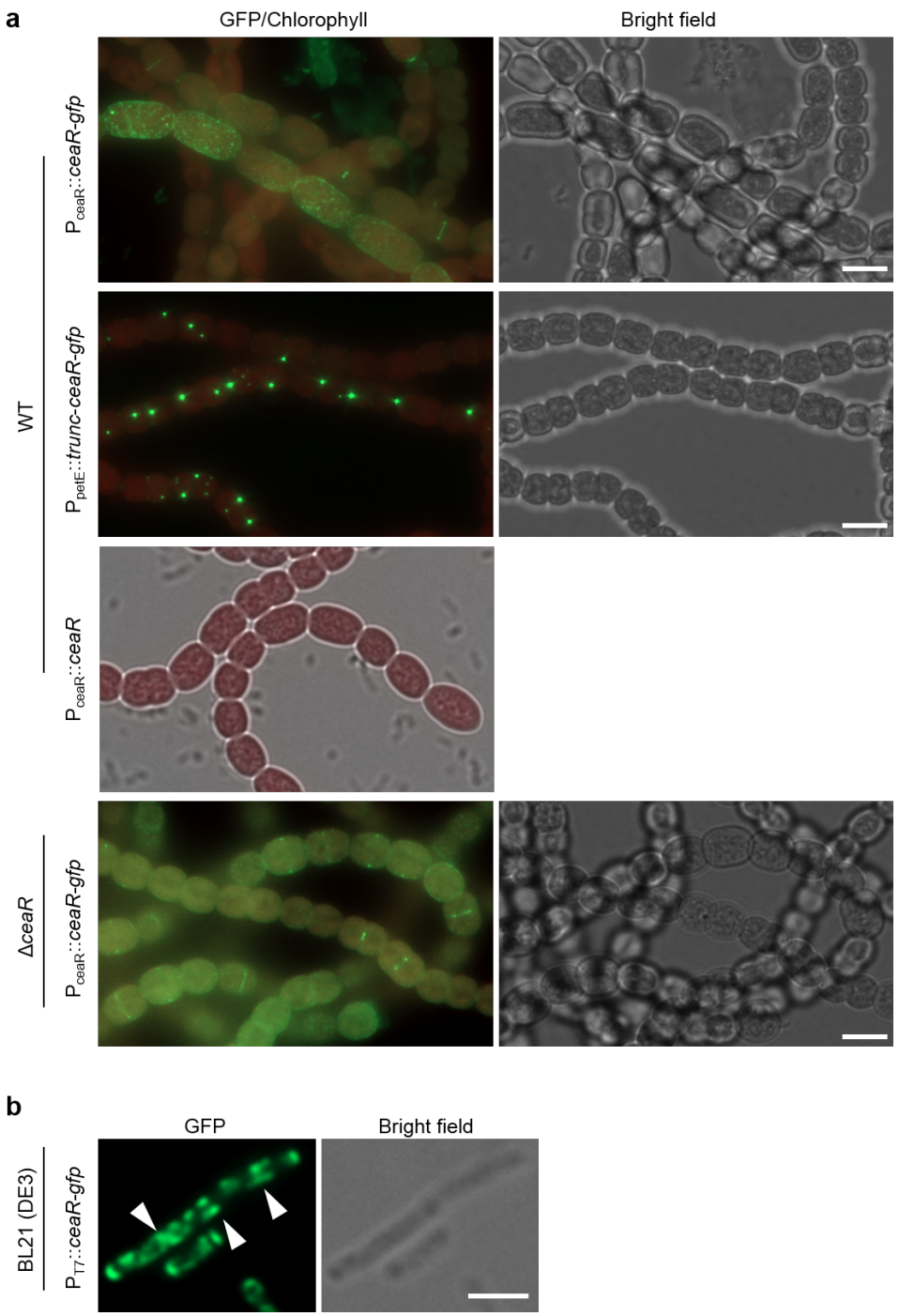

Supplementary Fig. 8: *In vivo* localization of CeaR-GFP in *Anabaena* and *E. coli*

(a) Merged GFP-fluorescence and chlorophyll autofluorescence and bright field micrographs of *Anabaena* WT or Δ*ceaR* mutant strain expressing CeaR-GFP, CeaR-GFP without the N-terminal transmembrane domain (first 52 aa removed; *trunc-ceaR*) or CeaR form P_{petE} or P_{ceaR}. Additional expression of CeaR-GFP from P_{ceaR} or P_{petE} and CeaR from P_{ceaR} induces a swollen cell phenotype. This phenomenon is not present upon expression of CeaR-GFP or CeaR (Supplementary Fig. 9a) from P_{ceaR} in the Δ*ceaR* mutant strain, indicating that *ceaR* expression or protein level is tightly regulated in *Anabaena* WT. Expression of truncated CeaR-GFP in *Anabaena* WT cells was induced for 1 d with 0.2 µM $CuSO_4$. Scale bars: 5 µm.

(b) GFP-fluorescence and bright field micrographs of *E. coli* BL21 (DE3) cells expressing CeaR-GFP. Cells were grown till an OD_{600} of 0.5 and induced for 48 h at 20 °C with 0.05 mM IPTG. White triangles indicate banded and helical localization of CeaR-GFP. Scale bar: 5 µm.

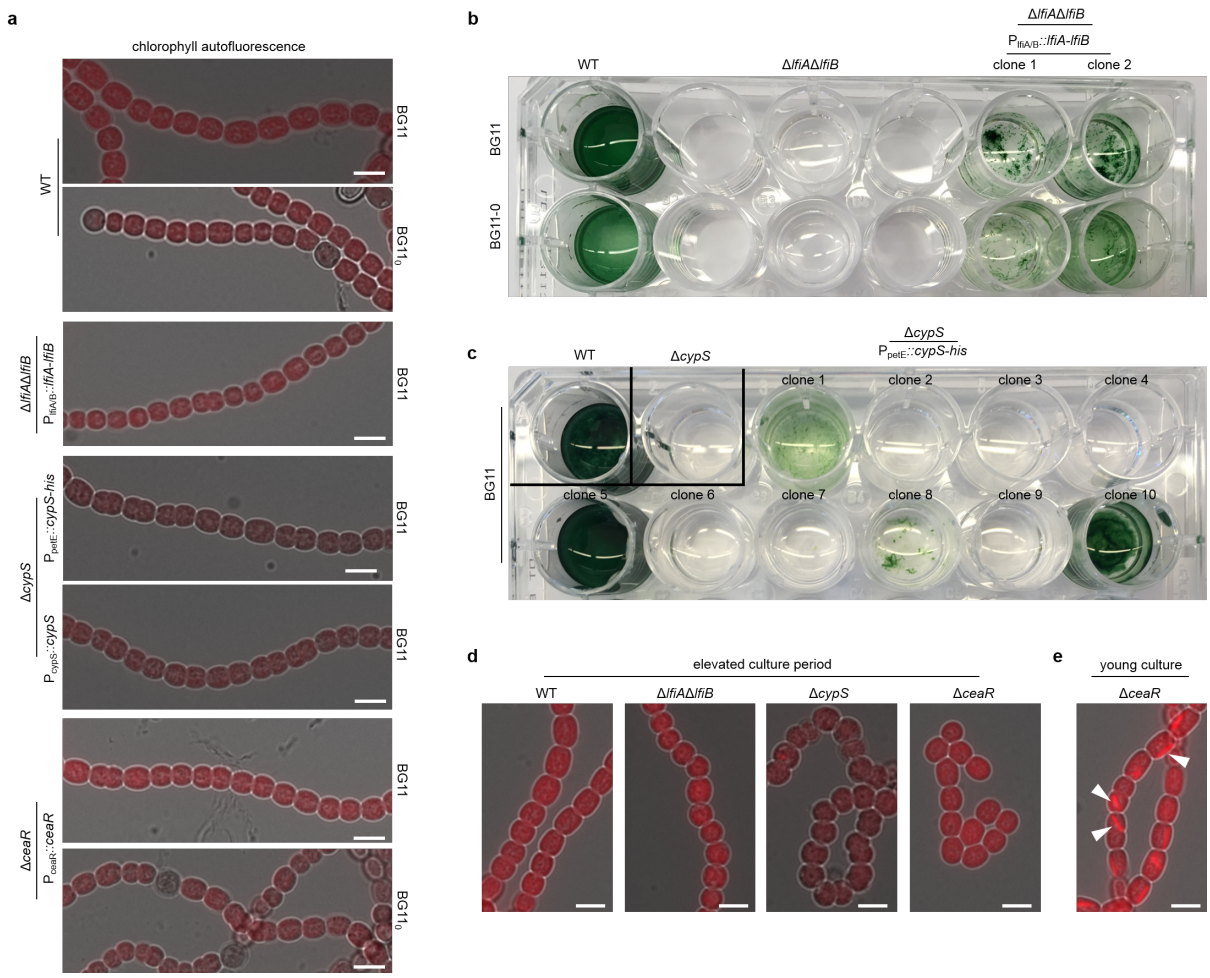

Supplementary Fig. 9: Mutant phenotype complementation and culture age-dependency of *Anabaena* mutant phenotypes

(a) Morphological complementation of *Anabaena* CCRP mutant strains as a result of native expression of *lfiA-lfiB*, *cypS* and *ceaR* from pRL25C. Notably, CypS-His expressed from P_{petE} also complemented the morphological defect of the Δ*cypS* mutant strain and rescues the linear *Anabaena* filament shape. The ability to complement the mutant phenotypes using the pRL25C plasmid shows that pDU1-based plasmids can be successfully employed to rescue WT phenotypes despite their variation in the relative copy number[100]. Scale bars: 5 µm.

(b,c) Complementation of (b) Δ*lfiA*Δ*lfiB* and (c) Δ*cypS* mutant strains by expressing *lfiA-lfiB* from $P_{lfiA/B}$ or *cypS-his* from P_{petE} from the replicative pRL25C plasmid. Note, not all tested clones successfully complemented the mutant growth defects in liquid culture, likely due to the phenotypic variation caused by the copy number variation of pRL25C[100,101].

(d) Merged bright field and chlorophyll autofluorescence micrographs of (a) *Anabaena* WT and Δ*lfiA*Δ*lfiB*, Δ*cypS* and Δ*ceaR* mutant strains grown on BG11 plates for an elevated time period (about 3 weeks) or (d) Δ*ceaR* mutant strain grown on BG11 plates for about one week. White triangles indicate red fluorescent filaments. Note: a decreased viability of the Δ*cypS* mutant strain is evident by a decreased chlorophyll autofluorescence signal. Scale bars: 5 µm.

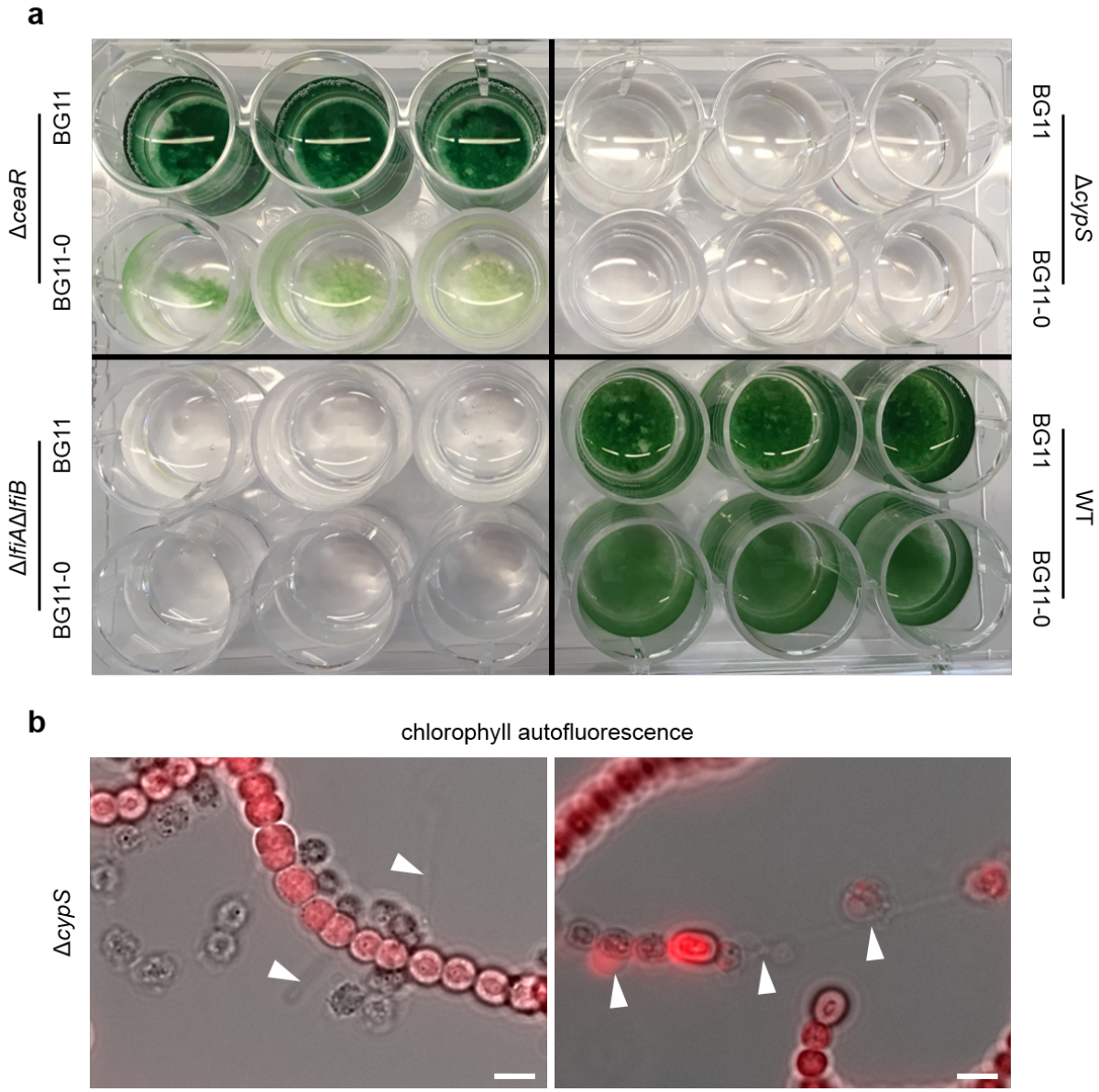

Supplementary Fig. 10: *Anabaena* CCRP mutant strains show growth defects in liquid culture

(a) *Anabaena* WT, Δ*cypS,* Δ*lfiA*Δ*lfiB* and Δ*ceaR* mutant strains were grown on BG11 plates, transferred to liquid BG11 and $BG11_0$ medium and incubated for 12 d at standard growth conditions without shaking. The Δ*ceaR* mutant strain can somewhat manage to survive in $BG11_0$ liquid medium without agitation. Nevertheless, prolonged incubation usually led to cell death. On the contrary, Δ*ceaR* mutant cells are not viable when grown in liquid media with agitation.

(b) Merged bright field and chlorophyll autofluorescence micrographs of Δ*cypS* mutant strain resuspended in BG11 liquid medium from BG11 plates. Cells were visualized immediately after transfer. White triangles indicate material released from cells upon cell rupture. Scale bars: 5 µm.

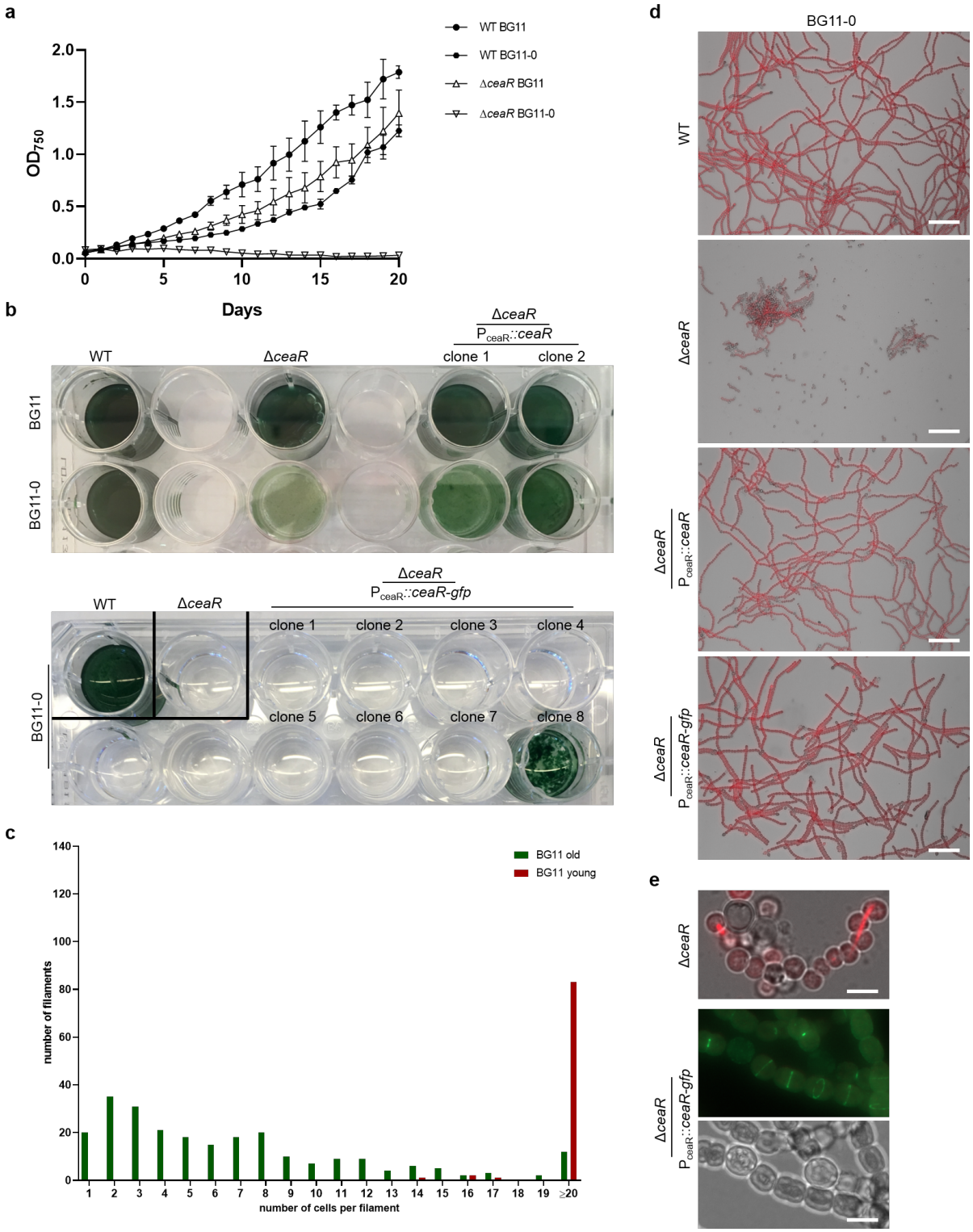

Supplementary Fig. 11: Fragmentation and decreased viability of the *ΔceaR* mutant strain

(a) *Anabaena* WT and Δ*ceaR* mutant strain were grown in BG11, washed three times in BG11 or $BG11_0$, adjusted to an OD_{750} of 0.1 and then grown in triplicates at standard growth conditions. OD_{750} values were recorded once a day for 20 d. Error bars show the standard deviation (n = 3).

(b) *Anabaena* WT grows in BG11 and $BG11_0$ while the Δ*ceaR* mutant strain only grows in BG11. Growth in $BG11_0$ can, however, be rescued using the pRL25C plasmid bearing P_{ceaR}::*ceaR* or P_{ceaR}::*ceaR-gfp*, showing that the CeaR-GFP fusion protein is active.

743 (c) Filament length (number of cells per filament) of Δ*ceaR* mutant strain from young and older cultures grown in
744 BG11 liquid medium. Filament length of filaments with up to 19 cells were individually counted while filaments with
745 with more than 20 cells are listed with ≥20.

746 (d) Merged bright field and chlorophyll autofluorescence micrographs of *Anabaena* WT, Δ*ceaR* mutant and the
747 Δ*ceaR* mutant carrying a pRL25C plasmid bearing P_{ceaR}::*ceaR* or P_{ceaR}::*ceaR-gfp*. Micrographs show cells from
748 Supplementary Fig. 11b 48 h after transfer to $BG11_0$. The Δ*ceaR* mutant fragments into short filaments that clump
749 together with cells losing their chlorophyll auto-fluorescence signal. However, the Δ*ceaR* mutant
750 fragmentation/aggregation can be fully complemented with a pRL25C plasmid bearing P_{ceaR}::*ceaR* or P_{ceaR}::*ceaR-*
751 *gfp*.

752 (e) Micrographs of Δ*ceaR* mutant and Δ*ceaR* mutant expressing CeaR-GFP from P_{ceaR} on the pRL25C plasmid
753 48 h after transfer to $BG11_0$

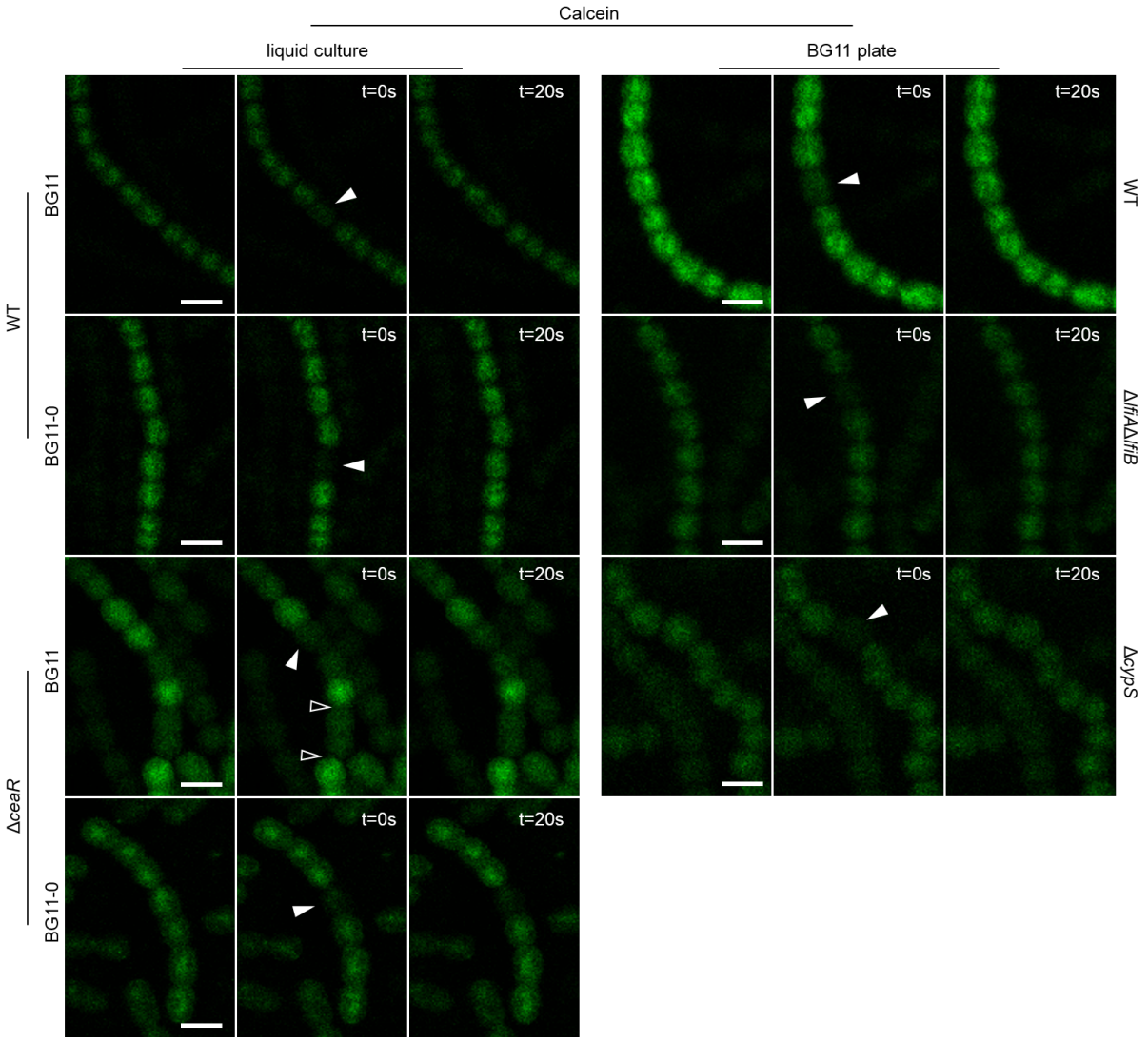

754

755 **Supplementary Fig. 12: *Anabaena* CCRP mutant strains display defects in cell-cell solute diffusion**

756 Representative calcein fluorescence micrographs depicting intercellular molecular exchange following laser-based
757 bleaching of calcein fluorescence in *Anabaena* WT or Δ*ceaR* mutant strain grown in liquid BG11 and liquid $BG11_0$
758 as well as in *Anabaena* WT and Δ*lfiA*Δ*lfiB* and Δ*cypS* mutant strains grown on BG11 plates. White triangles indicate
759 bleached cells. Translucent triangles show diffusion barriers present in the Δ*ceaR* mutant strain. Fluorescence
760 images show respective cells prior bleaching, immediately after bleaching (t = 0) and after 20 seconds after
761 bleaching (t = 20s). Images show representative examples. Scale bars: 5 µm.

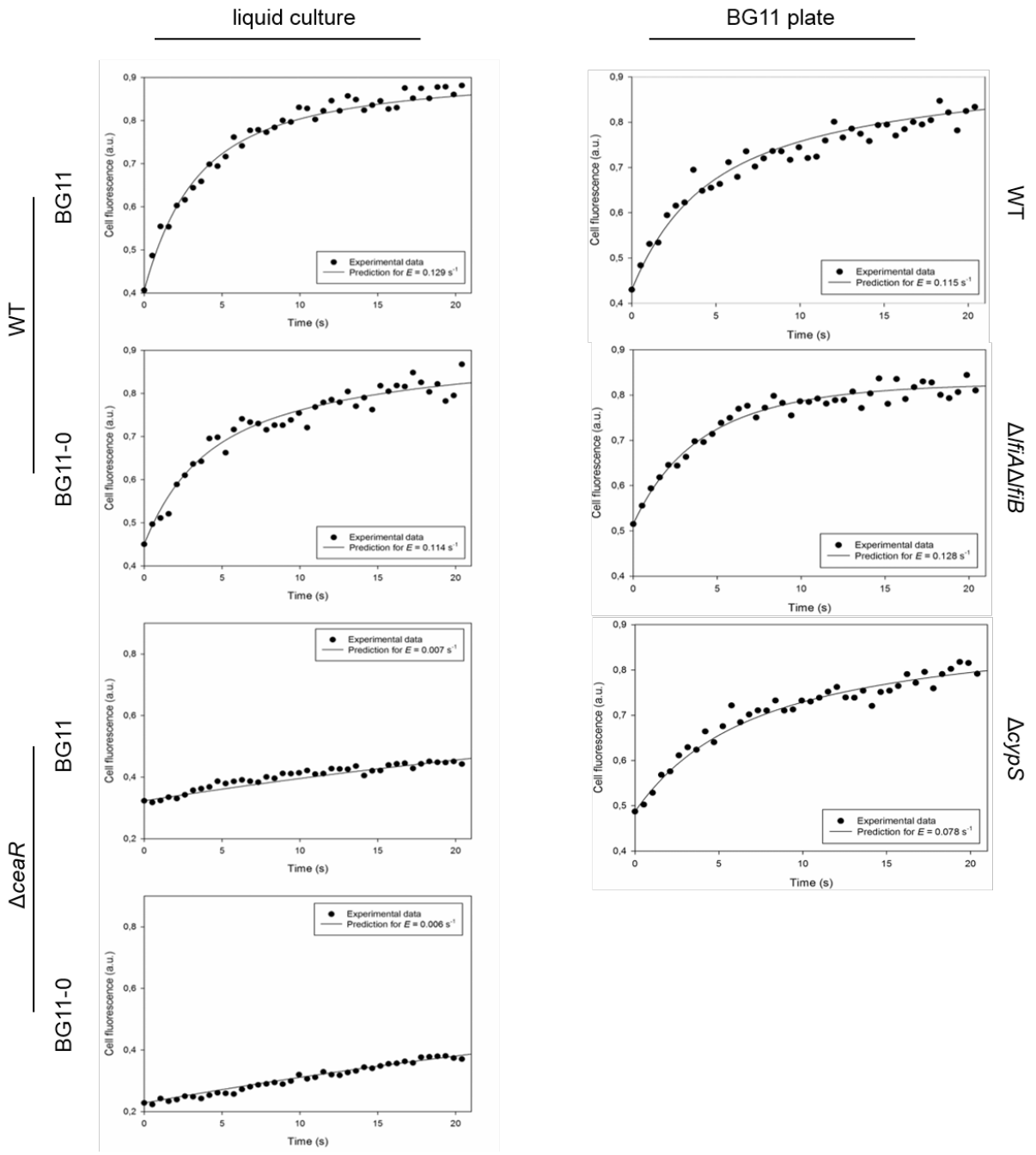

Supplementary Fig. 13: Exchange coefficients of FRAP assays

Fluorescence recovery curves with their predicted exchange coefficient values (*E*)[43] for selected bleached cells of *Anabaena* WT or Δ*ceaR* mutant strain grown in liquid BG11 and liquid $BG11_0$ as well as in *Anabaena* WT and Δ*lfiA*Δ*lfiB* and Δ*cypS* mutant strains grown on BG11 plates. Fluorescence values are given in arbitrary units (a.u.)[43] over a time course of 20 s post bleaching.

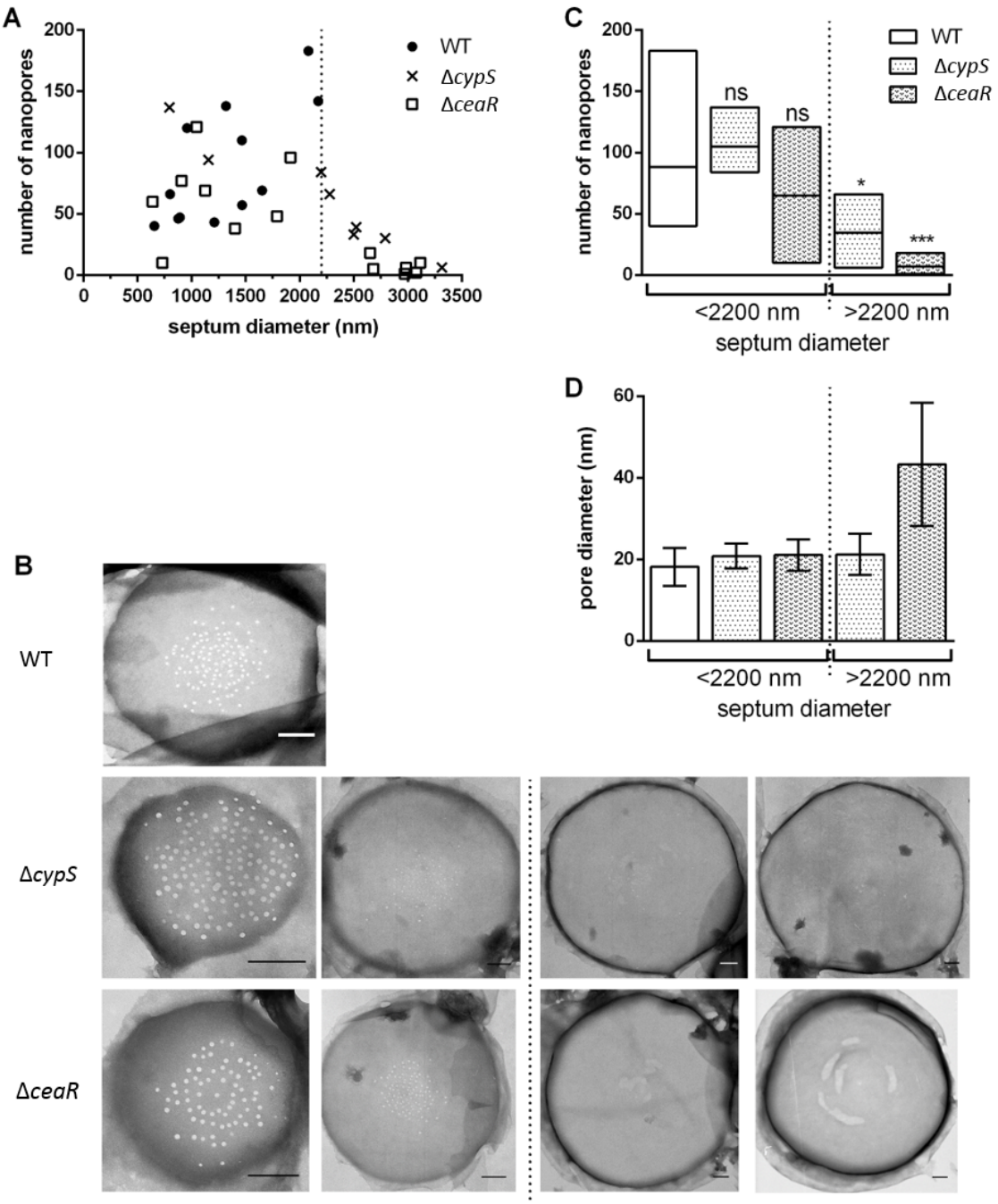

Supplementary Fig. 14: Septal nanopore array

(a) The number of nanopores is shown correlated to the septum size. In contrast to the WT, *Anabaena* CCRP mutants show a subset of large septa (>2200 nm) with few nanopores.

(b) Representative transmission electron microscopy images of indicated strains are shown. The dotted line divides the septa into a diameter of <2200 nm (left) and >2200 nm (right) derived from (a). Scale bars: 250 nm.

(c) Number of pores per septum (</> 2200 nm). Student's t-test (mutants vs. WT). P-values are indicated (ns: not significant, *P<0.05, ***P<0.001). P-values were calculated from the following number of septa: n (WT) = 12; n (Δ*cypS* <2200 nm) = 3; n (Δ*ceaR* <2200 nm) = 8; n (Δ*cypS* >2200 nm) = 5; n (Δ*ceaR* >2200 nm) = 6. WT data were derived from Bornikoel, *et al*[102].

(d) Nanopore diameter. Floating bars show the mean value from the number of analyzed nanopores. Sample size was n (WT) = 1061; n (Δ*cypS* <2200 nm) = 315; n (Δ*ceaR* <2200 nm) = 371; n (Δ*cypS* >2200 nm) = 174; n (Δ*ceaR* >2200 nm) = 42.

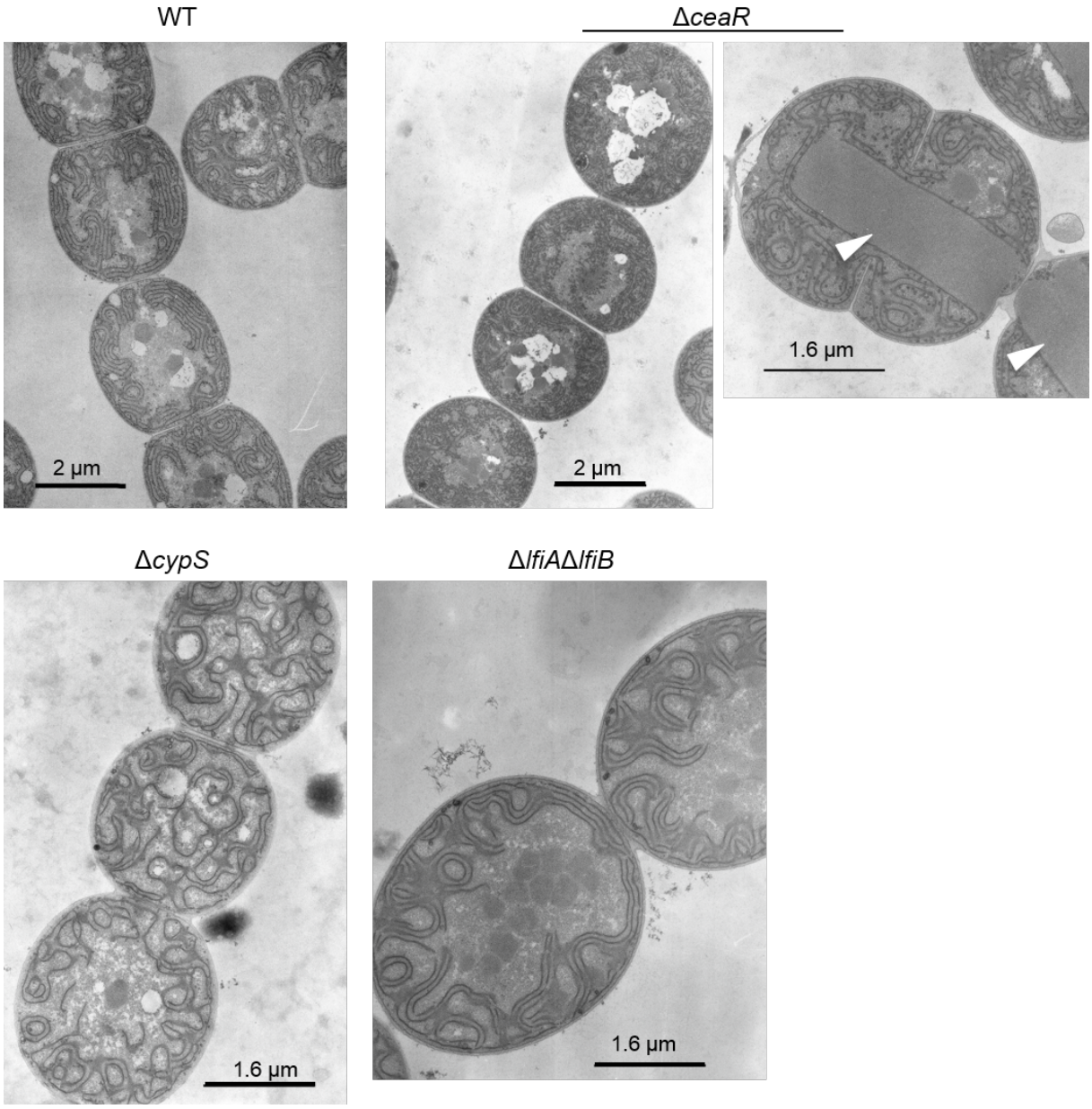

781

782 **Supplementary Fig. 15: Ultrastructure of *Anabaena* WT and CCRP mutant strains**

783 Ultrathin sections of *Anabaena* WT and *Anabaena* CCRP mutant strains grown on BG11 plates. White triangles indicate
784 unusual structures in the Δ*ceaR* mutant that coincide with the observed red fluorescent filaments in the Δ*ceaR* mutant
785 visualized by live cell fluorescence microscopy (Fig. 3d, Supplementary Fig. 9e).

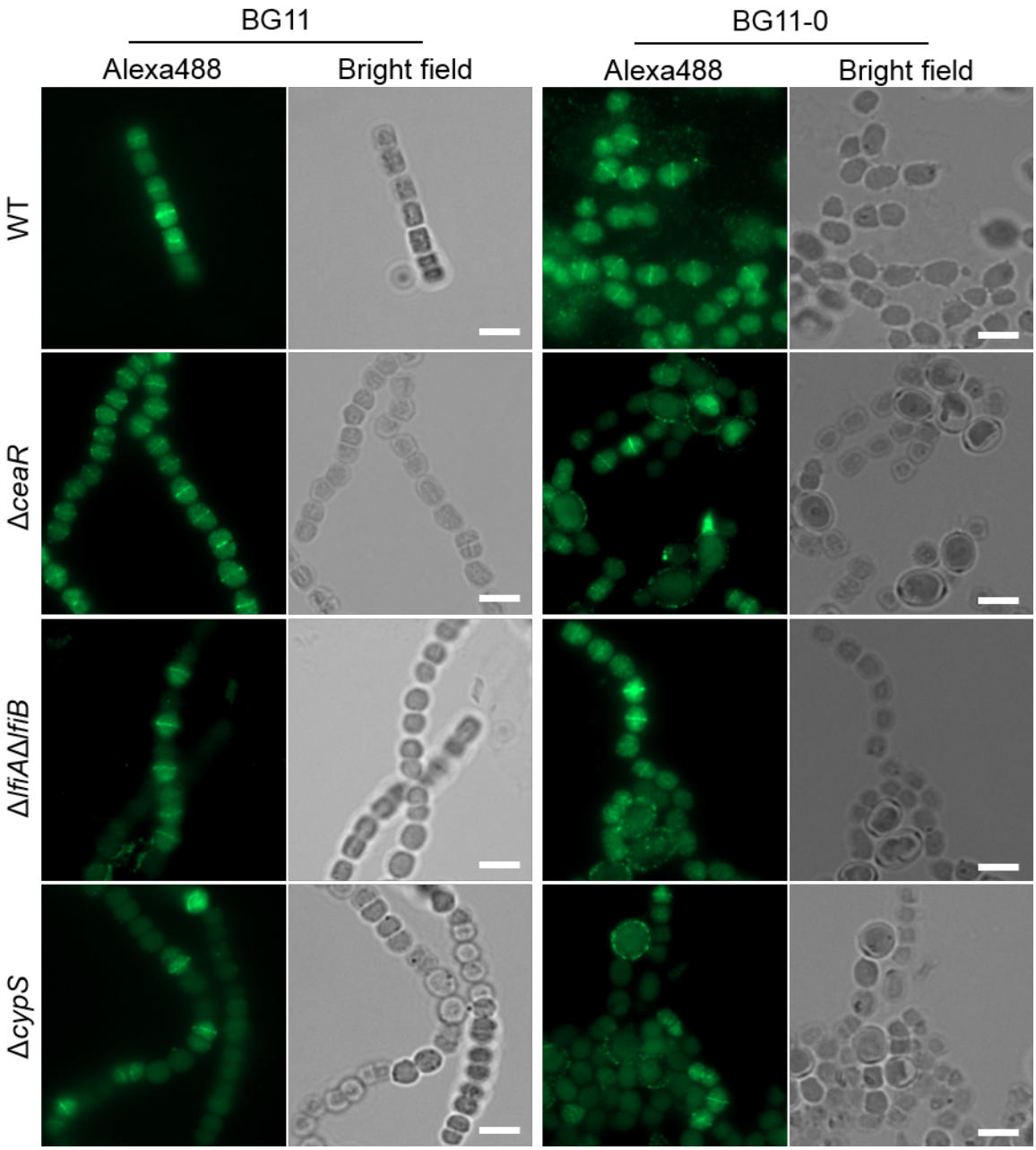

Supplementary Fig. 16: FtsZ localization is unaffected in *Anabaena* CCRP mutant strains

Alexa Flour-488 fluorescence and bright field micrographs of *Anabaena* WT and Δ*ceaR*, Δ*IfiA*Δ*IfiB* and Δ*cypS* mutant strains grown on BG11 or $BG11_0$ growth plates. Cells were subjected to immunofluorescence staining using anti-FtsZ primary antibody and Alexa Fluor-488 coated secondary antibody essentially as described by Ramos-León *et al.*[82]. Cells were mounted in ProLong Diamond antifade mountant (Thermo Fischer Scientific). Scale bars: 5 µm.

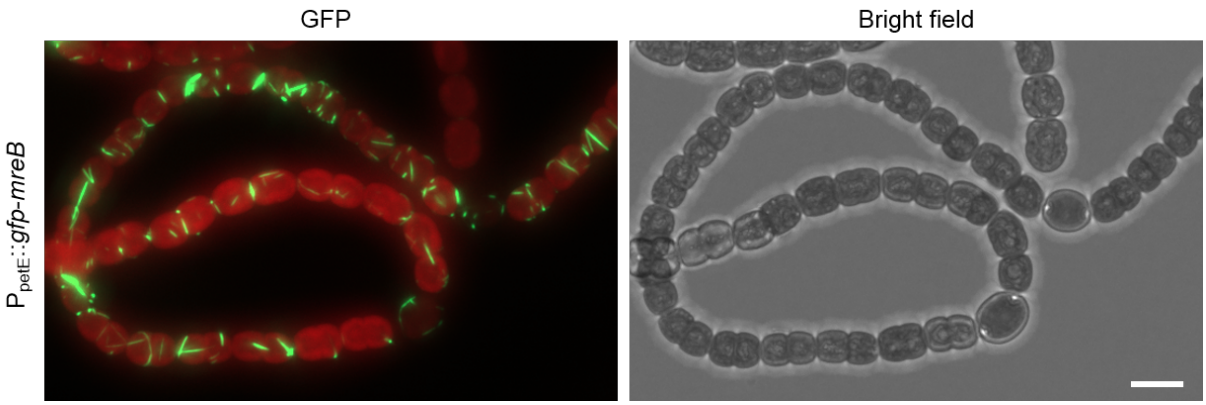

Supplementary Fig. 17: GFP-MreB forms extensive filaments in *Anabaena* WT

Merged GFP fluorescence and chlorophyll autofluorescence and bright field micrographs of *Anabaena* WT expressing GFP-MreB from P_{petE}. Cells were grown on $BG11_0$ growth plates. Maximum intensity projections of a Z-stack. Scale bar: 5 µm.

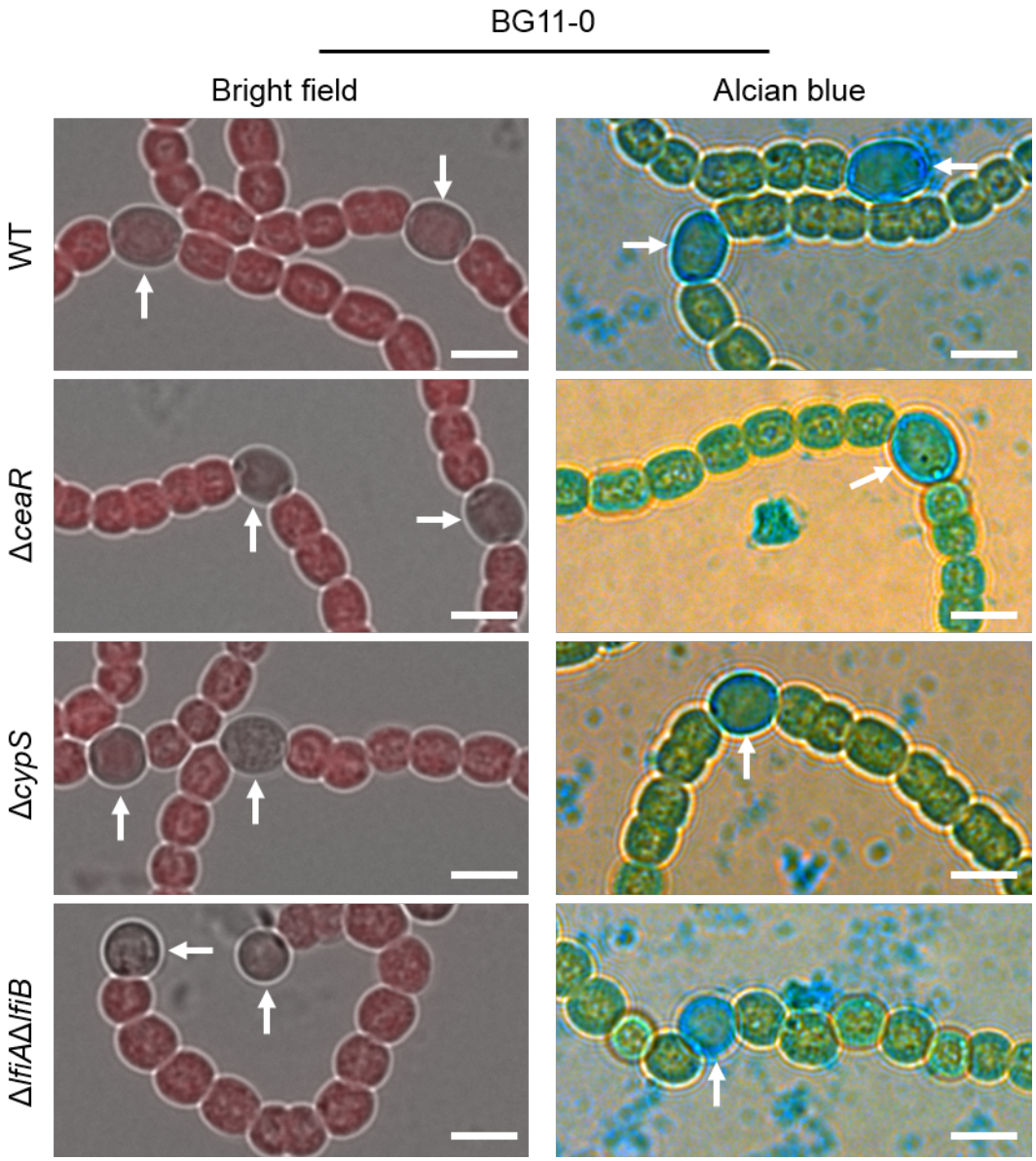

Supplementary Fig. 18: Alcian blue staining is unaltered in *Anabaena* CCRP mutant strains

Bright field micrographs of *Anabaena* WT and Δ*ceaR*, Δ*lfiA*Δ*lfiB* and Δ*cypS* mutant strains grown on $BG11_0$ plates. Cells were either observed directly by bright field microscopy or previously stained with 0.5% alcian blue (final concentration). Heterocysts are indicated by white arrows. Scale bars: 5 µm.

803

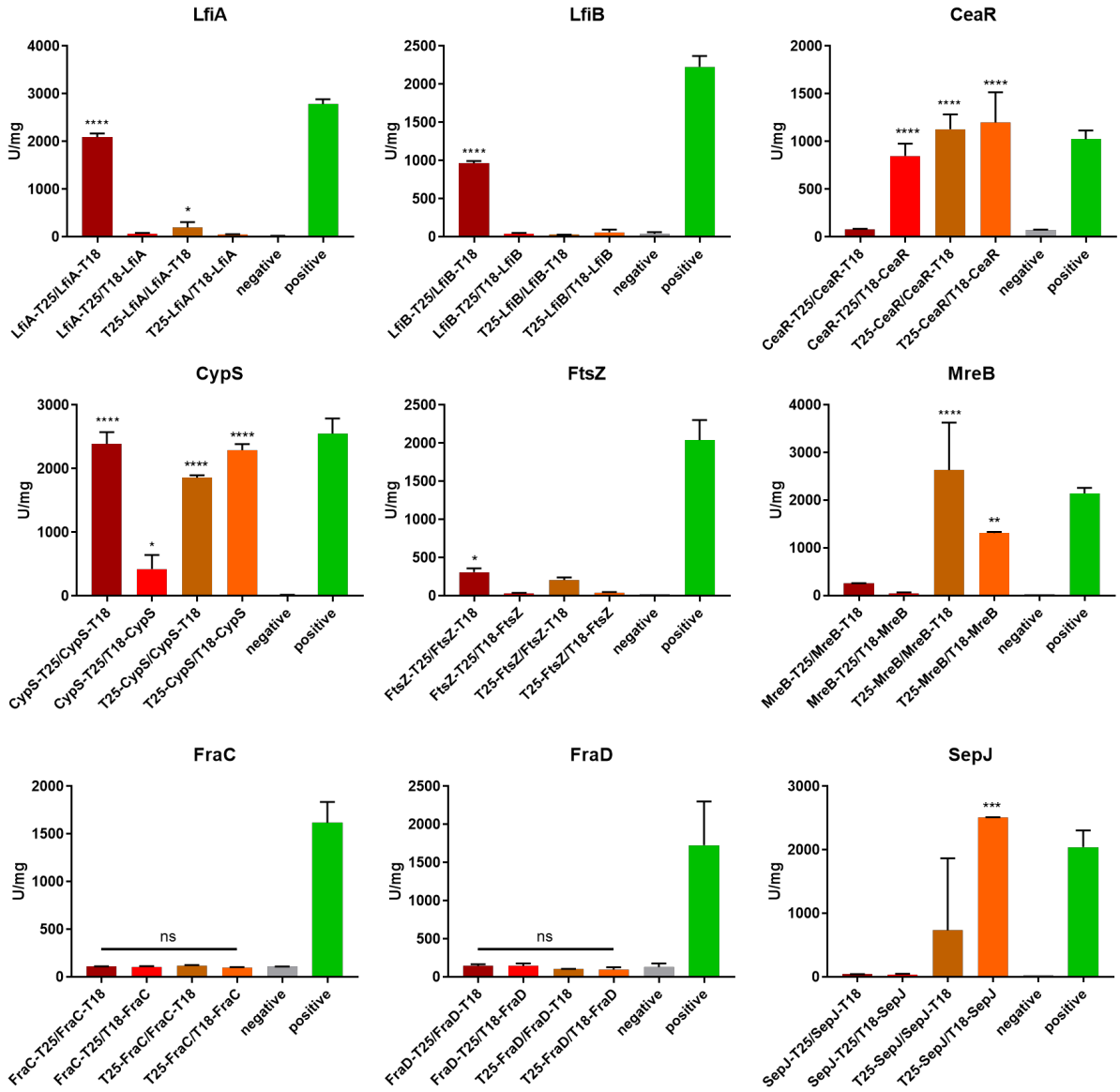

804

805 Figure description follows on page 47.

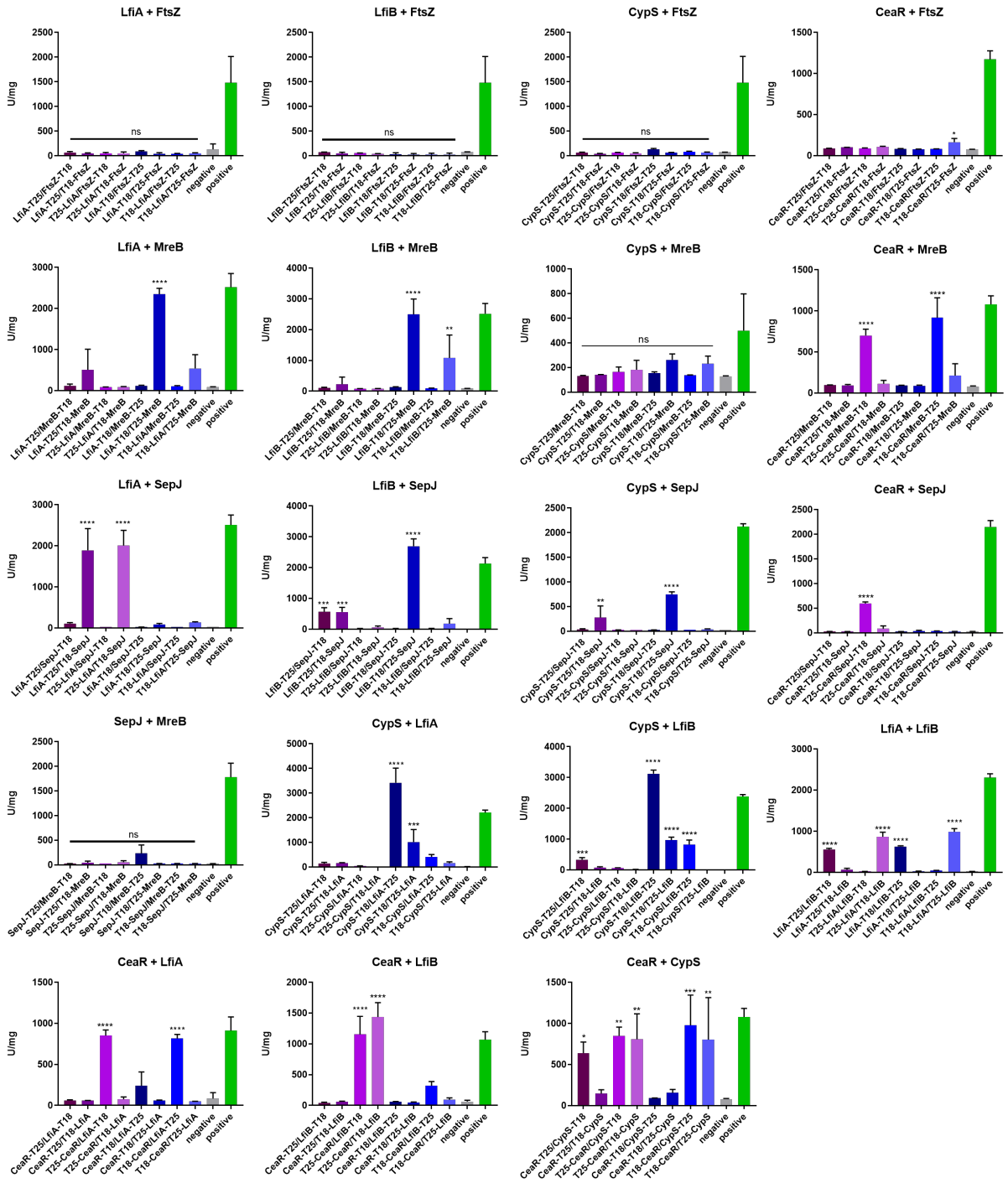

Figure description follows on page 47.

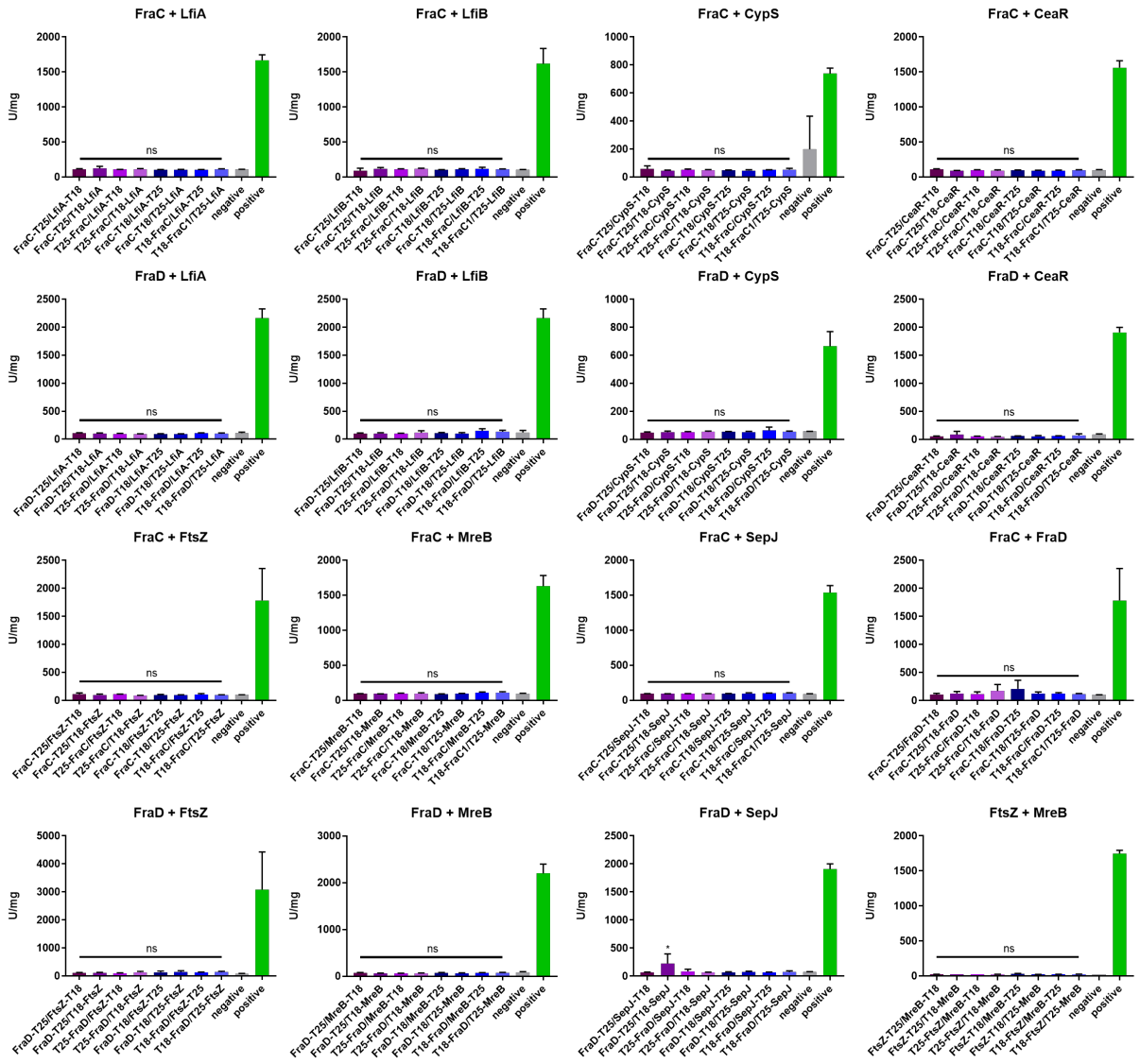

Supplementary Fig. 19: *Anabaena* possess a complex cytoskeletal network that is linked to a septal junction protein

Beta-galactosidase assays of *E. coli* BTH101 cells co-expressing indicated T25 and T18 translational fusions of all possible pair-wise combinations. *E. coli* cells carrying the respective plasmids were subjected to beta-galactosidase assay as described by Karimova *et al.*[103] in triplicates from three independent colonies grown for 2 d at 20 °C. Quantity values are given in Miller Units per milligram LacZ of the mean results from three independent colonies. Negative: N-terminal T25 fusion construct of the respective protein co-transformed with empty pUT18C. Positive: Zip/Zip control. Error bars indicate standard deviations (n = 3). *: $P < 0.05$, **: $P < 0.01$, ***: $P < 0.001$, ****: $P < 0.0001$ (Dunnett's multiple comparison test and one-way ANOVA).

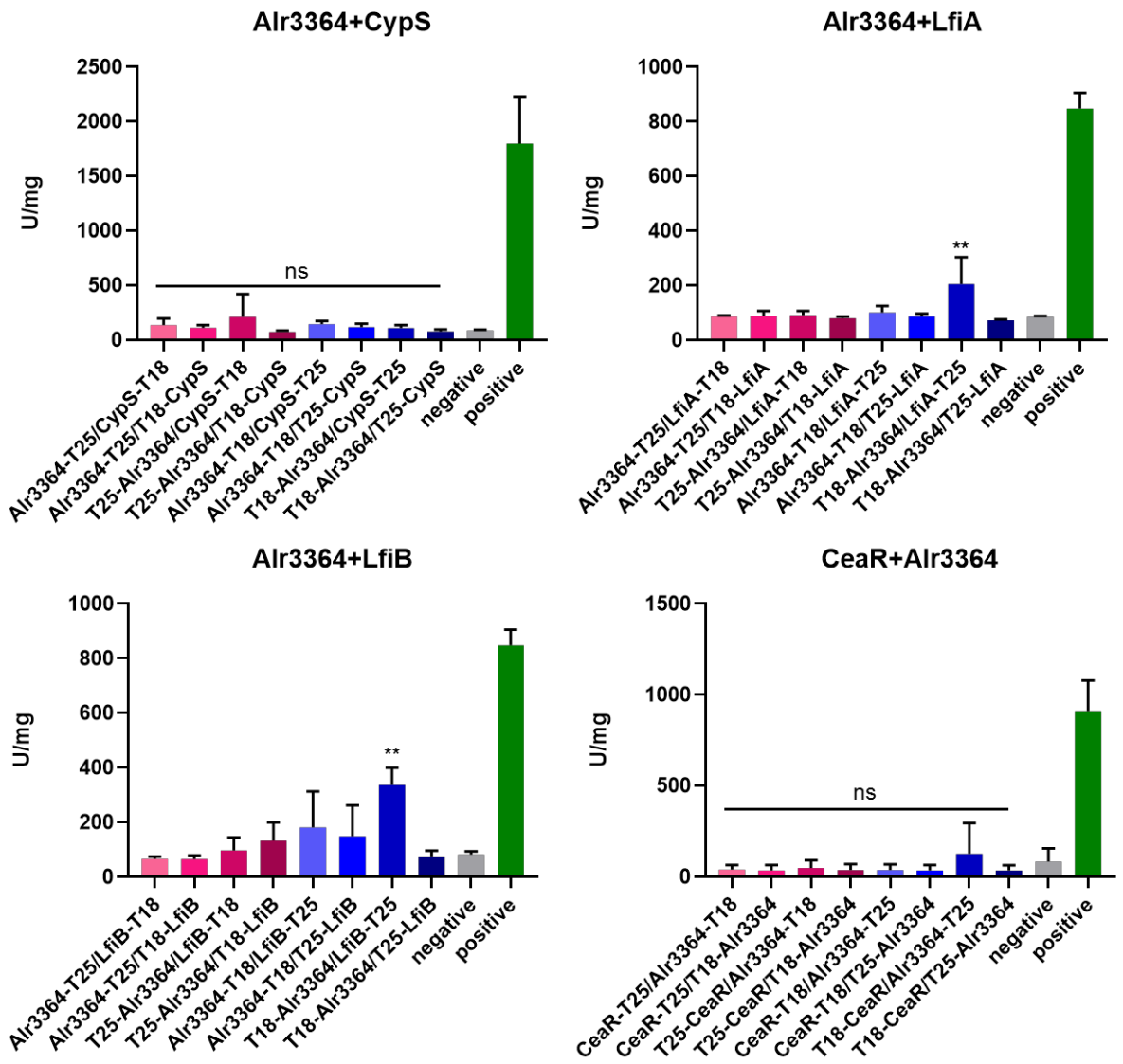

Supplementary Fig. 20: Interaction of *Anabaena* IF-like CCRPs is specific in a bacterial two hybrid system

Beta-galactosidase assays of *E. coli* BTH101 cells co-expressing indicated T25 and T18 translational fusions of all possible pair-wise combinations. *E. coli* cells carrying the respective plasmids were subjected to beta-galactosidase assay as described by Karimova *et al.*[103] in triplicates from three independent colonies grown for 2 d at 20 °C. Quantity values are given in Miller Units per milligram LacZ of the mean results from three independent colonies. Negative: N-terminal T25 fusion construct of the respective protein co-transformed with empty pUT18C. Positive: Zip/Zip control. Error bars indicate standard deviations (n = 3). Values indicated with * are significantly different from the WT. **: $P < 0.01$ (Dunnett's multiple comparison test and one-way ANOVA).

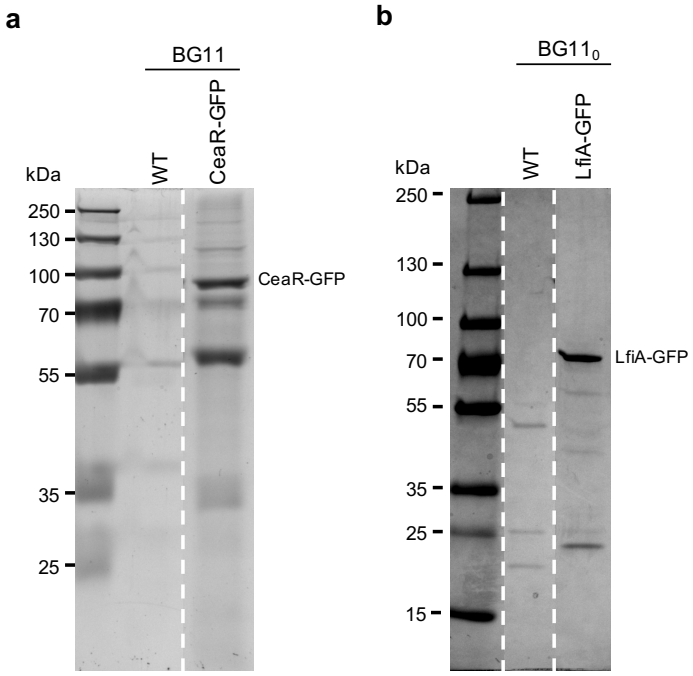

c

CeaR-GFP	LfiA-GFP
All4981	LfiB
MreB	MreB
ParA	ParA
MinD	
SepJ	
All2981 (PBP1a)	
All2952 (PBP1a)	
Alr0718 (PBP2)	
Alr3365	
Alr4550 (S-layer protein)	

PBP: Penicillin-binding protein

Supplementary Fig. 21: Identification of proteins interacting with *Anabaena* CCRPs

(a,b) Cell-free extracts of *Anabaena* WT expressing (a) CeaR-GFP or (b) LfiA-GFP from P_{petE} were subjected to co-immunoprecipitation using anti-GFP magnetic beads (µMACS GFP isolation Kit; Miltenyi Biotec). CeaR-GFP-expressing cells were grown in BG11 without copper and protein expression was induced for 1 d with 0.5 µM $CuSO_4$. LfiA-GFP expressing cells were grown in BG11$_0$ without copper and protein expression was induced for 5 d with 0.5 µM $CuSO_4$. *Anabaena* WT cells were grown in BG11 and BG11$_0$ supplemented with 0.5 µM $CuSO_4$ for 1 or 5 d, respectively. Cells were lysed in PBS-N and pooled duplicates of precipitated proteins of two independent experiments were analyzed by mass spectrometry and 25 µl of the co-precipitate were resolved in a (a) 10% SDS-polyacrylamide gel or in a (b) 4-15% TGX precast gel (Bio-Rad) and detected by Quick Coomassie stain (Serva).

(c) Excerpt of the identified specific interactors of CeaR-GFP and LfiA-GFP. The full list is listed in Supplementary File 3. Notably, CeaR directly interacts with All4981, another filament forming protein in *Anabaena* (covered in a separate report) as well as Alr3365 that lies directly downstream of *alr3364* in the *Anabaena* genome, which we also identified in our screening for CCRPs in *Anabaena* (Supplementary Fig. 1). Both, CeaR and LfiA, interact with ParA, hinting for a putative role in chromosome or plasmid segregation in *Anabaena*.

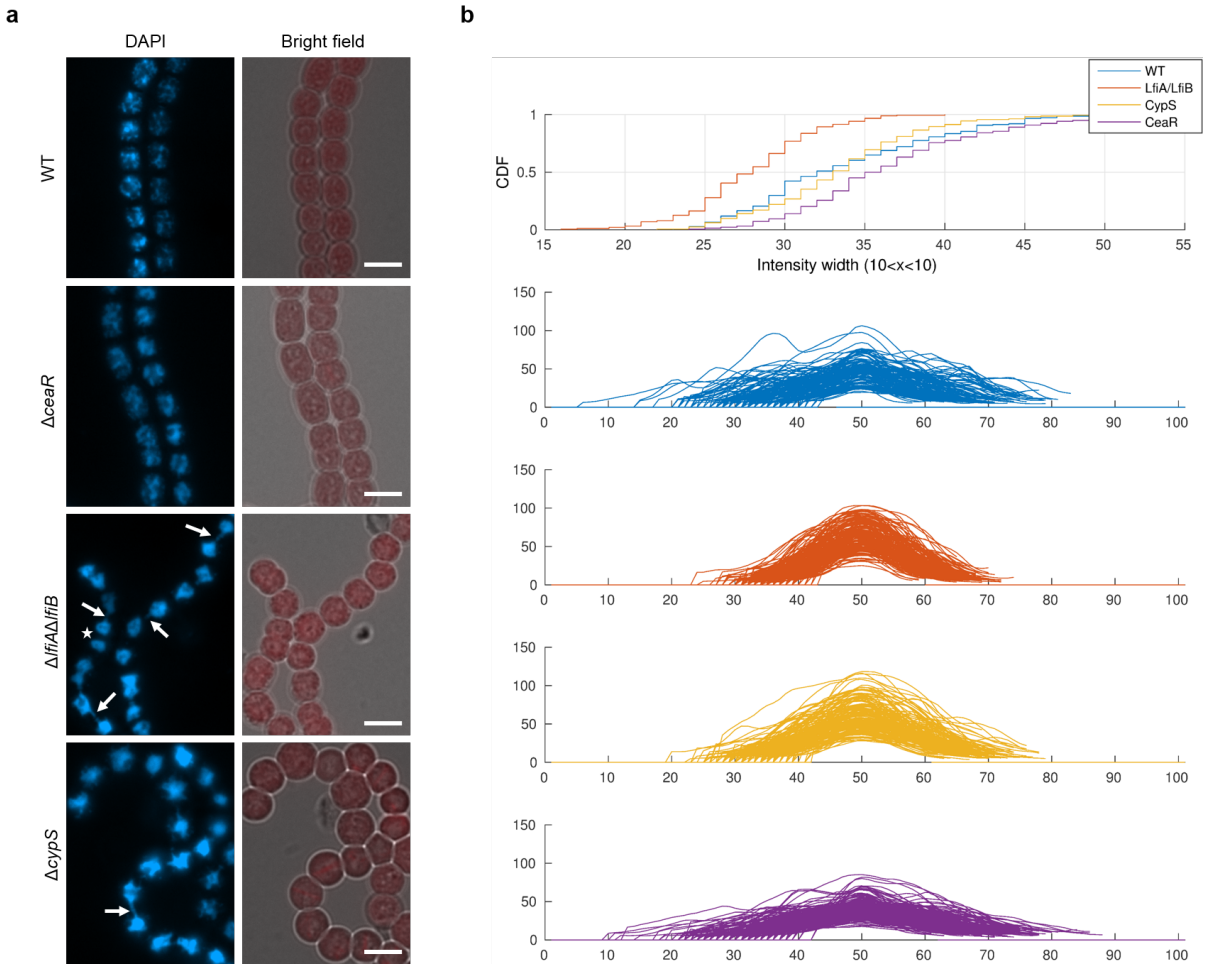

Supplementary Fig. 22: Condensation of intracellular DNA in Anabaena CCRPs

(a) DAPI fluorescence and merged bright field and chlorophyll autofluorescence micrographs of *Anabaena* WT and Δ*ceaR*, Δ*lfiA*Δ*lfiB* and Δ*cypS* mutant strains grown on BG11 growth plates. Cells were resuspended in BG11 and incubated with 10 µg ml^{-1} DAPI (final concentration). White arrows indicate strings of DNA that traverse from one cell to the other. Notably, no such strings are observed in dividing cells (white star), suggesting that it is an effect that occurs after complete cell division. Scale bars: 5 µm.

(b) Plot profile showing the DAPI signal intensities of pixels (grey value) along *Anabaena* WT and *Anabaena* mutant cells (n =151 for each strain) in arbitrary units (a.u.) and arranged to the respective peak maxima. The focal area size in the Δ*lfiA*Δ*lfiB* mutant was smallest in comparison to the other strains, Δ*ceaR* was larger than the others, and the area size in WT was not significantly different than Δ*cypS* (alpha=0.05, using Tukey test). Notably, the comparison of cell size among the strains reveals a similar result: the Δ*lfiA*Δ*lfiB* mutant cell size was smallest in comparison to the other strains, Δ*ceaR* was larger than the others, and the area size in WT was not significantly different than the Δ*cypS* mutant ($P=1.75x10^{-54}$, using Kruskal-wallis; alpha=0.05, using Tukey test). Consequently, we compared the area of the focal DAPI staining decided by the cell size among the strains. This reveals that this ratio is smallest in Δ*ceaR*, largest in Δ*cypS* and not significantly different between Δ*lfiA*Δ*lfiB* and the WT.

8 **Supplementary Table 1: Characteristics of protein candidates**

Locus tag	Genus	Subsection	Homolog distribution	Predicted proteins of similar structure (I-TASSER)	Conserved domains	Others 859
crescentin	*C. crescentus*	n/a	n/a	Cytoplasmic domain of bacterial cell division protein EzrA	SMC_N, CCDC158	Validated IF-like protein[86,107–109]
cypS (*alr0931*)	*Anabaena*	IV	I, II, III, IV, V	Cytoplasmic domain of bacterial cell division protein EzrA	SMC_N, CCDC158 DUF3084, Neuromodulin_N	
all4981	*Anabaena*	IV	III, IV, V	TTC7B/Hyccin Complex or Clathrin coat	TPR	4 bp overlap to *all4982*
lfiA (*alr4504*)	*Anabaena*	IV	I, II, III, IV, V	Spectrin repeats 7, 8, and 9 of the plakin domain of plectin	SMC_N	*lfiB* localized downstream of *lfiA*
lfiB (*alr4505*)	*Anabaena*	IV	I, II, III, IV, V	Cytoplasmic domain of bacterial cell division protein EzrA	SMC_N, DUF3552	
ceaR (*all2460*)	*Anabaena*	IV	III, IV, V	Cytoplasmic domain of bacterial cell division protein EzrA	SMC_N, TerB_C, CALCOCO1, Spc7	Two N-terminal TMHs
alr0347	*Anabaena*	IV	I, II, III, IV, V	*Bacillus subtilis* Smc coiled-coil middle fragment	Filament superfamily	
alr3364	*Anabaena*	IV	II, III, IV, V	Cytoplasmic domain of bacterial cell division protein EzrA	SMC_N, FtsK, DUF4696	
all8023	*Anabaena*	IV	IV	Human ATR-ATRIP complex	SMC_N, Pentapeptide, Yjbl	
alr4393	*Anabaena*	IV	I, II, III, IV, V	Cytoplasmic domain of bacterial cell division protein EzrA	SMC_N, DUF3084	
alr4911	*Anabaena*	IV	I, II, III, IV, V	Structure of the Smc head domain with a coiled coil and joint derived from *Pyrococcus yayanosii*	SMC_N, P-loop_NTPase DNA_S_dndD, Spc7, SbcC	
all4935	*Anabaena*	IV	IV	Cytoplasmic domain of bacterial cell division protein EzrA	DUF4114, DUF3084	
alr2043	*Anabaena*	IV	IV, V	Human ATR-ATRIP complex (replication stress response)	SMC_N, Tubulin_2	
alr3988	*Anabaena*	IV	I, II, III, IV, V	Two dynein tail domains bound to dynactin and BICDR1	SMC_N, SbcC	

The first column indicates the respective locus tags of protein candidates and Crescentin. The second and third column indicate the respective subsection of the corresponding genus according to Rippka *et al.* (1979)[36]. Column four lists the subsections that contain homologous proteins to the respective candidate. Column five contains proteins predicted to be structurally similar to the protein candidates in the PDB (Protein Data Bank) based on I-TASSER[104–106]. The sixth column indicates predicted sub-domains of protein candidates identified by BLAST CDS. Column seven states other features of interest. Abbreviations: (TMH) Transmembrane helix; (DUF) Domain of unknown function; (CCDC158) Coiled-coil domain-containing protein 158; (SMC) Structural maintenance of chromosomes; (SbcC) DNA repair exonuclease SbcCD ATPase; (CALCOCO1) Calcium binding and coiled-coil domain; (TRP): Tetratricopeptide repeat; (Spc7) Spc7 kinetochore protein; (TerB_C) TerB-C occurs C-terminal of TerB in TerB-N containing proteins, putative metal chelating; (Filament superfamily) Intermediate filament protein; (FtsK) DNA segregation ATPase FtsK; (Pentapeptide) Pentapeptide repeats often found in many cyanobacterial proteins with unknown function (predicted to be a β-helix); (Yjbl) Uncharacterized protein containing pentapeptide repeats; (DNA_S_dndD) DNA sulfur modification protein DndD; (Tubulin_2 superfamily) Tubulin like; Many of the residues conserved in Tubulin (pfam00091) are also conserved in this family; (P-loop_NTPase) P-loop containing Nucleoside Triphosphate Hydrolases superfamily. n/a: not applicable.

860 **Material and methods**

861 Bacterial strains and growth conditions

862 *Anabaena* WT was obtained from the Pasteur Culture Collection (PCC) of cyanobacteria
863 (France). Cells were grown photoautotropically in BG11 or without combined nitrogen ($BG11_0$)
864 at constant light with a light intensity of 30 µmol m^{-2} s^{-1}. When appropriate, 5 µg ml^{-1}
865 spectinomycin (Sp), 5 µg ml^{-1} streptomycin (Sm) or 30 µg ml^{-1} neomycin (Nm) was added to
866 strains carrying respective plasmids or chromosomal insertions. In some cases, basal copper-
867 regulated *petE*-driven expression of gene candidates in *Anabaena* cells was lethal or growth
868 inhibiting, therefore these strains were grown in BG11 without copper and protein expression
869 was later induced by the addition of $CuSO_4$ at indicated concentrations to the culture. *E. coli*
870 strains DH5α, DH5αMCR, XL1-blue and HB101 were used for cloning and conjugation by
871 triparental mating. BTH101 was used for BACTH system and BL21 (DE3) was used for
872 expression of His_6- and GFP-tagged proteins in *E. coli*. All strains were grown in LB medium
873 containing the appropriate antibiotics at standard concentrations. Supplementary Tables 2-5
874 list all used bacterial strains, plasmids and oligonucleotides.

875

876 Prediction of coiled-coil rich proteins

877 Genome sequence of *Anabaena* (GCA_000009705.1) was analyzed by the COILS algorithm[98]
878 as described by Bagchi *et al.*[32]. The algorithm was run with a window width of 21 and the cut-
879 off for amino acids in coiled-coil conformation was set to ≥ 80 amino acid residues. The
880 resulting set of protein candidates was further manually examined with online available
881 bioinformatic tools (NCBI Conserved Domain Search, NCBI BLAST, TMHMM Server,
882 PSORTb, I-TASSER). Protein candidates exhibiting BLAST hits involved in cytoskeletal
883 processes or similar domain architectures as known IF proteins like CreS, FilP, vimentin,
884 desmin or keratin were selected, and enzymatic proteins as well as proteins predicted to be
885 involved in other cellular processes were excluded.

886

887 Distribution of homologs in cyanobacteria

888 Cyanobacteria species tree is according to Dagan *et al.*[110] with the root of the tree as recently
889 inferred by Tria, Landan and Dagan[111]. Homologs to the *Anabaena* proteins were detected by
890 amino acid sequence similarity using stand-alone BLAST[112] ver. 2.2.26. Protein sequences
891 that were found as BLAST hits with a threshold of E-value ≤ $1x10^{-5}$ were further compared to
892 the *Anabaena* protein by global alignment using needle[113]. Hits having ≥30% identical amino

893 acids in the global alignment were considered as homologs. The phylogenetic tree was
894 visualized with iTOL[114].

895

896 Genomic DNA and RNA isolation and cDNA synthesis

897 Genomic DNA (gDNA) from *Anabaena* was isolated using the GeneJET Plant Genomic DNA
898 Purification Kit (Thermo Fischer Scientific) and the DNeasy Plant Mini Kit (QIAGEN) according
899 to the manufacturer's instructions from 10 ml cyanobacterial cultures.

900 RNA from *Anabaena* WT was isolated using the Direct-zol™ RNA MiniPrep Kit (Zymo
901 Research) according to the manufacturer's instructions. RNA was isolated in technical
902 triplicates from 10 ml cultures. Isolated RNA was treated with DNA-free™ Kit (2 units
903 rDNAs/reaction; Thermo Fischer Scientific) and 200 ng RNA was reverse transcribed using
904 the qScript™ cDNA Synthesis Kit (Quanta Biosciences). RT-PCR of cDNA samples for *mpB*,
905 *cypS*, *ceaR*, *lfiA*, *lfiB* and *lfiA*+*lfiB* was done using primer pairs #1/#2, #3/#4, #5/#6, #7/#8,
906 #9/#10, #7/#10, respectively.

907

908 Transformation

909 Transformation of chemically competent *E. coli* was performed by the standard heat shock
910 procedure[115]. *Anabaena* was transformed by triparental mating according to Ungerer and
911 Pakrasi[116]. Briefly, 100 µl of overnight cultures of DH5α carrying the conjugal plasmid pRL443
912 and DH5αMCR carrying the cargo plasmid and the helper plasmid pRL623, encoding for three
913 methylases, were mixed with 200 µl *Anabaena* culture (for transformation into *Anabaena*
914 mutant strains, cells were scraped from the plate and resuspended in 200 µl BG11). This
915 mixture was directly applied onto sterilized nitrocellulose membranes placed on top of BG11
916 plates supplemented with 5% LB medium. Cells were incubated in the dark at 30 °C for 6-8 h
917 with subsequent transfer of the membranes to BG11 plates. After another 24 h, membranes
918 were transferred to BG11 plates supplemented with appropriate antibiotics.

919

920 Plasmid construction

921 Ectopic expression of *Anabaena* protein candidates was achieved from a self-replicating
922 plasmid (pRL25C[117]) under the control of the copper-inducible *petE* promoter (P_{petE}) or the
923 native promoter (predicted by BPROM[61]) of the respective gene. All constructs were verified
924 by Sanger sequencing (Eurofins Genomics).

925 Initially, we generated pTHS1 (pRL25C, P_{petE}::*lfiA-gfp)*, which served as template for many
926 other pRL25C-based plasmids employed in this study. For this, P_{petE} and *lfiA* were amplified
927 from *Anabaena* gDNA using primers #11/#12 and #13/#14, respectively. *gfpmut3.1* was
928 amplified from pJET1.2 containing P_{petE}-*gfp*[118] using primers #15/#16. This *gfpmut3.1*
929 (hereafter *gfp*) is deprived of its internal NdeI site and contains a 5' linker sequence of 12
930 alternating codons encoding for alanine and serine. The PCR fragments were next ligated into
931 PCR-amplified pRL25C (using primers #17/#18) by Gibson assembly.

932 For pTHS2 (pRL25C, P_{petE}::*lfiB-gfp*) and pTHS3 (pRL25C, P_{petE}::*ceaR-gfp*), *lfiB* and *ceaR* were
933 amplified from *Anabaena* gDNA using primers #19/#20 or #21/#22, respectively and ligated
934 into PCR-linearized pTHS1 (using primers #23/#24; thereby removing only *lfiA* and leaving
935 P_{petE} and *gfp* in the vector) by Gibson assembly.

936 For pTHS4 (pRL25C, P_{petE}::*cypS-gfp*), *cypS* was amplified by PCR from *Anabaena* gDNA
937 using primers #36/#38, introducing NdeI and SacI sites, and then ligated into pJET1.2-
938 P_{petE}::*gfp*, thereby generating P_{petE}::*cypS-gfp* which is flanked by a 5' BamHI site and a 3' EcoRI
939 site. The P_{petE}::*cypS-gfp* fragment was excised by BamHI and EcoRI and ligated into BamHI
940 and EcoRI-digested pRL25C.

941 For pTSH5 (pRL25C, P_{petE}::*trunc-ceaR-gfp*), pTHS3 was amplified using primers #148/#148
942 and re-ligated using Quick Ligase (NEB). Thereby, the first 153 bp from *ceaR* were removed

943 For pTHS6 (P_{petE}::*cypS-his*), *cypS-his* was amplified from pTHS8 using primers #25/#26 and
944 ligated into PCR-linearized pRL25C (using primers #24/#27) by Gibson assembly.

945 For pTHS7 (pRL25C, P_{petE}-*lfiA*-ec*fp,* P_{petE}-*lfiB-gfp*), P_{petE}-*lfiA* was amplified from pTHS1 using
946 primers #28/#29 and ligated into ClaI-digested pRL25C by Gibson assembly together with
947 *myc-link-ecfp* (initially amplified with primers #30/#31, purified and then again amplified with
948 primers #32/#33). This construct was digested by BamHI and ligated by Gibson assembly with
949 PCR-amplified P_{petE}::*lfiB-gfp* from pTHS2 (using primers #34/#35).

950 pET21a(+) plasmids bearing C-terminal His-tag translational fusions of CCRPs were
951 generated by restriction-based cloning techniques. For this, *cypS*, *lfiA*, *lfiB* or *ceaR* were
952 amplified by PCR from *Anabaena* gDNA using primers #36/#37, #39/#40, #41/#42 or #43/#44,
953 respectively, introducing NdeI and XhoI sites. NdeI and XhoI-digested fragments were then
954 ligated into pET21a(+) using Quick Ligase (NEB). This procedure yielded plasmids pTHS8,
955 pTHS9, pTHS10 and pTSH11, respectively.

956 pET21a(+) bearing C-terminal *gfp* translational fusions were generated based on pTHS12
957 (pET21a(+), P_{T7}::*cypS-gfp*). For this, *cypS* was amplified by PCR from *Anabaena* gDNA with
958 primers 36#/#38, introducing NdeI and SacI sites, and ligated into NdeI and SacI-digested

959 pJET1.2 bearing P_{petE}-*gfp*. *cypS-gfp* was excised by NdeI and EcoRI and ligated into NdeI and
960 EcoRI-digested pET21a(+), generating pTHS12. For pTHS13 (pET21a(+), P_{T7}::*ceaR-gfp*),
961 *ceaR-gfp* was amplified by PCR from pTHS3 using primers #47/#48 and ligated into PCR-
962 linearized pTHS12 (primers #49/#50) by Gibson assembly.

963 GFP-fragment reassembly plasmids were generated by Gibson assembly. For this aim, *lfiA*
964 was amplified by PCR from *Anabaena* gDNA with primer 51/52 or 53/54 and ligated into XhoI
965 and BamHI or NheI digested pET11a-link-NGFP, generating pTHS15 or pTHS16. *lfiB* was
966 amplified by PCR from *Anabaena* gDNA with primers 55/56 and ligated into NcoI and AatII
967 digested pMRBAD-link-CGFP, generating pTHS17.

968 Clonings for bacterial two-hybrid plasmids were done using Gibson assembly of PCR-
969 linearized pKNT25, pKT25, pUT18 or pUT18C plasmids, using primers #57/#58 for pKNT25
970 and pUT18, primers #59/#60 for pKT25 and primers 61/62 for pUT18C. For each gene, three
971 primer combinations were used for amplification from *Anabaena* gDNA. The first primer pair
972 was always used for cloning of the respective gene into pKNT25 and pUT18 while the second
973 and third primer pairs were used for cloning into pKT25 or pUT18C, respectively: *cypS* (primers
974 #63/#64, #65/#66 or #67/#68), *lfiA* (primers #69/#70, #71/#72 or #73/#74), *lfiB* (primers
975 #75/#76, #77/#78 or #79/#80), *ceaR* (primers #81/#82, #83/#84 or #85/#86), *sepJ* (primers
976 #87/#88, #89/#90 or #91/#92), *ftsZ* (primers #93/#94, #95/#96 or #97/#98), *mreB* (primers
977 #99/#100, #101/#102 or #103/#104), *fraC* (primers #105/#106, #107/#108 or #109/#110) and
978 *fraD* (primers #111/#112, #113/#114 or #115/#116). This yielded plasmids pTHS17-pTHS52,
979 respectively.

980 Like for P_{petE}-driven expression, native expression of *Anabaena* CCRPs was mediated from
981 the pRL25C plasmid. For pTHS56 (pRL25C, P_{cypS}::*cypS-gfp*), P_{cypS} was amplified from
982 *Anabaena* gDNA using primers #150/#151 and ligated into BamHI and EcoRI-digested
983 pRL25C by Gibson assembly together with *cypS-gfp*, which was amplified from pTHS4 using
984 primers #152/#153.

985 For pTHS57 (pRL25C, P_{ceaR}::*ceaR-gfp*), P_{ceaR} was amplified from *Anabaena* gDNA using
986 primers #154/#155 and ligated into BamHI and EcoRI-digested pRL25C by Gibson assembly
987 together with *ceaR-gfp*, which was amplified from pTHS3 using primers #156/#153.

988 For pTHS58 (pRL25C, P_{lfiA}::*lfiA-gfp*), P_{lfiA} was amplified from *Anabaena* gDNA using primers
989 #157/#158 and ligated into BamHI and EcoRI-digested pRL25C by Gibson assembly together
990 with *lfiA-gfp*, which was amplified from pTHS1 using primers #159/#153.

991 For pTHS59 (pRL25C, P_{lfiB}::*lfiB-gfp*), P_{lfiB} was amplified from *Anabaena* gDNA using primers
992 #160/#161 and ligated into BamHI and EcoRI-digested pRL25C by Gibson assembly together
993 with *lfiB-gfp*, which was amplified from pTHS2 using primers #162/#153.

994 For pTHS60 (pRL25C, P_{cypS}::*cypS-his*), P_{cypS} was amplified from *Anabaena* gDNA using
995 primers #150/#151 and ligated into BamHI and EcoRI-digested pRL25C by Gibson assembly
996 together with *cypS-his*, which was amplified from pTHS8 using primers #152/#163.

997 For pTHS61 (pRL25C, P_{ceaR}::*ceaR*), P_{ceaR}::*ceaR* was amplified from *Anabaena* gDNA using
998 primers #154/#164 and ligated into BamHI and EcoRI-digested pRL25C by Gibson assembly.

999 For pTHS58 (pRL25C, $P_{lfiA/B}$::*lfiA-lfiB*), $P_{lfiA/B}$::*lfiA-lfiB* was amplified from *Anabaena* gDNA using
1000 primers #157/#165 and ligated into BamHI and EcoRI-digested pRL25C by Gibson assembly.

1001

1002 *Anabaena* mutant strain construction

1003 All *Anabaena* mutant strains were generated using the pRL278-based double homologous
1004 recombination system employing the conditionally lethal *sacB* gene[119]. For this, 1500 bp
1005 upstream and downstream of the gene to be replaced were generated by PCR from *Anabaena*
1006 gDNA. Upstream and downstream regions of *cypS* and *ceaR*, were amplified using primers
1007 #121/#122 and #123/#124 or #125/#126 and #127/#128, respectively. Upstream region of *lfiA*
1008 was amplified using primers #129/#130 and downstream region of *lfiB* was amplified using
1009 primers #131/#132. The respective upstream and downstream homology regions flanking the
1010 CS.3 cassette (amplified with primer #119/#120 from pCSEL24) were then inserted into PCR-
1011 amplified pRL278 (using primer #117/#118) by Gibson assembly, yielding pTHS55, pTHS56
1012 and pTHS57, respectively. *Anabaena* transformed with those plasmids was subjected to
1013 several rounds of re-streaking on new plates (about 5-8 rounds for each strain). To test for fully
1014 segregated clones, colony PCRs were performed. For this, *Anabaena* cells were resuspended
1015 in 10 µl sterile H_2O of which 1 µl was used for standard PCR with internal gene primers #3/#4,
1016 #5/#6 and #7/#10 for Δ*cypS*, Δ*ceaR* and Δ*lfiA*Δ*lfiB,* respectively. Correct placement of the
1017 CS.3 cassette was then further confirmed using primers CS.3 cassette primers with primers
1018 binding outside of the 5' and 3' flanks used for homologous recombination (#137/#118 and
1019 #117/#138 for Δ*cypS*, #135/#118 and #117/#136 for Δ*ceaR* and #133/#118 and #117/#134 for
1020 Δ*lfiA*Δ*lfiB*).

1021 Growth curve analysis

1022 For analysis of mutant viability, growth curves of *Anabaena* WT and Δ*ceaR* mutant strain were
1023 performed. For this, cells were grown in BG11 liquid medium, washed three times by
1024 centrifugation (6500 x *g*, RT, 3 min) in BG11 or $BG11_0$, adjusted to an OD_{750} of 0.1 and then
1025 grown in triplicates at standard growth conditions in 15 ml culture volumes. OD_{750} values were
1026 recorded once a day for 24 d.

1027 Fluorescence microscopy

1028 Bacterial strains grown in liquid culture were either directly applied to a microscope slide or
1029 previously immobilized on a 2% low-melting agarose in PBS (10 mM Na_2HPO_4, 140 mM NaCl,
1030 2.7 mM KCl, 1.8 mM KH_2PO_4, pH 7.4) agarose pad and air dried before microscopic analysis.
1031 Epifluorescence was done using an Axio Imager.M2 light microscope (Carl Zeiss) equipped
1032 with Plan-Apochromat 63x/1.40 Oil M27 objective and the AxioCam MR R3 imaging device
1033 (Carl Zeiss). GFP, Alexa Fluor 488 and BODIPY™ FL Vancomycin (Van-FL) fluorescence was
1034 visualized using filter set 38 (Carl Zeiss; excitation: 470/40 nm band pass (BP) filter; emission:
1035 525/50 nm BP). Chlorophyll auto-fluorescence was recorded using filter set 15 (Carl Zeiss;
1036 excitation: 546/12 nm BP; emission: 590 nm long pass). When applicable, cells were previously
1037 incubated in the dark at RT for about 5 min with 10 µg ml^{-1} DAPI (final concentration) to stain
1038 intracellular DNA. For visualization of DAPI fluorescence filter set 49 (Carl Zeiss; excitation: G
1039 365 nm; emission: 455/50 nm) was employed. For confocal laser scanning microscopy, the
1040 LSM 880 Axio Imager 2 equipped with a C-Apochromat 63x/1.2 W Korr M27 objective and an
1041 Airyscan detector (Carl Zeiss) was used and visualization of GFP, eCFP and chlorophyll auto-
1042 fluorescence was done using Zen black smart setup settings. Also, to investigate putative
1043 alterations of the polysaccharide sheath of *Anabaena* mutants, cells were grown on $BG11_0$
1044 agar plates, re-suspended in $BG11_0$ liquid medium and stained with 0.05% alcian blue (final
1045 concentration). Polysaccharide staining of *Anabaena* cells immobilized on an agarose pad was
1046 then observed with an Axiocam ERc 5s color camera (Carl Zeiss). *E. coli* BL21 (DE3) cells
1047 expressing C-terminally GFP-tagged protein candidates were were grown over night in LB and
1048 then diluted 1:40 in the same medium the following day. Cells were grown for 2 h at 37 °C,
1049 briefly acclimated to 20 °C for 10 min and induced with 0.05 mM IPTG at 20 °C. Protein
1050 localization of GFP-tagged proteins was then observed after indicated time points of cells
1051 immobilized on an agarose pad.

1052 Transmission electron microscopy and sacculi preparation

1053 For ultra-structure analysis, *Anabaena* filaments were fixed with 2.5% glutaraldehyde,
1054 immobilized in 2% agaorse, treated with 2% potassium permanganate and dehydrated through
1055 a graded ethanol series. The fixed cells were infiltrated by ethanol:EPON (2:1 to 1:2 ratio) and
1056 embedded in pure EPON. Ultrathin sections were prepared with a Leica UC6iUltramicrotome,
1057 transferred to formvar coated copper grids and post-stained with uranyl acetate and lead
1058 citrate[120]. Micrographs were recorded at a Philips Tecnai10 electron microscope at 80 kV.

1059 Peptidoglycan sacculi were isolated from filaments grown on BG11 agar plates by the method
1060 of Kühner *et al.*[121] with the following modifications: Cells were sonicated (Branson Sonifier 250;
1061 duty cycle 50%, output control 1, 2 min) prior to boiling in 0.1 M Tris-HCl pH 6.8 with 3% SDS.
1062 After incubation in a sonifier waterbath, the samples were incubated with α-Chymotrypsin (600
1063 µg ml^{-1}) at 37 °C over night in 50 mM Na_3PO_4 buffer pH 6.8. After inactivation of the enzyme,
1064 the sample was sonified again and loaded on a formvar/carbon film coated copper grid
1065 (Science Services GmbH, Munich) and stained with 1 % (w/v) uranyl acetate as described
1066 previously[122]. Images were taken with a Philips Tecnai10 electron microscope at 80 kV.

1067

1068 Calcein labelling and fluorescence recovery after photobleaching (FRAP) experiments

1069 *Anabaena* WT and mutant strains were either grown on BG11 plates and resuspended in BG11
1070 or directly taken from liquid cultures, washed several times in BG11, resuspended in 0.5 ml
1071 BG11 and incubated with 10 µl calcein-AM (1 mg ml^{-1} in DMSO). The cells were incubated in
1072 the dark at 30 °C for 1 hour and then subjected to four washing steps with 1 ml BG11.
1073 Subsequently, cells were resuspended in a small volume of BG11, spotted on BG11 agar
1074 plates (1 % w/v) and air dried. Samples were visualized by using an inverted confocal laser
1075 scanning microscope (Leica TCS SP5) with a x63 oil immersion objective (HCX PL APO 63x
1076 1.40-0.60 OIL CS). Fluorescence was excited at 488 nm and emission monitored by collecting
1077 across a window of 500 to 530 nm with a maximally opened pinhole (600 µm). FRAP
1078 experiments were carried out by an automated routine as previously described (Mullineaux *et*
1079 *al.* EMBO). After recording an initial image, selected cells were bleached by increasing the
1080 laser intensity by a factor of 5 for two subsequent scans and the fluorescence recovery followed
1081 in 0.5 s intervals for 30 s was recorded using the Leica LAS X software. Exchange coefficients
1082 (*E*) were then calculated according to Mullineaux *et al*. and Nieves-Morión *et al.*[43,101].

1083 BODIPY™ FL Vancomycin (Van-FL) staining

1084 Van-FL staining of BG11-grown filaments of the *Anabaena* WT and mutant strains was
1085 essentially performed as previously described by Lehner *et al.*[47] and Rudolf *et al.*[123]. Briefly,
1086 cells were resuspended in BG11 medium, washed once in BG11 by centrifugation (6500 x *g*,
1087 4 min, RT) and incubated with 5 µg ml^{-1} Van-FL (dissolved in methanol). Cells were incubated
1088 in the dark for 1 hour at 30 °C, washed three times with BG11 and immobilized on an agarose
1089 pad. Van-FL fluorescence signals were then visualized using epifluorescence microscopy with
1090 an excitation time of 130 ms. Arithmetic mean fluorescence intensities were then recorded
1091 from the septa between two cells with a measured area of 3.52 μm^2 using the histogram option
1092 of the Zen blue 2.3 software (Carl Zeiss).

1093

1094 Data analysis

1095 Cell length, volume and roundness were determined using the imaging software ImageJ. Cell
1096 volume was calculated based on the assumption of an elliptic cell shape of *Anabaena* cells
1097 using the Major Axis and Minor Axis values given by ImageJ and the formula for the volume of
1098 an ellipse ($V = \frac{4}{3}\pi abc$):

1099 • $V = \frac{4}{3}\pi\left(\left(\frac{Major\ Axis}{2}\right)^2 \frac{Minor\ Axis}{2}\right)$

1100 Distribution of DAPI fluorescence signals was done in ImageJ with the Plot Profile option along
1101 151 single cells with rectangle tool. The resulting grey values were arranged according to the
1102 maximum intensity focus and the width of the DAPI focal area was calculated as the range of
1103 DAPI staining around the maximum (± 10 grey value in arbitrary units).

1104

1105 Bacterial two-hybrid and beta galactosidase assays

1106 Chemically competent *E. coli* BTH101 cells were co-transformed with 5 ng of plasmids carrying
1107 the respective T18 and T25 translational fusion constructs, plated onto LB plates
1108 supplemented with 200 µg ml^{-1} X-gal, 0.5 mM IPTG, Amp, Km and grown at 30°C for 24-36 h.
1109 Interactions were quantified by beta-galactosidase assays from three independent colonies.
1110 For this aim, cultures were either grown over night at 30 °C or for two days at 20 °C in LB Amp,
1111 Km, 0.5 mM IPTG and beta-galactosidase activity was recorded as described in the
1112 manufacturer's instructions (Euromedex; BACTH System Kit Bacterial Adenylate Cyclase
1113 Two-Hybrid System Kit) in a 96 well plate according to Karimova, Davi and Ladant[103].

1114 GFP-fragment reassembly assay

1115 Chemically competent *E. coli* BL21 (DE3) were co-transformed with indicated plasmid
1116 combinations, plated on LB Amp, Km and grown over night at 37 °C. Liquid overnight cultures
1117 of single colonies of the respective plasmid-bearing *E. coli* strains were then diluted 1:40 in the
1118 same medium the following day. Cells were grown for 2 h at 37 °C, briefly acclimated to 20 °C
1119 for 10 min and protein expression was induced with 0.05 mM IPTG and 0.2% L-arabinose.
1120 Pictures of induced cultures grown at 20 °C were taken after 48 h of cells immobilized on an
1121 agarose pad.

1122

1123 Co-immunoprecipitation

1124 About 20-30 ml of the respective *Anabaena* culture was pelleted by centrifugation (4800 x *g*,
1125 10 min, RT), cells were washed twice by centrifugation (4800 x *g*, 10 min, RT) with 40 ml PBS
1126 and then resuspended in 1 ml lysis buffer (PBS-N: PBS supplemented with 1% NP-40)
1127 supplemented with protease inhibitor cocktail (PIC; cOmplete™, EDTA-free Protease Inhibitor
1128 Cocktail, Sigma-Aldrich). Cells were lysed using the VK05 lysis kit (Bertin) in a Precellys® 24
1129 homogenizer (3 strokes for 30 seconds at 6500 rpm) and cell debris was pelleted by
1130 centrifugation (30 min, 21,100 x *g*, 4 °C). 50 µl µMACS anti-GFP MicroBeads (Miltenyi Biotec)
1131 was added to the resulting cell-free supernatant and incubated for 1 h at 4 °C with mild rotation.
1132 Afterwards, the sample was loaded onto µColumns (Miltenyl Biotec), washed two times with 1
1133 ml lysis buffer and eluted in 50 µl elution Buffer (50 mM Tris HCl pH 6.8, 50 mM DTT, 1% SDS,
1134 1 mM EDTA, 0.005% bromphenol blue, 10% glycerol; Miltenyl Biotec). Until further use,
1135 samples were stored at -80 °C.

1136

1137 Mass spectrometry analysis

1138 Coomassie stained gel bands were excised and protein disulfide bonds were reduced with 10
1139 mM dithiotreitol at 56 °C for 45 min and alkylated with 55 mM iodoacetamide at RT for 30 min
1140 in the dark. The gel bands were washed 50 mM ammonium bicarbonate and subsequently
1141 dehydrated with acetonitrile. 10 µl trypsin (5 ng μl^{-1} in 25 mM ammonium bicarbonate) were
1142 added and the gel bands were rehydrated for 5 min at 37 °C. Samples were digested over
1143 night at 37 °C. Prior to peptide extraction samples were acidified with 10% formic acid. After
1144 transferring the supernatant into a new Eppendorf tube, 5% formic acid was added to the gel
1145 bands and incubated for 10 min. Subsequently the samples were sonicated for 1 min in ice-
1146 cooled water and the supernatant was combined with the one from the step before. Two
1147 additional extraction steps with 60% acetonitrile/1% formic acid and 100% acetonitrile were

1148 performed in the same manner. The combined supernatants were dried in the SpeedVac and
1149 the samples were reconstituted in 30 µL 3% acetonitrile/0.1% trifluoroacetic acid. LC-MS/MS
1150 analysis was performed using a Dionex U3000 nanoUHPLC coupled to a Q Exactive Plus
1151 mass spectrometer (both from Thermo Scientific). The LC-MS/MS parameters were as follows:
1152 Six microliter were injected and loaded on a trap column (Acclaim Pepmap 100 C18, 10 mm ×
1153 300 µm, 3 µm, 100 Å, Dionex) and washed for 3 min with 2% ACN/0.05% TFA at a flow-rate
1154 of 30 µL min^{-1}. separation was performed using an Acclaim PepMap 100 C18 analytical column
1155 (50 cm × 75 µm, 2 µm, 100 Å, Dionex) with a flow-rate of 300 nL/min and following eluents: A
1156 (0.05% FA) and B (80% ACN/0.04% FA); linear gradient 5-40% B in 60 min, 50-90% B in 5
1157 min, 90% B for 10 min, 90-5% B in 1 min and equilibrating at 5% B for 11 min. Ionization was
1158 performed with 1.5 kV spray voltage applied on a non-coated PicoTip emitter (10 µm tip size,
1159 New Objective, Woburn, MA) with the source temperature set to 250°C. MS data were acquired
1160 from 5 to 85 min with MS full scans between 300 and 1,800 m/z at a resolution of 70,000 at
1161 m/z 200. The 10 most intense precursors with charge states ≥2+ were subjected to
1162 fragmentation with HCD with NCE of 27%; isolation width of 3 m/z; resolution, 17,500 at m/z
1163 200. Dynamic exclusion for 30 s was applied with a precursor mass tolerance of 10 ppm. Lock
1164 mass correction was performed based on the polysiloxane contaminant signal of 445.120025
1165 m/z. Additional wash runs were performed between samples from gel bands to reduce carry
1166 over while cytochrome C was used to monitor mass accuracy and LC quality control. The
1167 acquired MS/MS data were searched with the SequestHT algorithm against the entire
1168 reviewed Uniprot protein database of *Nostoc* sp. PCC 7120 including plasmids (6922
1169 sequences in total). Static modifications applied were carbamidomethylation on cysteine
1170 residues, while oxidation on methionine residues was set as dynamic modification. Spectra
1171 were searched with full enzyme specificity. A MS mass tolerance of 10 ppm and a MS/MS
1172 tolerance of 0.02 Da was used. Proteins were identified with at least three unique peptides
1173 with a FDR confidence ≤ 0.01 (high).
1174

1175 Immunofluorescence

1176 Immunolocalization of CypS-His and FtsZ in *Anabaena* was essentially performed as
1177 described by Ramos-León *et al.*[82]. For visualization of FtsZ, *Anabaena* WT and mutant strains
1178 were streaked from growth plates (BG11 and $BG11_0$ plates), resuspended in a small volume
1179 of distilled water and air-dried on Polysine® adhesion slides (Menzel) at RT followed by fixation
1180 and permeabilization with 70% ethanol for 30 min at -20 °C. Cells were allowed to air dry for
1181 30 min at RT and then washed two times with PBST (PBS supplemented with 0.1% (v/v)
1182 Tween-20) for 2 min. Unspecific binding sites were blocked for 30 min at RT with blocking
1183 buffer (1x Roti®-ImmunoBlock in PBST; Carl Roth) and afterwards rabbit anti-FtsZ (Agrisera;

1184 1:150 diluted) antibody in blocking buffer was added to the cells and incubated for 1.5 h at RT
1185 in a self-made humidity chamber followed by five washing steps with PBST. 7.5 µg ml^{-1} Alexa
1186 Fluor 488-conjugated goat anti-rabbit IgG (H+L) secondary antibody (Thermo Fischer
1187 Scientific) in blocking buffer was added to the cells and incubated for 1 h at RT in the dark in
1188 a self-made humidity chamber. Subsequently, cells were washed five times with PBST, air
1189 dried and mounted with ProLong™ Diamond Antifade Mountant (Thermo Fischer Scientific)
1190 overnight at 4 °C. Immunolocalization of FtsZ was then analyzed by epifluorescence
1191 microscopy. Similarly, *in vivo* localization of CypS-His expressed in *Anabaena* was evaluated
1192 by immunolocalization of $BG11_0$ grown liquid cultures, induced with 0.25 µM $CuSO_4$ for two
1193 days, and compared to *Anabaena* WT cells using mouse anti-His primary antibody (1:500
1194 diluted; Thermo Fischer Scientific).

1195

1196 Spot assays

1197 Spot assays were essentially performed as described by Dörrich *et al.*[124]. *Anabaena* WT and
1198 mutant strains were grown on BG11 growth plates, resuspended in BG11 liquid medium and
1199 adjusted to an OD_{750} of 0.4. Cells were then spotted in triplicates of 5 µl onto the respective
1200 growth plates containing either no additives (BG11 or $BG11_0$), 50 µg ml^{-1} Proteinase K or
1201 100 µg ml^{-1} lysozyme in serial 1/10 dilutions and incubated under standard growth conditions
1202 until no further colonies arose in the highest dilution.

1203

1204 Protein purification and *in vitro* filamentation assays

1205 For protein purification, *E. coli* BL21 (DE3) cells carrying His-tagged protein candidates were
1206 grown in overnight cultures at 37 °C and 250 rpm. The next day, overnight cultures were diluted
1207 1:40 in the same medium and grown at 37 °C until they reached an OD_{600} of 0.5-0.6. Protein
1208 expression was induced with 0.5 mM IPTG for 3-4 h at 37 °C and 250 rpm. Afterwards, cell
1209 suspensions of 50 ml aliquots were harvested by centrifugation, washed once in PBS and
1210 stored at -80 °C until further use. For *in vitro* filamentation assays, cell pellets were
1211 resuspended in urea lysis buffer (ULB: 50 mM NaH_2PO_4, 300 mM NaCl, 25 mM imidazole,
1212 6 M urea; pH 8.0) and lysed in a Precellys® 24 homogenizer (3x 6500 rpm for 30 s) using the
1213 2 ml microorganism lysis kit (VK01; Bertin) or self-packed Precellys tubes with 0.1 mm glass
1214 beads. The resulting cell debris was pelleted by centrifugation at 21,000 x *g* (30 min, 4 °C) and
1215 the supernatant was incubated with 1 ml HisPur™ Ni-NTA resin (Thermo Fischer Scientific)
1216 for 1 h at 4°C in an overhead rotator. The resin was washed 5 times with 4x resin-bed volumes
1217 ULB and eluted in urea elution buffer (UEB: ULB supplemented with 225 mM imidazole). Total

1218 protein concentration was measured using the Qubit® 3.0 Fluorometer (Thermo Fischer
1219 Scientific) and generally adjusted to 0.5-1.0 mg ml^{-1} before dialysis. Filament formation of
1220 purified proteins was induced by overnight dialysis against polymerization buffer (PLB: 50 mM
1221 PIPES, 100 mM KCl, pH 7.0; HLB: 25 mM HEPES, 150 mM NaCl, pH 7.4; or 25 mM HEPES
1222 pH 7.5) at 20 °C and 180 rpm with three bath changes using a Slide-A-Lyzer™ MINI Dialysis
1223 Device (10K MWCO, 0.5 ml or 2 ml; Thermo Fischer Scientific). Purified proteins were stained
1224 with an excess of NHS-Fluorescein (dissolved in DMSO; Thermo Fischer Scientific) and
1225 *in vitro* filamentation was analyzed by epifluorescence microscopy.

1226

1227 **Data availability**

1228 All data generated or analyzed during this study are included in this published article (and its
1229 supplementary information files). The datasets generated during and/or analyzed during the
1230 current study are available from the corresponding authors on reasonable request.

1231 **Supplementary Table 2: Cyanobacterial strains used in this study**

Strain	Genotype	Resistance Marker	Source
Anabaena sp. PCC 7120	WT		Pasteur culture collection of Cyanobacteria (PCC)
BLS1	*Anabaena* Δ*cypS*::CS.3	Sp, Sm	This study
BLS2	*Anabaena* (Δ*lfiA*Δ*lfiB*)::CS.3	Sp, Sm	This study
BLS3	*Anabaena* Δ*ceaR*::CS.3	Sp, Sm	This study

1232 Sp = spectinomycin, Sm = streptomycin

1233 **Supplementary Table 3: *E. coli* strains used in this study**

Strain	Genotype	Resistance	Source
DH5αMCR	F- *endA1 supE44 thi-1* λ^- *recA1 gyrA96 relA1 deoR* Δ(*lacZYA-argF*)U169 Φ80d*lac*ZΔM15 *mcrA* Δ(*mrr* hsdRMS *mcrBC*)		Grant *et al.,*1990 ([125])
BL21 (DE3)	F^- *ompT gal dcm lon hsdS*$_B$($r_B^- m_B^-$) λ(DE3 [*lacI lacUV5-T7p07 ind1 sam7 nin5*]) [*malB*$^+$]$_{K-12}$(λ^S)		Studier *et al.,* 1986 ([126])
BTH101	F^-, *cya-99*, *araD139*, *galE15*, *galK16*, *rpsL1* (*Str*$_r$), *hsdR2, mcrA1,mcrB1*	Sm	Euromedex
XL1-blue	endA1 gyrA96(nal^R) thi-1 recA1 relA1 lac glnV44 F'[::Tn10 proAB$^+$ lacI^q Δ(*lacZ*)M15] *hsdR17*(r_K^- m_K^+)	Tet	Stratagene
HB101	F^- *mcrB mrr hsd*S20(r_B^- m_B^-) *rec*A13 *leuB*6 *ara*-14 *pro*A2 *lac*Y1 *gal*K2 *xyl*-5 mtl-1 rpsL20(Sm^R) glnV44 λ^-	Sm	Boyer & Roulland-Dessoix, 1969 ([127])

1234 Tet = tetracycline

1235 **Supplementary Table 4: Plasmids used in this study**

Name	Description	Resistance	Source
pET21a(+)	Bacterial vector for expressing N- terminal T7 and/or C-terminal His6-tagged proteins in *E. coli*	Amp	Novagen
pRL25C	Shuttle cosmid vector for cyanobacteria and *E. coli*	Km, Nm	Wolk *et al.,* 1988 ([117])
pRL623	Methylation plasmid	Cm	Wolk *et al.,* 1988 ([117])
pRL443	Conjugation plasmid	Amp	Wolk *et al.,* 1988 ([117])
pRL278	Suicide vector used for homologous recombination in cyanobacteria; contains *sacB* for positive selection of double recombination events	Km, Nm	Wolk *et al.,* 1988 ([117])
pKNT25	P_{lac}::-*T25*	Km	Euromedex
pKT25	P_{lac}::*T25*-	Km	Euromedex
pUT18	P_{lac}::-*T18*	Amp	Euromedex
pUT18C	P_{lac}::*T18*-	Amp	Euromedex
pKT25-zip	pKT25; P_{lac}::*T25-zip*	Km, Nm	Euromedex
pUT18C-zip	pUT18C, P_{lac}::*T18-zip*	Amp	Euromedex

pET11a-link-NGFP	IPTG-inducible expression vector for translational fusion of target gene with a N-terminal *gfp* fragment in *E. coli*	Amp	Wilson *et al.,* 2004 ([99])
pMRBAD-link-CGFP	L-arabinose-inducible expression vector for translational fusion of target gene with a C-terminal *gfp* fragment in *E. coli*	Km	Wilson *et al.,* 2004 ([99])
pAM5084	P_{trc}::*ecfp-kaiC*	Amp	Cohen *et al.,* 2014 ([128])
pCSEL24	Integrates into the *nucA-nuiA* region of *Anabaena*	Amp, Sm, Sp	Olmedo-Verd *et al.,* 2006 ([129])
pJET1.2-P*petE-gfp*	pJET1.2 vector containing P_{petE}::*gfp*[a)]	Amp	Stucken *et al.,* 2012 ([118])
pTHS1	pRL25C, P_{petE}::*lfiA-gfp*	Km, Nm	This study
pTHS2	pRL25C, P_{petE}::*lfiB-gfp*	Km, Nm	This study
pTHS3	pRL25C, P_{petE}::*ceaR-gfp*	Km, Nm	This study
pTHS4	pRL25C, P_{petE}::*cypS-gfp*	Km, Nm	This study
pTHS5	pRL25C, P_{petE}::*trunc-ceaR-gfp* (truncated *ceaR* without the N-terminal transmembrane domain; first 156 base pairs removed)	Km, Nm	This study
pTHS6	pRL25C, P_{petE}::*cypS-his*	Km, Nm	This study
pTHS7	pRL25C, P_{petE}::*lfiA*-ec*fp*[b)], P_{petE}::*lfiB-gfp*	Km, Nm	This study
pTHS8	pET21a(+),P_{T7}::*cypS-his*	Amp	This study
pTHS9	pET21a(+), P_{T7}::*lfiA-his*	Amp	This study
pTHS10	pET21a(+), P_{T7}::*lfiB-his*	Amp	This study
pTHS11	pET21a(+), P_{T7}::*ceaR-his*	Amp	This study
pTHS12	pET21a(+); P_{T7}::*cypS-gfp*	Amp	This study
pTHS13	pET21a(+), P_{T7}::*ceaR-gfp*	Amp	This study
pTHS14	pET11a-link-NGFP, P_{T7}::*ngfp-lfiA*	Amp	This study
pTHS15	pET11a-link-NGFP, P_{T7}::*lfiA-ngfp*	Amp	This study
pTHS16	pMRBAD-link-CGFP, P_{ara}::*lfiB-cgfp*	Km	This study
pTHS17	pKNT25, P_{lac}::*cypS-T25*	Km, Nm	This study
pTHS18	pKT25, P_{lac}::*T25-cypS*	Km, Nm	This study
pTHS19	pUT18, P_{lac}::*cypS-T18*	Amp	This study
pTHS20	pUT18C, P_{lac}::*T18-cypS*	Amp	This study
pTHS21	pKNT25, P_{lac}::*lfiA-T25*	Km, Nm	This study
pTHS22	pKT25, P_{lac}::*T25-lfiA*	Km, Nm	This study
pTHS23	pUT18, P_{lac}::*lfiA-T18*	Amp	This study
pTHS24	pUT18C, P_{lac}::*T18-lfiA*	Amp	This study
pTHS25	pKNT25, P_{lac}::*lfiB-T25*	Km, Nm	This study
pTHS26	pKT25, P_{lac}::*T25-lfiB*	Km, Nm	This study
pTHS27	pUT18, P_{lac}::*lfiB-T18*	Amp	This study
pTHS28	pUT18C, P_{lac}::*T18-lfiB*	Amp	This study
pTHS29	pKNT25, P_{lac}::*ceaR-T25*	Km, Nm	This study
pTHS30	pKT25, P_{lac}::*T25-ceaR*	Km, Nm	This study
pTHS31	pUT18, P_{lac}::*ceaR-T18*	Amp	This study

pTHS32	pUT18C, P_{lac}::*T18-ceaR*	Amp	This study
pTHS33	pKNT25, P_{lac}::*sepJ-T25*	Km, Nm	This study
pTHS34	pKT25, P_{lac}::*T25-sepJ*	Km, Nm	This study
pTHS35	pUT18, P_{lac}::*sepJ-T18*	Amp	This study
pTHS36	pUT18C, P_{lac}::*T18-sepJ*	Amp	This study
pTHS37	pKNT25, P_{lac}::*ftsZ-T25*	Km, Nm	This study
pTHS38	pKT25, P_{lac}::*T25-ftsZ*	Km, Nm	This study
pTHS39	pUT18, P_{lac}::*ftsZ-T18*	Amp	This study
pTHS40	pUT18C, P_{lac}::*T18-ftsZ*	Amp	This study
pTHS41	pKNT25, P_{lac}::*mreB-T25*	Km, Nm	This study
pTHS42	pKT25, P_{lac}::*T25-mreB*	Km, Nm	This study
pTHS43	pUT18, P_{lac}::*mreB-T18*	Amp	This study
pTHS44	pUT18C, P_{lac}::*T18-mreB*	Amp	This study
pTHS45	pKNT25, P_{lac}::*fraC-T25*	Km, Nm	This study
pTHS46	pKT25, P_{lac}::*T25-fraC*	Km, Nm	This study
pTHS47	pUT18, P_{lac}::*fraC-T18*	Amp	This study
pTHS48	pUT18C, P_{lac}::*T18-fraC*	Amp	This study
pTHS49	pKNT25, P_{lac}::*fraD-T25*	Km, Nm	This study
pTHS50	pKT25, P_{lac}::*T25-fraD*	Km, Nm	This study
pTHS51	pUT18, P_{lac}::*fraD-T18*	Amp	This study
pTHS52	pUT18C, P_{lac}::*T18-fraD*	Amp	This study
pTHS53	pRL278 containing 1500 bp upstream and downstream of *cypS* flanking the CS.3 cassette	Nm, Km, Sm, Sp	This study
pTHS54	pRL278 containing 1500 bp upstream and downstream of *ceaR* flanking the CS.3 cassette	Nm, Km, Sm, Sp	This study
pTHS55	pRL278, containing 1500 bp upstream of *lfiA* and 1500 bp downstream of *lfiB* flanking the CS.3 cassette	Nm, Km, Sm, Sp	This study
pTHS56	pRL25C, P_{cypS}::*cypS-gfp*	Nm, Km,	This study
pTHS57	pRL25C, P_{ceaR}::*ceaR-gfp*	Nm, Km,	This study
pTHS58	pRL25C, P_{lfiA}::*lfiA-gfp*	Nm, Km,	This study
pTHS59	pRL25C, P_{lfiB}::*lfiB-gfp*	Nm, Km,	This study
pTHS60	pRL25C, P_{cypS}::*cypS-his*	Nm, Km,	This study
pTHS61	pRL25C, P_{ceaR}::*ceaR*	Nm, Km,	This study
pTHS62	pRL25C, $P_{lfiA/B}$::*lfiA-lfiB*	Nm, Km,	This study

Km = kanamycin, Nm = neomycin, Amp = ampicillin; Cm = chloramphenicol

- a) Modified gfpmut3.1[118] in which the internal NdeI site was removed by replacing CAT by the synonymous CAC codon. The GFP is N-terminally preceded by 12 alanine and serine residues. Abbreviated: *gfp*.
- b) eCFP from Cohen *et al.* (2014)[128] was adjusted for C-terminal translational fusion instead of N-terminal fusion. For this, a N-terminal Myc sequences followed by a seven amino acid linker (GSGSGSG) and an additional stop codon at the C-terminus were added.

1243 **Supplementary Table 5: Oligonucleotides used in this study**

#	Given name	Sequence (5' - > 3')
1	rnpB_intern_A	TGCTGGATAACGTCCAGTGC
2	rnpB_intern_B	GGTTTACCGAGCCAGTACCTC
3	Nos295_intern_A	CAAAGTCAGGCGATGAGTGA
4	Nos295_intern_B	GGAACCGCATTACCAGAAGT
5	Nos842_intern_A	TCGGGCAGAAATTACCCAGT
6	Nos842_intern_B	TGCCATTCTTCAGGCAAAGC
7	Nos903_intern_A	TCAGCTAGACGTAAAGAGTGGC
8	Nos903_intern_B	TAATTCTGCTGGGAATGCAGC
9	Nos904_intern_A	TGGAATTAGCGAAGGGGTGG
10	Nos904_intern_B	TGTTCATAGCCATCTGTTGCCA
11	petE_903_Fwd	GAGATTATCAAAAAGGATCCCAGTACTCAGAATTTTTTGCTGAGGTACT
12	petE_903_Rev	TTGAGTGCAACTGTCGTCATGGCGTTCTCCTAACCTGTAGTTTTATTTTT
13	pRL25-Nos903_Fwd	CTACAGGTTAGGAGAACGCCATGACGACAGTTGCACTCAAAGATAG
14	pRL25-Nos903_Rev	GCACTAGCAGATGCACTAGCTTTAGCCGTAGAACTATCAAAAGCTCTCATTGC
15	GFP_903_Fwd	TTGATAGTTCTACGGCTAAAGCTAGTGCATCTGCTAGTGCTAGT
16	GFP_903_Rev	CTTTCGTCTTCAAGAATTCTTTATTTGTATAGTTCATCCATGCCATGTGTAATCC
17	pRL25c-903_V_F	TGGATGAACTATACAAATAAAGAATTCTTGAAGACGAAAGGGCC
18	pRL25c-903_V_R	GCAAAAAATTCTGAGTACTGGGATCCTTTTTGATAATCTCATGACCAAAATCC
19	Nos904-2A	CTACAGGTTAGGAGAACGCCATGGCAGTCAAAAAGTTAACAGACAAAAAC
20	Nos904_2B	GCACTAGCAGATGCACTAGCTTTATTTTTCACTTGACTTTTTGCCTGTTCTAAAGC
21	Nos842_2A	TACAGGTTAGGAGAACGCCATGCAACAAGTCATAGTAAGTAATCGATT
22	Nos842_2B	CACTAGCAGATGCACTAGCGGATGCGTATCTAGCTATTAGATGTTC
23	pRL25c_NEB_Fwd	GCTAGTGCATCTGCTAGTGCTAGTG
24	pRL25c_NEB_Rev	GGCGTTCTCCTAACCTGTAGTTTTATTTTTCT
25	Nos295His_2A	TACAGGTTAGGAGAACGCCATGCTGTATTTAGCAGAAGTACAAAAG
26	Nos295His_2B	CCTTTCGTCTTCAAGAATTCTTCAGTGGTGGTGGTGGTG
27	MBP7_1A	AGAATTCTTGAAGACGAAAGGGCC
28	petE_2A	ACTACCGCATTAAAGCTTATCAGTACTCAGAATTTTTTGCTGAGGTAC
29	Nos903_2B	TTCGCTGATAAGCTTCTGTTCTTTAGCCGTAGAACTATCAAAAGCTCTC
30	Linker_eCFP_3A	GGCTCTGGATCGGGTTCAGGAATGGTGAGCAAGGGCGAG
31	eCFP_3B	CTGCTGCTTACTTGTACAGCTCGTCCATGCC

32	MYC_Linker_3A2	GAACAGAAGCTTATCAGCGAAGAAGATCTGGGCTCTGGATCGGGTTCAG
33	eCFP_3B2	TCATGTTTGACAGCTTATCATTTACTTGTACAGCTCGTCCATGCC
34	petE_BamHI_2A	TTGGTCATGAGATTATCAAAAAGCAGTACTCAGAATTTTTTGCTGAGG
35	GFP_BamHI_2B	ATTGATTTAAAACTTCATTTTTAATTTAAAAGTTATTTGTATAGTTCATCCATGCCATGTG
36	Nos295_NdeI_Fwd	GCTACATATGCTGTATTTAGCAGAAGTACAAA
37	Nos295_XhoI_wo_R	GCTACTCGAGAGATGCCAACAACTCAGG
38	Nos295_SacI_wo_R	GCTAGAGCTCAGATGCCAACAACTCAGG
39	Nos903_NdeI_F	GCTACATATGACGACAGTTGCACTCA
40	Nos903_XhoI_R_w/o	GCTACTCGAGTTTAGCCGTAGAACTATCAAAAGC
41	Nos904_NdeI_F	GCTACATATGGCAGTCAAAAAGTTAACAGAC
42	Nos904_XhoI_wo_R	GCTACTCGAGTTTATTTTTCACTTGACTTTTTGCCT
43	Nos842_NdeI_F	GCTACATATGCAACAAGTCATAGTAAGTAATCG
44	Nos842_XhoI_wo_R	GCTACTCGAGGGATGCGTATCTAGCTATTAGATG
45	Nos903_pET_2A	GTTTAACTTTAAGAAGGAGATATACATATGACGACAGTTGCACTCAAAG
46	Nos904_pET_2A	GTTTAACTTTAAGAAGGAGATATACATATGGCAGTCAAAAAGTTAACAGAC
47	Nos842_pET_2A	GTTTAACTTTAAGAAGGAGATATACATATGCAACAAGTCATAGTAAGTAATCG
48	GFP_pET21a_2B	AGTGGTGGTGGTGGTGGTGTTTGTATAGTTCATCCATGCCATGTGTAATC
49	pET21a_1A	CACCACCACCACCACCAC
50	pET21a_1B	ATGTATATCTCCTTCTTAAAGTTAAACAAAATTATTTCTAGAGG
51	903_split_A	AAGGTGGCTCTGGCTCTGGCTCGAGCATGACGACAGTTGCACTCAAAG
52	903_split_B	CGGGCTTTGTTAGCAGCCGTTATTTAGCCGTAGAACTATCAAAAGCTCTC
53	903_split_A2	TTAACTTTAAGAAGGAGATATACATATGACGACAGTTGCACTCAAAG
54	903_split_B2	CCATGGTGATGGTGGTGATGAGATGCACTAGCTTTAGCCGTAGAACTATCAAAAGCTCT
55	904_split_A	TTTAACTTTAAGAAGGAGATATACCATGGCAGTCAAAAAGTTAACAGACA
56	904_split_B	TTACCGCTTCCACCCGACGTTTTATTTTTCACTTGACTTTTTGCCTGTTC
57	N-term_1A	GAGGATCCCCGGGTACC
58	N-term_1B	TAGAGTCGACCTGCAGGCA
59	pKT25_1A	CCCCGGGTACCTAAGTAAGTAAG
60	pKT25_1B	ATCCTCTAGAGTCGACCCTGC
61	pUT18C_1A	CCGAGCTCGAATTCATCGAT
62	pUT18C_1B	TACCCGGGGATCCTCTAGAGT
63	MB_5A	TGCCTGCAGGTCGACTCTAATGCTGTATTTAGCAGAAGTACAAAAG
64	MB_5B	TCGGTACCCGGGGATCCTCAGATGCCAACAACTCAGGC
65	MB_6A	AGGGTCGACTCTAGAGGATATGCTGTATTTAGCAGAAGTACAAAAGC
66	MB_6B	CTTACTTAGGTACCCGGGGAGATGCCAACAACTCAGGC
67	MB_8A	TCTAGAGGATCCCCGGGTAATGCTGTATTTAGCAGAAGTACAAAAG

68	MB_8B	TCGATGAATTCGAGCTCGGAGATGCCAACAACTCAGGC
69	MB_17A	TGCCTGCAGGTCGACTCTAATGACGACAGTTGCACTCAAAG
70	MB_17B	TCGGTACCCGGGGATCCTCTTTAGCCGTAGAACTATCAAAAGCTCTC
71	MB_18A	AGGGTCGACTCTAGAGGATATGACGACAGTTGCACTCAAAG
72	MB_18B	CTTACTTAGGTACCCGGGGTTTAGCCGTAGAACTATCAAAAGCTCTC
73	MB_20A	TCTAGAGGATCCCCGGGTAATGACGACAGTTGCACTCAAAG
74	MB_20B	TCGATGAATTCGAGCTCGGTTTAGCCGTAGAACTATCAAAAGCTCTC
75	MB_21A	TGCCTGCAGGTCGACTCTAATGGCAGTCAAAAAGTTAACAGACAA
76	MB_21B	TCGGTACCCGGGGATCCTCTTTATTTTTCACTTGACTTTTTGCCTGTTC
77	MB_22A	AGGGTCGACTCTAGAGGATATGGCAGTCAAAAAGTTAACAGACAA
78	MB_22B	CTTACTTAGGTACCCGGGGTTTATTTTTCACTTGACTTTTTGCCTGTTC
79	MB_24A	TCTAGAGGATCCCCGGGTAATGGCAGTCAAAAAGTTAACAGACAA
80	MB_24B	TCGATGAATTCGAGCTCGGTTTATTTTTCACTTGACTTTTTGCCTGTTC
81	MB_25A	TGCCTGCAGGTCGACTCTAATGCAACAAGTCATAGTAAGTAATCGAT
82	MB_25B	TCGGTACCCGGGGATCCTCGGATGCGTATCTAGCTATTAGATGTTC
83	MB_26A	AGGGTCGACTCTAGAGGATATGCAACAAGTCATAGTAAGTAATCGAT
84	MB_26B	CTTACTTAGGTACCCGGGGGGATGCGTATCTAGCTATTAGATGTTC
85	MB_28A	TCTAGAGGATCCCCGGGTAATGCAACAAGTCATAGTAAGTAATCGAT
86	MB_28B	TCGATGAATTCGAGCTCGGGGATGCGTATCTAGCTATTAGATGTTC
87	MB_41A	TGCCTGCAGGTCGACTCTAATGGGGCGATTTGAGAAGC
88	MB_41B	TCGGTACCCGGGGATCCTCACCTTCTGCATTGGCAGG
89	MB_42A	AGGGTCGACTCTAGAGGATATGGGGCGATTTGAGAAGC
90	MB_42B	CTTACTTAGGTACCCGGGGACCTTCTGCATTGGCAGG
91	MB_44A	TCTAGAGGATCCCCGGGTAATGGGGCGATTTGAGAAGC
92	MB_44B	TCGATGAATTCGAGCTCGGACCTTCTGCATTGGCAGG
93	MB_49A	ATGCCTGCAGGTCGACTCTAATGACACTTGATAATAACCAAGAGCTTACC
94	MB_49B	CTCGGTACCCGGGGATCCTCATTTTTGGGTGGTCGCCGTC
95	MB_50A	CAGGGTCGACTCTAGAGGATATGACACTTGATAATAACCAAGAGCTTACC
96	MB_50B	TACTTACTTAGGTACCCGGGGATTTTTGGGTGGTCGCCGTC
97	MB_52A	CTCTAGAGGATCCCCGGGTAATGACACTTGATAATAACCAAGAGCTTACC
98	MB_52B	TATATCGATGAATTCGAGCTCGGATTTTTGGGTGGTCGCCGTC
99	MB_53A	ATGCCTGCAGGTCGACTCTAATGGGGCTTTTTAGGAACTTTCG
100	MB_53B	CTCGGTACCCGGGGATCCTCCATATTTCGAGATCGTCCGCTAAAAAC
101	MB_54A	CAGGGTCGACTCTAGAGGATATGGGGCTTTTTAGGAACTTTCG
102	MB_54B	TACTTACTTAGGTACCCGGGGCATATTTCGAGATCGTCCGCTAAAAAC
103	MB_56A	CTCTAGAGGATCCCCGGGTAATGGGGCTTTTTAGGAACTTTCG
104	MB_56B	TATATCGATGAATTCGAGCTCGGCATATTTCGAGATCGTCCGCTAAAAAC
105	MB_69A	ATGCCTGCAGGTCGACTCTAATGTTTGAAGATTTGACTATACCCAGG
106	MB_69B	CTCGGTACCCGGGGATCCTCCCTATTACGTATCAATAAAATAATAGTTATAGCGGTG
107	MB_70A	CAGGGTCGACTCTAGAGGATATGTTTGAAGATTTGACTATACCCAGG

108	MB_70B	TACTTACTTAGGTACCCGGGGCCTATTACGTATCAATAAAATAATAGTTATAGCGGTG
109	MB_72A	CTCTAGAGGATCCCCGGGTAATGTTTGAAGATTTGACTATACCCAGG
110	MB_72B	ATATCGATGAATTCGAGCTCGGCCTATTACGTATCAATAAAATAATAGTTATAGCGGTG
111	MB_73A	ATGCCTGCAGGTCGACTCTAGTGAATTTATTATTTAAAGACCTTTTCGGAATATT
112	MB_73B	CTCGGTACCCGGGGATCCTCCTGCTGCGGTGGCGCTG
113	MB_74A	GGGTCGACTCTAGAGGATGTGAATTTATTATTTAAAGACCTTTTCGGAAT
114	MB_74B	TACTTACTTAGGTACCCGGGGCTGCTGCGGTGGCGCTG
115	MB_76A	CTAGAGGATCCCCGGGTAGTGAATTTATTATTTAAAGACCTTTTCGGAAT
116	MB_76B	TATATCGATGAATTCGAGCTCGGCTGCTGCGGTGGCGCTG
117	pRL271_Fwd	GAGCTCGCGAAAGCTTGCATG
118	pRL271_Rev	CTCGAGATCTAGATATCGAATTTCTGCCAT
119	CS.3_Fwd	GATCCGTGCACAGCACCTTG
120	CS.3_Rev	TTATTTGCCGACTACCTTGGTGATCT
121	295KO_2A	ATTCGATATCTAGATCTCGAGACTCAACATAATCATCGGTATATACCGAAAT
122	295KO_2B	CAAGGTGCTGTGCACGGATCACCGTTCTTCCTCTTGTGTACTTGA
123	295KO_4A	CCAAGGTAGTCGGCAAATAACAATTCAAAATTCAAAATTCAAAATATTTAGGACTTACG
124	295KO_4B	ATGCAAGCTTTCGCGAGCTCTGTAAATTTCTCACTAAGTGATGGATCAACACT
125	842KO_2A	ATTCGATATCTAGATCTCGAGATGGATAATCCAGCAATGTCGGC
126	842KO_2B	AAGGTGCTGTGCACGGATCATTGCTGATTTTTAGCGTAGTTAAGCTTT
127	842KO_4A	CAAGGTAGTCGGCAAATAAAATTTAATATCCCTAGCTCATCGTAAAATTTTTATAAAAATATG
128	842KO_4B	ATGCAAGCTTTCGCGAGCTCTTTAAAACTAGAACTATGAACTAGCTCGCTAAAC
129	903KO_2A	ATTCGATATCTAGATCTCGAGAAGCAACGGCAACGCC
130	903KO_2B	AAGGTGCTGTGCACGGATCATTTCAACTCCCTTGATTAGATAATGATTAATCGAG
131	904KO_4A	CAAGGTAGTCGGCAAATAAAATACAAATAATAAAAATAAATAAAAAGACGTAACGAAAATTACG
132	904KO_4B	TGCAAGCTTTCGCGAGCTCGTAGTGGGTTTCGCACAAGCTATC
133	903KO_Seq_A	TGCGAATTCCAGTAGGTCTTGGTAA
134	904KO_Seq_B	GGTGGCGCAGAAGTATTTTTG
135	842KO_Seq_A	TCAACAGTCAACAGTCAATAGTGAAGG
136	842KO_Seq_B	TTCATCTACACCGATATCTTGACCC
137	295KO_Seq_A	GCCATCCTAGCTCTGATTTGATC
138	295KO_Seq_B	CAGGGTTATCGGTAAGGAATCG
139	Fragment1.FOR	GATTTCGAACCCGGGGTACCACCTGTAGAGAAGAGTCCCTGAATATCAA
140	Fragment1.REV	TTTTTCGTATTTTCCCTCATTGAATTAATCTCCTACTTGACTTTATGAGTTGGGA
141	Fragment4.FOR	TGGATGAACTATACAAATAAACCGGTGTTTGGATTGTCGG
142	Fragment4.REV	CCCTGCAGGTCGAGGAATTCGCTGTCGAAGTTGAACATCAGTAAGC
143	Nos903_pIGA_2A	TAAAGTCAAGTAGGAGATTAATTCAATGACGACAGTTGCACTCAAAG
144	Fragment3.FOR	ATTTAATGACTGCCTTAGTCGCTAGTGCATCTGCTAGTGCTAGT

145	Fragment3.REV	CCGACAATCCAAACACCGGTTTATTTGTATAGTTCATCCATGCCATGTGTAATCC
146	Vector.FOR	TGATGTTCAACTTCGACAGCGAATTCCTCGACCTGCAGGG
147	Vector.REV	AGGGACTCTTCTCTACAGGTGGTACCCCGGGTTCGAAATCG
148	842_petE_F	CTACAGGTTAGGAGAACGCCATGGATAAGCGACGGAGGAAT
149	petE_842_R	CTCCGTCGCTTATCCATGGCGTTCTCCTAACCTGTAGTTTTATTTTTCT
150	p295_25C_long_A	TTTTGGTCATGAGATTATCAAAAAGATTGACGCAGCATGGC
151	pNos295_Rev	ACCGTTCTTCCTCTTGTGTACT
152	Nos295_pNos295_A	CACAAGAGGAAGAACGGTGTGCTGTATTTAGCAGAAGTACAAAAG
153	GFP_25C_R	AGGCCCTTTCGTCTTCAAGTTATTTGTATAGTTCATCCATGCCATGTGT
154	p842_25C_long_A	TTTTGGTCATGAGATTATCAAAAAGTCTCTCTATCCCCAAGTACAATTTCTCC
155	pNos842_2B	CTTGTTGCATATTGCTGATTTTTAGCG
156	Nos842_pNos842_3A	AATCAGCAATATGCAACAAGTCATAGTAAGTAATCGATTTATTTTAG
157	p903_25C_long_A	TTTTGGTCATGAGATTATCAAAAAGACCCGACACTCTTGAGG
158	pNos903_2B	ACTGTCGTCATATTTCAACTCCCTTG
159	Nos903_pNos903_3A	GGAGTTGAAATATGACGACAGTTGCACTCAAAG
160	pNos904_25C_F	ATTTTGGTCATGAGATTATCAAAAAGAGAAATATCAGCTAGACGTAAAGAGTGG
161	pNos904_2B	TGACTGCCATAAAAACCTCTATTTATTGC
162	Nos904_pNos904_3A	AGAGGTTTTTATGGCAGTCAAAAAGTTAACAGACAAAAAC
163	295_His_25C_R	GGCCCTTTCGTCTTCAAGTTAGTGGTGATGGTGATGATGAGATGC
164	Nos842_25C_B	GAGGCCCTTTCGTCTTCAAGTCAGGATGCGTATCTAGCTATTAGATG
165	Nos904_25C_Ba	GGCCCTTTCGTCTTCAAGTTATTTATTTTTCACTTGACTTTTTGCCTGT

Employed enzymatic cut sites are underlined.

1245 **References**

1246 1. Shapiro, J. A. Thinking about bacterial populations as multicellular organisms. *Annu.*
1247 *Rev. Microbiol.* **52**, 81–104 (1998).

1248 2. Lyons, N. A. & Kolter, R. On the evolution of bacterial multicellularity. *Curr. Opin.*
1249 *Microbiol.* **24**, 21–28 (2015).

1250 3. Claessen, D., Rozen, D. E., Kuipers, O. P., Søgaard-Andersen, L. & Van Wezel, G. P.
1251 Bacterial solutions to multicellularity: A tale of biofilms, filaments and fruiting bodies.
1252 *Nat. Rev. Microbiol.* **12**, 115–124 (2014).

1253 4. Smith, W. P. J. *et al.* Cell morphology drives spatial patterning in microbial communities.
1254 *Proc. Natl. Acad. Sci.* **114**, E280–E286 (2017).

1255 5. Lin, T.-Y., Santos, T. M. A., Kontur, W. S., Donohue, T. J. & Weibel, D. B. A Cardiolipin-
1256 Deficient Mutant of Rhodobacter sphaeroides Has an Altered Cell Shape and Is
1257 Impaired in Biofilm Formation. *J. Bacteriol.* **197**, 3446–3455 (2015).

1258 6. Lam, H. *et al.* D-amino acids govern stationary phase cell wall remodeling in bacteria.
1259 *Science* **325**, 1552–1555 (2009).

1260 7. Kolodkin-Gal, I. *et al.* D-amino acids trigger biofilm disassembly. *Science* **328**, 627–629
1261 (2010).

1262 8. Typas, A. *et al.* Regulation of peptidoglycan synthesis by outer-membrane proteins. *Cell*
1263 **143**, 1097–1109 (2010).

1264 9. Reichenbach, H. The ecology of the myxobacteria. *Environ. Microbiol.* **1**, 15–21 (1999).

1265 10. Flärdh, K., Richards, D. M., Hempel, A. M., Howard, M. & Buttner, M. J. Regulation of
1266 apical growth and hyphal branching in Streptomyces. *Curr. Opin. Microbiol.* **15**, 737–
1267 743 (2012).

1268 11. Flores, E. & Herrero, A. Compartmentalized function through cell differentiation in
1269 filamentous cyanobacteria. *Nat. Rev. Microbiol.* **8**, 39–50 (2010).

1270 12. Rossetti, V. & Bagheri, H. C. Advantages of the division of labour for the long-term
1271 population dynamics of cyanobacteria at different latitudes. *Proceedings. Biol. Sci.* **279**,
1272 3457–3466 (2012).

1273 13. Fuchs, E. & Weber, K. INTERMEDIATE FILAMENTS: Structure, Dynamics, Function
1274 and Disease. *Annu. Rev. Biochem.* **63**, 345–382 (1994).

1275 14. Köster, S., Weitz, D. A., Goldman, R. D., Aebi, U. & Herrmann, H. Intermediate filament
1276 mechanics in vitro and in the cell: From coiled coils to filaments, fibers and networks.
1277 *Curr. Opin. Cell Biol.* **32**, 82–91 (2015).

1278 15. Ausmees, N., Kuhn, J. R. & Jacobs-Wagner, C. The bacterial cytoskeleton: An
1279 intermediate filament-like function in cell shape. *Cell* **115**, 705–713 (2003).

1280 16. Fuchino, K. *et al.* Dynamic gradients of an intermediate filament-like cytoskeleton are
1281 recruited by a polarity landmark during apical growth. *Proceedings of the National*
1282 *Academy of Sciences* **110**, E1889–E1897 (2013).

1283 17. Holmes, N. A. *et al.* Coiled-coil protein Scy is a key component of a multiprotein
1284 assembly controlling polarized growth in Streptomyces. *Proceedings of the National*
1285 *Academy of Sciences* **110**, E397–E406 (2013).

1286 18. Fenton, A. K., Hobley, L., Butan, C., Subramaniam, S. & Sockett, R. E. A coiled-coil-
1287 repeat protein 'Ccrp' in Bdellovibrio bacteriovorus prevents cellular indentation, but is
1288 not essential for vibroid cell morphology. *FEMS Microbiology Letters* **313**, 89–95 (2010).

1289 19. Waidner, B. *et al.* A novel system of cytoskeletal elements in the human pathogen
1290 Helicobacter pylori. *PLoS Pathogens* **5**, (2009).

1291 20. Ent, F. van den, Amos, L. A. & Löwe, J. Prokrayotic origin of the actin cytoskeleton.
1292 *Nature* **413**, 39–44 (2001).

1293 21. de Boer, P., Crossley, R. & Rothfield, L. The essential bacterial cell-division protein FtsZ
1294 is a GTPase. *Nature* **359**, 254–256 (1992).

1295 22. Lin, L. & Thanbichler, M. Nucleotide-independent cytoskeletal scaffolds in bacteria.
1296 *Cytoskeleton* **70**, 409–423 (2013).

1297 23. Kaiser, D. & Crosby, C. Cell movement and its coordination in swarms of Myxococcus
1298 xanthus. *Cell Motil.* **3**, 227–245 (1983).

1299 24. Yang, R. *et al.* AglZ Is a Filament-Forming Coiled-Coil Protein Required for Adventurous
1300 Gliding Motility of Myxococcus xanthus. *J. Bacteriol.* **186**, 6168–6178 (2004).

1301 25. Nan, B., Mauriello, E. M. F., Sun, I. H., Wong, A. & Zusman, D. R. A multi-protein
1302 complex from Myxococcus xanthus required for bacterial gliding motility. *Mol. Microbiol.*
1303 **76**, 1539–1554 (2010).

1304 26. Nan, B. *et al.* Myxobacteria gliding motility requires cytoskeleton rotation powered by
1305 proton motive force. *Proc. Natl. Acad. Sci.* **108**, 2498–2503 (2011).

1306 27. Mauriello, E. M. F. *et al.* Bacterial motility complexes require the actin-like protein, MreB
1307 and the Ras homologue, MglA. *EMBO J.* **29**, 315–326 (2010).

1308 28. Schumacher, D. & Søgaard-Andersen, L. Regulation of Cell Polarity in Motility and Cell
1309 Division in Myxococcus xanthus. *Annu. Rev. Microbiol. Regul.* **71**, 61–78 (2017).

1310 29. Letek, M. *et al.* DivIVA is required for polar growth in the MreB-lacking rod-shaped
1311 actinomycete Corynebacterium glutamicum. *J. Bacteriol.* **190**, 3283–3292 (2008).

1312 30. Puffal, J., García-Heredia, A., Rahlwes, K. C., Siegrist, M. S. & Morita, Y. S. Spatial
1313 control of cell envelope biosynthesis in mycobacteria. *Pathog. Dis.* **76**, fty027 (2018).

1314 31. Surovtsev, I. V & Jacobs-Wagner, C. Subcellular organization: a critical feature of
1315 bacterial cell replication. *Cell* **172**, 1271–1293 (2018).

1316 32. Bagchi, S., Tomenius, H., Belova, L. M. & Ausmees, N. Intermediate filament-like
1317 proteins in bacteria and a cytoskeletal function in Streptomyces. *Mol. Microbiol.* **70**,
1318 1037–1050 (2008).

1319 33. Hempel, A. M., Wang, S., Letek, M., Gil, J. A. & Flärdh, K. Assemblies of DivIVA mark
1320 sites for hyphal branching and can establish new zones of cell wall growth in
1321 Streptomyces coelicolor. *J. Bacteriol.* **190**, 7579–7583 (2008).

1322 34. Wagstaff, J. & Löwe, J. Prokaryotic cytoskeletons: protein filaments organizing small
1323 cells. *Nat. Rev. Microbiol.* (2018). doi:10.1038/nrmicro.2017.153

1324 35. Schwedock, J., McCormick, J. R., Angert, E. R., Nodwell, J. R. & Losick, R. Assembly
1325 of the cell division protein FtsZ into ladder-like structures in the aerial hyphae of
1326 Streptomyces coelicolor. *Mol. Microbiol.* **25**, 847–858 (1997).

1327 36. Rippka, R., Stanier, R. Y., Deruelles, J., Herdman, M. & Waterbury, J. B. Generic

1328 Assignments, Strain Histories and Properties of Pure Cultures of Cyanobacteria.
1329 *Microbiology* **111**, 1–61 (1979).

1330 37. Herrero, A., Stavans, J. & Flores, E. The multicellular nature of filamentous heterocyst-
1331 forming cyanobacteria. *FEMS Microbiol. Rev.* **40**, 831–854 (2016).

1332 38. Zhang, C.-C. C., Hugenin, S., Friry, A., Huguenin, S. & Friry, A. Analysis of genes
1333 encoding the cell division protein FtsZ and a glutathione synthetase homologue in the
1334 cyanobacterium Anabaena sp. PCC 7120. *Res. Microbiol.* **146**, 445–455 (1995).

1335 39. Hu, B., Yang, G., Zhao, W., Zhang, Y. & Zhao, J. MreB is important for cell shape but
1336 not for chromosome segregation of the filamentous cyanobacterium Anabaena sp. PCC
1337 7120. *Mol. Microbiol.* **63**, 1640–1652 (2007).

1338 40. Burnat, M., Schleiff, E. & Flores, E. Cell envelope components influencing filament
1339 length in the heterocyst-forming cyanobacterium Anabaena sp. strain PCC 7120. *J.*
1340 *Bacteriol.* **196**, 4026–4035 (2014).

1341 41. Cho, H., Uehara, T. & Bernhardt, T. G. Beta-lactam antibiotics induce a lethal
1342 malfunctioning of the bacterial cell wall synthesis machinery. *Cell* **159**, 1310–1311
1343 (2014).

1344 42. Fenton, A. K., Mortaji, L. El, Lau, D. T. C., Rudner, D. Z. & Bernhardt, T. G. CozE is a
1345 member of the MreCD complex that directs cell elongation in Streptococcus
1346 pneumoniae. *Nat. Microbiol.* **2**, 1–9 (2016).

1347 43. Mullineaux, C. W. *et al.* Mechanism of intercellular molecular exchange in heterocyst-
1348 forming cyanobacteria. *EMBO J.* **27**, 1299–1308 (2008).

1349 44. Wilk, L. *et al.* Outer membrane continuity and septosome formation between vegetative
1350 cells in the filaments of Anabaena sp. PCC 7120. *Cell. Microbiol.* **13**, 1744–1754 (2011).

1351 45. Weiss, G. L., Kieninger, A.-K., Maldener, I., Forchhammer, K. & Pilhofer, M. Structure
1352 and function of a bacterial gap junction analog. *bioRxiv* 462465 (2018).
1353 doi:10.1101/462465

1354 46. Flores, E. *et al.* Septum-localized protein required for filament integrity and diazotrophy
1355 in the heterocyst-forming cyanobacterium Anabaena sp. strain PCC 7120. *J. Bacteriol.*
1356 **189**, 3884–3890 (2007).

1357 47. Lehner, J. *et al.* Prokaryotic multicellularity: A nanopore array for bacterial cell
1358 communication. *FASEB J.* **27**, 2293–2300 (2013).

1359 48. Nayar, A. S., Yamaura, H., Rajagopalan, R., Risser, D. D. & Callahan, S. M. FraG is
1360 necessary for filament integrity and heterocyst maturation in the cyanobacterium
1361 Anabaena sp. strain PCC 7120. *Microbiology* **153**, 601–607 (2007).

1362 49. Merino-Puerto, V. *et al.* FraC/FraD-dependent intercellular molecular exchange in the
1363 filaments of a heterocyst-forming cyanobacterium, Anabaena sp. *Mol. Microbiol.* **82**, 87–
1364 98 (2011).

1365 50. Merino-Puerto, V., Mariscal, V., Mullineaux, C. W., Herrero, A. & Flores, E. Fra proteins
1366 influencing filament integrity, diazotrophy and localization of septal protein SepJ in the
1367 heterocyst-forming cyanobacterium Anabaena sp. *Mol. Microbiol.* **75**, 1159–1170
1368 (2010).

1369 51. Herrmann, H. & Aebi, U. Intermediate Filaments: Molecular Structure, Assembly
1370 Mechanism, and Integration Into Functionally Distinct Intracellular Scaffolds. *Annu. Rev.*
1371 *Biochem.* **73**, 749–789 (2004).

1372 52. Specht, M., Schätzle, S., Graumann, P. L. & Waidner, B. Helicobacter pylori Possesses
1373 Four Coiled-Coil-Rich Proteins That Form Extended Filamentous Structures and Control
1374 Cell Shape and Motility. *J. Bacteriol.* **193**, 4523–4530 (2011).

1375 53. Herrmann, H., Bär, H., Kreplak, L., Strelkov, S. V. & Aebi, U. Intermediate filaments:
1376 From cell architecture to nanomechanics. *Nat. Rev. Mol. Cell Biol.* **8**, 562–573 (2007).

1377 54. Kelemen, G. H. Intermediate Filaments Supporting Cell Shape and Growth in Bacteria
1378 BT - Prokaryotic Cytoskeletons: Filamentous Protein Polymers Active in the Cytoplasm
1379 of Bacterial and Archaeal Cells. in (eds. Löwe, J. & Amos, L. A.) 161–211 (Springer
1380 International Publishing, 2017). doi:10.1007/978-3-319-53047-5_6

1381 55. Camberg, J. L., Hoskins, J. R. & Wickner, S. ClpXP protease degrades the cytoskeletal
1382 protein, FtsZ, and modulates FtsZ polymer dynamics. *Proc Natl Acad Sci U S A* **106**,
1383 10614–10619 (2009).

1384 56. Charbon, G., Cabeen, M. T. & Jacobs-Wagner, C. Bacterial intermediate filaments: In
1385 vivo assembly, organization, and dynamics of crescentin. *Genes and Development* **23**,
1386 1131–1144 (2009).

1387 57. Weissenbach, J. *et al.* Evolution of Chaperonin Gene Duplication in Stigonematalean
1388 Cyanobacteria (Subsection V). *Genome Biol. Evol.* **9**, 241–252 (2017).

1389 58. Elhai, J., Vepritskiy, A., Muro-Pastor, A. M., Flores, E. & Wolk, C. P. Reduction of
1390 conjugal transfer efficiency by three restriction activities of Anabaena sp. strain PCC
1391 7120. *J. Bacteriol.* **179**, 1998–2005 (1997).

1392 59. Sakr, S., Thyssen, M., Denis, M. & Zhang, C. C. Relationship among several key cell
1393 cycle events in the developmental cyanobacterium Anabaena sp. strain PCC 7120. *J.*
1394 *Bacteriol.* **188**, 5958–5965 (2006).

1395 60. Sakr, S., Jeanjean, R., Zhang, C.-C. & Arcondeguy, T. Inhibition of cell division
1396 suppresses heterocyst development in Anabaena sp. strain PCC 7120. *J. Bacteriol.*
1397 **188**, 1396–1404 (2006).

1398 61. Solovyev, V. & Salamov, A. Automatic Annotation of Microbial Genomes and
1399 Metagenomic Sequences. in *Metagenomics and its Applications in Agriculture,*
1400 *Biomedicine and Environmental Studies* (ed. Robert W. Li, pp) 61–78 (Nova Science
1401 Publishers, Inc., 2011).

1402 62. Buikema, W. J. & Haselkorn, R. Expression of the Anabaena hetR gene from a copper-
1403 regulated promoter leads to heterocyst differentiation under repressing conditions. *Proc.*
1404 *Natl. Acad. Sci.* **98**, 2729–2734 (2001).

1405 63. Callahan, S. M. & Buikema, W. J. The role of HetN in maintenance of the heterocyst
1406 pattern in Anabaena sp. PCC 7120. *Mol. Microbiol.* **40**, 941–950 (2001).

1407 64. Cabeen, M. T. & Jacobs-Wagner, C. Bacterial cell shape. *Nat. Rev. Microbiol.* **3**, 601–
1408 610 (2005).

1409 65. Rojas, E. R. & Huang, K. C. Regulation of microbial growth by turgor pressure. *Curr.*
1410 *Opin. Microbiol.* **42**, 62–70 (2018).

1411 66. Swulius, M. T. & Jensen, G. J. The helical mreb cytoskeleton in Escherichia coli
1412 MC1000/pLE7 is an artifact of the N-terminal yellow fluorescent protein tag. *J. Bacteriol.*
1413 **194**, 6382–6386 (2012).

1414 67. Wang, Y. *et al.* Coiled-coil networking shapes cell molecular machinery. *Mol. Biol. Cell*
1415 **23**, 3911–3922 (2012).

1416 68. Mason, J. M. & Arndt, K. M. Coiled coil domains: Stability, specificity, and biological
1417 implications. *ChemBioChem* **5**, 170–176 (2004).

1418 69. Lupas, A. N. & Gruber, M. B. T.-A. in P. C. The Structure of α-Helical Coiled Coils. in
1419 *Fibrous Proteins: Coiled-Coils, Collagen and Elastomers* **70**, 37–38 (Academic Press,
1420 2005).

1421 70. Newman, J. R. S., Wolf, E. & Kim, P. S. A computationally directed screen identifying
1422 interacting coiled coils from Saccharomyces cerevisiae. *Proc. Natl. Acad. Sci.* **97**,
1423 13203–13208 (2002).

1424 71. Litowski, J. R. & Hodges, R. S. Designing Heterodimeric Two-stranded α-Helical Coiled-
1425 coils. *J. Biol. Chem.* **277**, 37272–37279 (2002).

1426 72. Vinson, C. R., Hai, T. & Boyd, S. M. Dimerization specificity of the leucine zipper-
1427 containing bZIP motif on DNA binding: Prediction and rational design. *Genes Dev.* **7**,
1428 1047–1058 (1993).

1429 73. Shea, E. K. O., Rutkowski, R., Iii, W. F. S. & Kim, P. S. Preferential Heterodimer
1430 Formation by Isolated Leucine Zippers from Fos and Jun. *Science (80-.).* **245**, 646–648
1431 (1989).

1432 74. Mier, P., Alanis-Lobato, G. & Andrade-Navarro, M. A. Protein-protein interactions can
1433 be predicted using coiled coil co-evolution patterns. *J. Theor. Biol.* **412**, 198–203 (2017).

1434 75. Hai, T., Liu, F., Coukos, W. J. & Green, M. R. Transcription factor ATF cDNA clones: An
1435 extensive family of leucine zipper proteins able to selectively form DNA-binding
1436 heterodimers. *Genes Dev.* **3**, 2083–2090 (1989).

1437 76. Strauss, H. M. & Keller, S. Pharmacological Interference with Protein – Protein
1438 Interactions Mediated by Coiled-Coil Motifs. *Handb. Exp. Pharmacol.* 13125–13125
1439 (2008). doi:10.1007/978-3-540-72843-6_19

1440 77. Cabeen, M. T. & Jacobs-Wagner, C. The Bacterial Cytoskeleton. **44**, 365–392 (2010).

1441 78. Kerff, F., Terrak, M., Charlier, P., Sauvage, E. & Ayala, J. A. The penicillin-binding
1442 proteins: structure and role in peptidoglycan biosynthesis. *FEMS Microbiol. Rev.* **32**,
1443 234–258 (2008).

1444 79. van Teeseling, M. C. F., de Pedro, M. A. & Cava, F. Determinants of bacterial
1445 morphology: From fundamentals to possibilities for antimicrobial targeting. *Front.*
1446 *Microbiol.* **8**, 1–18 (2017).

1447 80. Lutkenhaus, J. The ParA/MinD family puts things in their place. *Trends Microbiol.* **20**,
1448 411–418 (2012).

1449 81. Leipe, D. D., Wolf, Y. I., Koonin, E. V & Aravind, L. Classification and evolution of P-
1450 loop GTPases and related ATPases. *J. Mol. Biol.* **317**, 41–72 (2002).

1451 82. Ramos-León, F., Mariscal, V., Frías, J. E., Flores, E. & Herrero, A. Divisome-dependent
1452 subcellular localization of cell-cell joining protein SepJ in the filamentous
1453 cyanobacterium Anabaena. *Mol. Microbiol.* **96**, 566–580 (2015).

1454 83. Heins, S. & Aebi, U. Making heads and tails of intermediate filament assembly,
1455 dynamics and networks. *Curr. Opin. Cell Biol.* **6**, 25–33 (1994).

1456 84. Herrmann, H. *et al.* Structure and assembly properties of the intermediate filament
1457 protein vimentin: The role of its head, rod and tail domains. *J. Mol. Biol.* **264**, 933–953
1458 (1996).

1459 85. England, P. *et al.* The Scc Spirochetal Coiled-Coil Protein Forms Helix-Like Filaments
1460 and Binds to Nucleic Acids Generating Nucleoprotein Structures. *J. Bacteriol.* **188**, 469–
1461 476 (2005).

1462 86. Ingerson-Mahar, M., Briegel, A., Werner, J. N., Jensen, G. J. & Gitai, Z. The metabolic
1463 enzyme CTP synthase forms cytoskeletal filaments. *Nature Cell Biology* **12**, 739–746
1464 (2010).

1465 87. Cabeen, M. T. *et al.* Bacterial cell curvature through mechanical control of cell growth.
1466 *The EMBO Journal* **28**, 1208–1219 (2009).

1467 88. Shieh, Y.-W. *et al.* Operon structure and cotranslational subunit association direct
1468 protein assembly in bacteria. *Science (80-.).* **350**, 678 LP – 680 (2015).

1469 89. Jones, L. J. F., Carballido-López, R. & Errington, J. Control of cell shape in bacteria:
1470 Helical, actin-like filaments in Bacillus subtilis. *Cell* **104**, 913–922 (2001).

1471 90. Alberts, B. *et al. Molecular Biology of the Cell*. (Garland Science, 2014).

1472 91. Herrmann, H. & Aebi, U. Intermediate filaments and their associates: Multi-talented
1473 structural elements specifying cytoarchitecture and cytodynamics. *Curr. Opin. Cell Biol.*
1474 **12**, 79–90 (2000).

1475 92. Leung, C. L., Green, K. J. & Liem, R. K. H. Plakins: A family of versatile cytolinker
1476 proteins. *Trends Cell Biol.* **12**, 37–45 (2002).

1477 93. Zhang, R., Zhang, C., Zhao, Q. & Li, D. Spectrin: Structure, function and disease. *Sci.*
1478 *China Life Sci.* **56**, 1076–1085 (2013).

1479 94. Typas, A., Banzhaf, M., Gross, C. A. & Vollmer, W. From the regulation of peptidoglycan
1480 synthesis to bacterial growth and morphology. *Nat. Rev. Microbiol.* **10**, 123–136 (2012).

1481 95. Persat, A. *et al.* The mechanical world of bacteria. *Cell* **161**, 988–997 (2015).

1482 96. Park, A., Jeong, H.-H., Lee, J., Kim, K. P. & Lee, C.-S. Effect of shear stress on the
1483 formation of bacterial biofilm in a microfluidic channel. *BioChip J.* **5**, 236–241 (2011).

1484 97. Young, K. D. The selective value of bacterial shape. *Microbiol. Mol. Biol. Rev.* **70**, 660–
1485 703 (2006).

1486 98. Lupas, A., Van Dyke, M. & Stock, J. Predicting coiled coils from protein sequences.
1487 *Science* **252**, 1162–1164 (1991).

1488 99. Wilson, C. G. M., Magliery, T. J. & Regan, L. Detecting protein-protein interactions with
1489 GFP-fragment reassembly. *Nat. Methods* **1**, 255–262 (2004).

1490 100. Yang, Y. *et al.* Phenotypic variation caused by variation in the relative copy number of
1491 pDU1-based plasmids expressing the GAF domain of Pkn41 or Pkn42 in Anabaena sp.
1492 PCC 7120. *Res. Microbiol.* **164**, 127–135 (2013).

1493 101. Nieves-Morión, M. *et al.* Specific Glucoside Transporters Influence Septal Structure and
1494 Function in the Filamentous, Heterocyst-Forming Cyanobacterium Anabaena sp. Strain
1495 PCC 7120. *J. Bacteriol.* **199**, e00876-16 (2017).

1496 102. Bornikoel, J. *et al.* Role of Two Cell Wall Amidases in Septal Junction and Nanopore
1497 Formation in the Multicellular Cyanobacterium Anabaena sp. PCC 7120. *Front. Cell.*
1498 *Infect. Microbiol.* **7**, 386 (2017).

1499 103. Karimova, G., Davi, M. & Ladant, D. The β-lactam resistance protein Blr, a small
1500 membrane polypeptide, is a component of the Escherichia coli cell division machinery.

1501 *J. Bacteriol.* **194**, 5576–5588 (2012).

1502 104. Roy, A., Yang, J. & Zhang, Y. COFACTOR: An accurate comparative algorithm for
1503 structure-based protein function annotation. *Nucleic Acids Res.* **40**, 471–477 (2012).

1504 105. Zhang, Y. I-TASSER: Fully automated protein structure prediction in CASP8. *Proteins*
1505 *Struct. Funct. Bioinforma.* **77**, 100–113 (2009).

1506 106. Yang, J. & Zhang, Y. I-TASSER server: New development for protein structure and
1507 function predictions. *Nucleic Acids Res.* **43**, W174–W181 (2015).

1508 107. Lutkenhaus, J. Another Cytoskeleton in the Closet. *Cell* **115**, 648–650 (2003).

1509 108. Jin, S. K. & Sun, S. X. Morphology of Caulobacter crescentus and the mechanical role
1510 of crescentin. *Biophysical Journal* **96**, (2009).

1511 109. Cabeen, M. T., Herrmann, H. & Jacobs-Wagner, C. The domain organization of the
1512 bacterial intermediate filament-like protein crescentin is important for assembly and
1513 function. *Cytoskeleton* **68**, 205–219 (2011).

1514 110. Dagan, T. *et al.* Genomes of stigonematalean cyanobacteria (subsection V) and the
1515 evolution of oxygenic photosynthesis from prokaryotes to plastids. *Genome Biol. Evol.*
1516 **5**, 31–44 (2013).

1517 111. Tria, F. D. K., Landan, G. & Dagan, T. Phylogenetic rooting using minimal ancestor
1518 deviation. *Nat. Ecol. Evol.* **1**, 0193 (2017).

1519 112. Altschul, S. F., Gish, W., Miller, W., Myers, E. W. & Lipman, D. J. Basic local alignment
1520 search tool. *J. Mol. Biol.* **215**, 403–410 (1990).

1521 113. Rice, P., Longden, I. & Bleasby, A. EMBOSS: the European Molecular Biology Open
1522 Software Suite. *Trends Genet.* **16**, 276–7 (2000).

1523 114. Letunic, I. & Bork, P. Interactive tree of life (iTOL) v3: an online tool for the display and
1524 annotation of phylogenetic and other trees. *Nucleic Acids Res.* **44**, W242–W245 (2016).

1525 115. Sambrook, J. & Green, M. R. *Molecular Cloning: A Laboratory Manual*. (Cold Spring
1526 Harbor Laboratory Press, 2012).

1527 116. Ungerer, J. & Pakrasi, H. B. Cpf1 Is A Versatile Tool for CRISPR Genome Editing Across
1528 Diverse Species of Cyanobacteria. *Sci. Rep.* **6**, 1–9 (2016).

1529 117. Wolk, C. P. *et al.* Isolation and complementation of mutants of Anabaena sp. strain PCC
1530 7120 unable to grow aerobically on dinitrogen. *J. Bacteriol.* **170**, 1239–1244 (1988).

1531 118. Stucken, K., Ilhan, J., Roettger, M., Dagan, T. & Martin, W. F. Transformation and
1532 conjugal transfer of foreign genes into the filamentous multicellular cyanobacteria
1533 (subsection V) Fischerella and Chlorogloeopsis. *Curr. Microbiol.* **65**, 552–560 (2012).

1534 119. Cai, Y. & Wolk, C. P. Use of a conditionally lethal gene in Anabaena sp. strain PCC
1535 7120 to select for double recombinats and to entrap insertion sequnces. *J. Bacteriol.*
1536 **172**, 3138–3145 (1990).

1537 120. Fiedler, G., Arnold, M., Hannus, S. & Maldener, I. The DevBCA exporter is essential for
1538 envelope formation in heterocysts of the cyanobacterium Anabaena sp. strain PCC
1539 7120. *Mol. Microbiol.* **27**, 1193–1202 (1998).

1540 121. Kühner, D., Stahl, M., Demircioglu, D. D. & Bertsche, U. From cells to muropeptide
1541 structures in 24 h: Peptidoglycan mapping by UPLC-MS . (2014).

122. Lehner, J. *et al.* The morphogene AmiC2 is pivotal for multicellular development in the cyanobacterium Nostoc punctiforme. *Mol. Microbiol.* **79**, 1655–1669 (2011).

123. Rudolf, M. *et al.* The Peptidoglycan-Binding Protein SjcF1 Influences Septal Junction Function and Channel Formation in the Filamentous Cyanobacterium Anabaena *MBio* **6**, e00376-15 (2015).

124. Dörrich, A. K., Mitschke, J., Siadat, O. & Wilde, A. Deletion of the Synechocystis sp. PCC 6803 kaiAB1C1 gene cluster causes impaired cell growth under light???dark conditions. *Microbiol. (United Kingdom)* **160**, 2538–2550 (2014).

125. Grant, S. G., Jessee, J., Bloom, F. R. & Hanahan, D. Differential plasmid rescue from transgenic mouse DNAs into Escherichia coli methylation-restriction mutants. *Proc. Natl. Acad. Sci.* **87**, 4645–4649 (1990).

126. Studier, F. W. & Moffatt, B. A. Use of bacteriophage T7 RNA polymerase to direct selective high-level expression of cloned genes. *J. Mol. Biol.* **189**, 113–130 (1986).

127. Boyer, H. & Roulland-Dessoix, D. A complementation analysis of the restrcition and modification of DNA in Escherichia coli. *J. Mol. Biol.* **41**, 459–472 (1969).

128. Cohen, S. E. *et al.* Dynamic localization of the cyanobacterial circadian clock proteins. *Curr. Biol.* **24**, 1836–1844 (2014).

129. Olmedo-Verd, E., Muro-Pastor, A. M., Flores, E. & Herrero, A. Localized induction of the ntcA regulatory gene in developing heterocysts of Anabaena sp. strain PCC 7120. *J. Bacteriol.* **188**, 6694–6699 (2006).